9950-351

PHASE I
FINAL REPORT
FOR THE
DEVELOPMENT OF AN
AIR BRAYTON SOLAR RECEIVER

CONTRACT NO. 955120

SUBMITTED TO

California Institute of Technology
Jet Propulsion Laboratory
4800 Oak Grove Drive
Pasadena, CA 91103

PREPARED BY

SANDERS ASSOCIATES, INC.
ENERGY SYSTEMS CENTER

95 Canal Street, Nashua, NH 03061

PHASE I
FINAL REPORT
FOR THE
DEVELOPMENT OF AN
AIR BRAYTON SOLAR RECEIVER

CONTRACT NO. 955120

SUBMITTED TO

California Institute of Technology
Jet Propulsion Laboratory
4800 Oak Grove Drive
Pasadena, CA 91103

PREPARED BY

SANDERS ASSOCIATES, INC.
ENERGY SYSTEMS CENTER

95 Canal Street, Nashua, NH 03061

TABLE OF CONTENTS

TABLE OF CONTENTS

TABLE OF CONTENTS

LIST OF ILLUSTRATIONS

LIST OF ILLUSTRATIONS (Continued)

LIST OF ILLUSTRATIONS (Continued)

LIST OF ILLUSTRATIONS (Continued)

SECTION 1

EXECUTIVE SUMMARY

1.1 INTRODUCTION

Small, point focus, Air Brayton Solar Power Systems consist of concentrators, receivers, energy transport, power conversion, and control subsystems. The technology and mass production techniques now available in industry make application experiments of air Brayton components and systems feasible in the early 1980's.

1.2 SYSTEM DESIGN APPROACH SELECTION

1.2.1 General

This receiver model is depicted in Figure 1-1 mounted on a typical low cost collector. The key elements of this receiver module are:

- Honeycomb, ceramic matrix receiver, heat exchanger
- A heat exchanger/storage module configured to minimize ducting pressure losses and conduction heat losses
- A valving mechanism, integral to the receiver module that allows for positive control of air flow in the storage system
- Low cost ceramic materials for both receiver and storage module

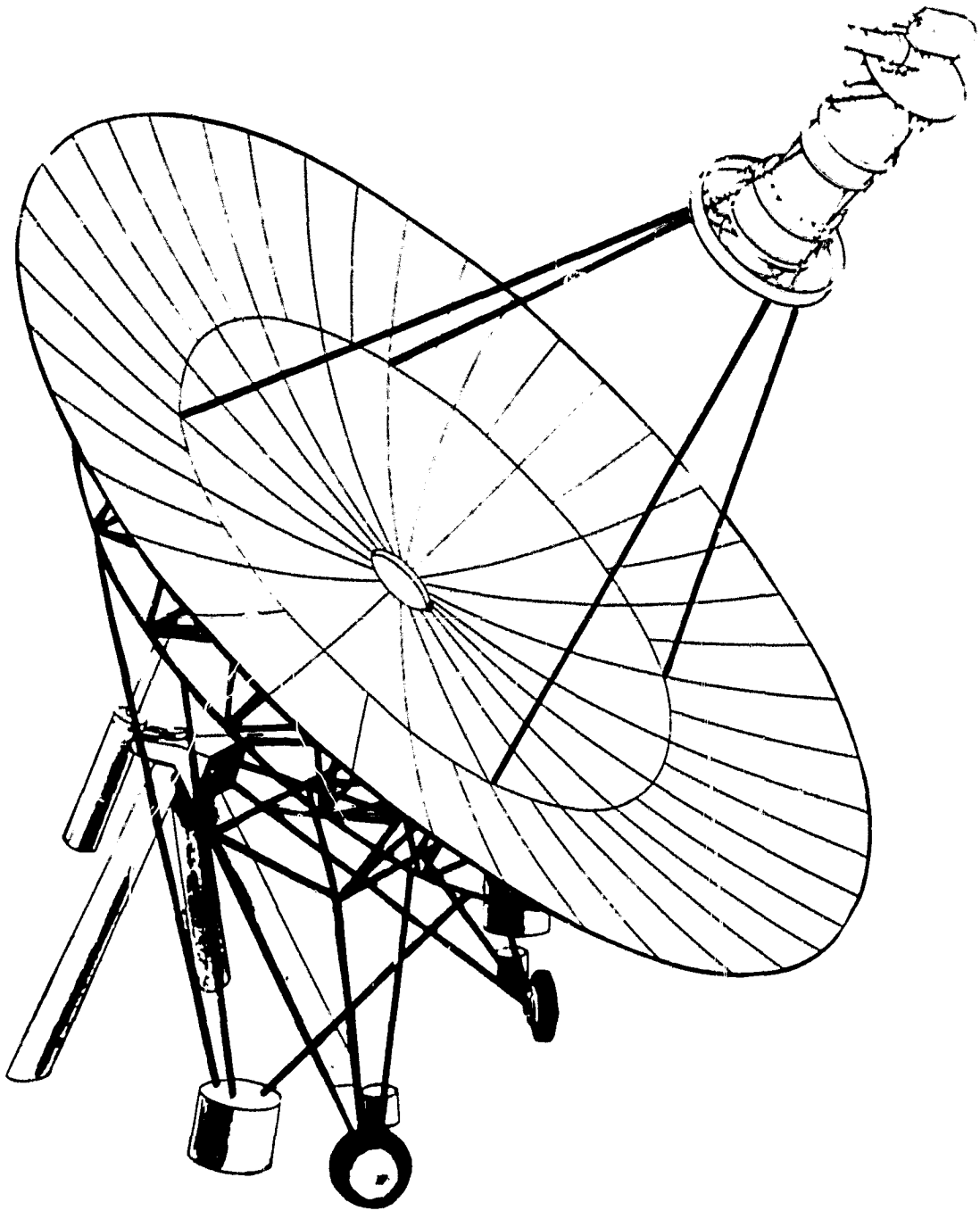

12088-20

Figure 1-1. Sanders' open cycle Air Brayton Receiver model is mounted on a low cost collector.

The principal factors influencing Sanders' selection of this specific receiver configuration are:

- Analytically and empirically validated high heat transfer efficiency of the matrix receiver (greater than 0.85@ 1700^{o}F).

- Compatability with automated, manufacturing processes that minimize requirements for labor intensive operations of drawing, fusing, brazing and welding. Utilization of these manufacturing cost efficiencies offers the potential for complete receiver modules of low cost and high reliability.

- Low thermal stress that minimizes mechanical failure of the receiver components.

- Proven fabrication, design and test experience with similar matrix receivers and storage modules that insures satisfactory operating performance well within the time frame of the Jet Propulsion Laboratory's schedule.

- The heat transfer efficiency, thermal stress and scalability of matrix honeycomb receivers were investigated and validated on earlier Department of Energy Programs.

The Phase I analysis program conducted by Sanders shows receivers compatible with Air Brayton Solar Systems are represented by two catagories:

- Matrix receivers
- Tube receivers

Performance contrasts between the types of receivers can be drawn around some key points, as described in the following paragraphs.

1.2.2 Heat Transfer Efficiency

The matrix honeycomb receiver has a high heat transfer surface area per unit volume compared to tube receiver. A great difference exists with tube receivers. The surface area/unit volume is low. This results in larger receivers to accomplish the same amount of heat transfer. If receiver overall size is maintained, then tube size must decrease, resulting in higher receiver pressure drops. These effects reduce the overall cycle efficiency and thus reduce output power compared to honeycomb matrix receivers.

1.2.3 Thermal Stress

In the tube receiver, circumferential temperature gradients are a limiting factor in the selection of tube sizes and spacing. This complication is eliminated by having a matrix which is supported in a compliant mounting structure. The receiver module that Sanders will build under Phase II program is designed using such a compliant mounting structure. This structure allows the matrix to move to relieve thermal stresses.

The low thermal stresses in matrix receivers minimizes the mechanical failures in the heat exchanger. In the event of cracking or hole obstruction the matrix receiver continues to operate without any change of performance. In a tube receiver, a crack or weld failure

results in loss of working fluid and eventual shutdown of the Air Brayton Solar Power System.

1.2.4 Tolerance to High Flux Variations

The ceramic honeycomb matrix is very tolerant to variation in flux intensities across the matrix. Sanders has conducted extensive measurements of the flux variation on matrix honeycomb receivers. These tests were conducted in Sanders laboratories, at the Department of Energy test sites at White Sands and DOE Advanced Component Test Facility at Georgia Institute of Technology. The results of the tests showed that for honeycomb configurations almost identical to those selected in the proposed receiver configuration, flux variations of 7 to 1 are tolerated with no adverse affect. In tube type receivers, variations of this magnitude often cause failure.

1.2.5 Convective Loss

Significant convective losses occur in open cavity receivers. A properly sealed aperture window design, as chosen for Sanders' design, completely eliminates convection losses. A window configuration of this type was demonstrated by Sanders during the 10 KWt receiver tests at White Sands, NM under a previously referenced DOE contract.

1.2.6 Sensible Heat Thermocline Storage Module

Sanders has selected a sensible heat thermocline storage module as the buffer storage subsystem in the ABSR system. This technique

provides high density storage and has relatively low pressure loss which improves the conversion efficiency of the Brayton engine.

1.2.7 Receiver/Storage Integrated Module

The Sanders designed receiver/storage module is integrated to minimize pressure losses and conduction losses due to ducting.

1.2.8 Positive Control of Mass Flow

Rather than relying on system pressure drops for distribution of flow between receiver and storage, Sanders has included an integrated valving mechanism that permits the positive control of mass flow through the storage module.

1.2.9 Potential Production Cost

Production cost of receiver modules is the final driving factor in any Air Brayton Solar Power System. The primary reason for selection of the honeycomb matrix receiver storage module is that potential production costs of this type of receiver configuration are lower than other alternatives. In addition, the matrix heat exchanger can be fabricated in large production quantities at a very low cost. The same production techniques can be applied to the buffer storage unit. This approach is superior to the high labor-intensive process of making either tubed receivers or heat pipe receivers.

The parametric study on Air Brayton Solar Receivers, indicated that the Pressurized Matrix receiver is the best candidate for meeting the performance and cost goals of Point Focusing Solar Thermal Power Conversion Systems.

SECTION 2

INTRODUCTION

This report discusses the results of the Phase I study on point focusing Air Brayton Solar receivers. The two phases of the program are:

Phase I: The development of a conceptual design for an Air Brayton Solar Receiver.

Phase II: Development and testing of an Air Brayton solar Receiver.

The objectives of Phase I were to perform a parametric study of receiver concepts and, based on the outcome of these studies, to present a conceptual design of a selected receiver. Phase II will involve a final design, prototype development and testing of the receiver prior to shipment to JPL. Subsequently, JPL will integrate the receiver with the concentrator and power conversion module. System tests will then be performed by JPL during 1980.

The following design goals were established during Phase I:

- Peak thermal input power: 85 KWt
- Receiver outlet air temperature: 1500^{o}F
- Receiver inlet air temperature: 1050^{o}F
- Design mass flow rate: 0.533 lb/sec
- Design receiver inlet pressure: 36.75 psia

Table 2-1 summarizes the statement of work for the Phase I contract. Task 1 involved a parametric study of various receiver configurations and operating conditions. During Task 2 a conceptual design was performed on the selected receiver design, based on the operating conditions provided by JPL. The interface requirements between the receiver/concentrator/power conversion module were addressed. Finally, production cost estimates were obtained to determine the cost of the ABSR during the 1980's. In addition, a proposal was prepared for Phase II of the contract to design, build and test a pressurized honeycomb matrix heat exchanger.

TABLE 2-1. STATEMENT OF WORK FOR CONCEPTUAL DESIGN OF OPEN CYCLE AIR BRAYTON SOLAR RECEIVER

Task	Activity
1	Perform parametric analyses of candidate designs
2	Provide conceptual design of the preferred receiver
3	Identify interface requirements • ABSR and power conversion unit (PCU) • ABSR/PCU mounting to concentrator • Control sequence and/or response capability to transients
4	Production cost estimates
5	Phase II proposal
6	Documentation and briefings

SECTION 3
DESIGN CONCEPT

3.1 SYSTEM CONCEPT

Figure 3-1 shows an artist's concept of the point focusing system. A two-axis, 36 ft diameter, tracking paraboloidal concentrator collects incident radiation and delivers 85 KWt to the receiver. The receiver aperture is located 21 ft from the concentrator surface; the receiver/power conversion module is held at the focus by four struts which are attached to a support ring on the concentrator. The receiver is supported independently of the power conversion module through a set of struts extending to a common attachment ring located at the receiver/power conversion module center of gravity.

A constant RPM mode of operation is used in the current design because it represents the simple and more conventional method of engine control where a synchronous or induction ac generator is geared to the output shaft. A reduction of solar flux affects engine performance by reducing power output. When the solar flux is insufficient to maintain adequate engine RPM, the generator drives the turbine.

The point focusing system operates utilizing the conventional, recuperated Brayton cycle illustrated in Figure 3-2. The power conversion unit is a high efficiency Brayton engine with a pressure ratio of

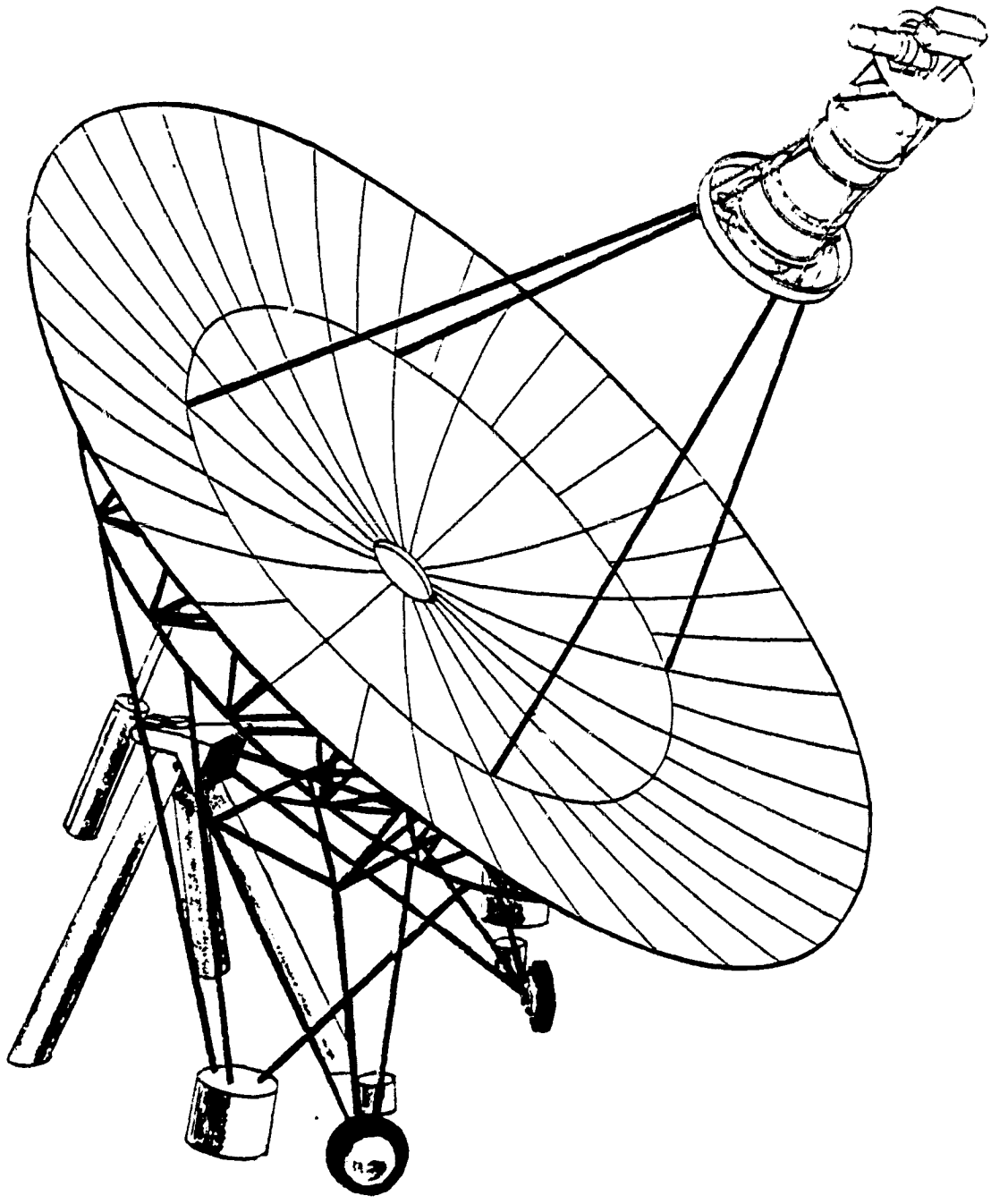

WICBO-008

Figure 3-1. The point focusing system artist's concept shows the receiver/power conversion module located at the concentrator focus.

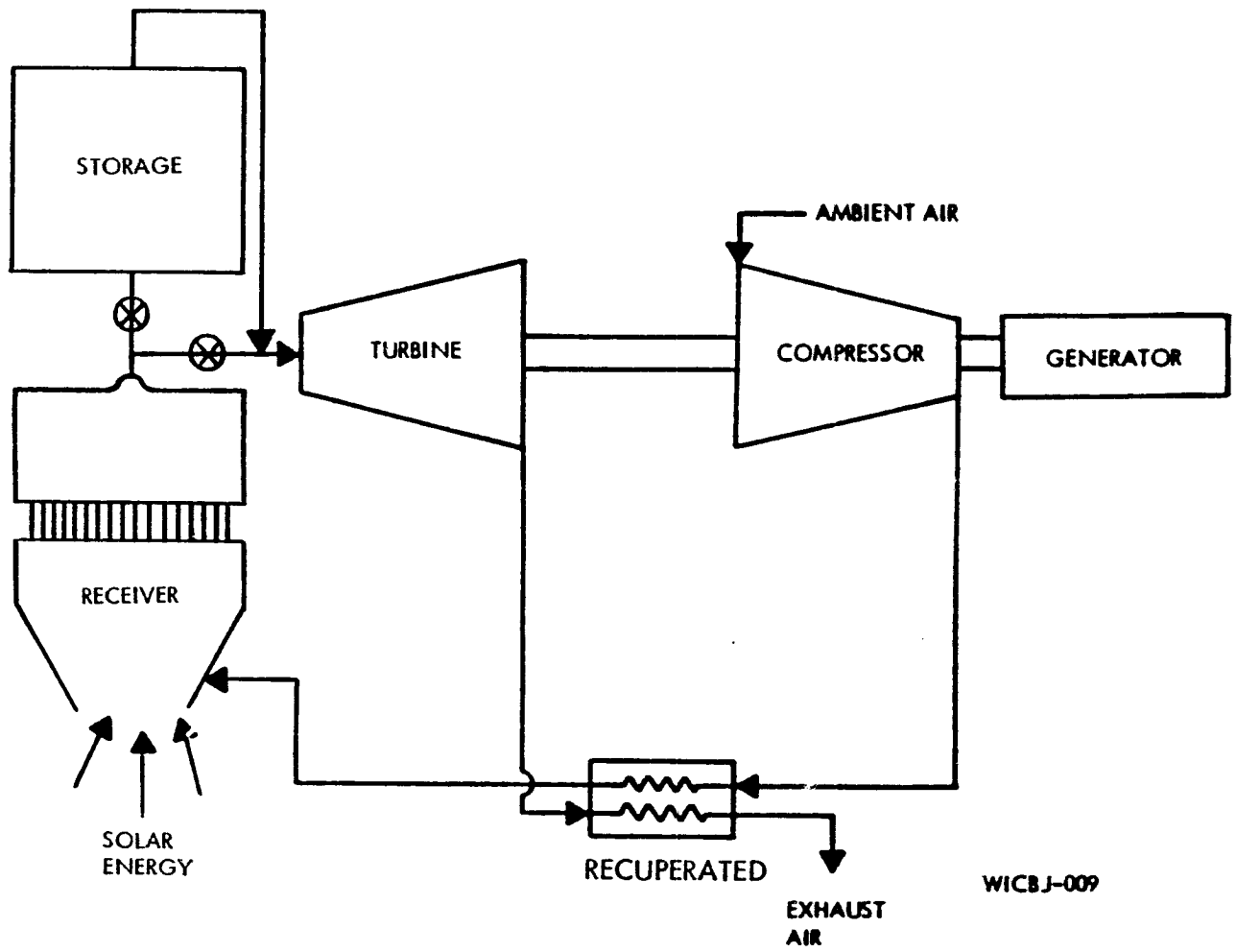

WICBO-007

Figure 3-2. The point focusing system utilizes a conventional, recuperated Brayton cycle.

2:5. The system is designed to operate at 35.8 psia pressure with receiver inlet and outlet temperatures at 1050°F and 1500°F, respectively.

Starting at the upper right, ambient air is drawn into the turbine-driven compressor. After compression, the air is routed to the recuperator where it is heated to 1050°F by the turbine exhaust gases. The heated air is then ducted to the receiver where additional energy is added to raise it to the turbine inlet temperature. A sensible heat storage module is integrated with the receiver as a buffer to isolate the turbine from short-term thermal transients caused by passing clouds. Based on component efficiencies and predicted cycle conditions, the overall system efficiency is estimated at 21%, resulting in an electric power output of 17 kW.

3.2 CYCLE DESCRIPTION

Figure 3-3 shows the Air Brayton Solar Receiver integrated with the power conversion module. The receiver aperture is 7.34 inches in diameter and is located at the focal plane of the concentrator. Focused energy is incident on the aperture; incoming rays diverge as they enter the receiver and uniformly illuminate the 22 inch diameter ceramic matrix heat exchanger. The solar energy is absorbed by the ceramic matrix; this energy is then transferred to the air stream as heat. At the design point, the receiver outlet air temperature is 1500°F. At a design mass flow of 0.53 lb/sec, this represents a power transfer of 66 kW. The receiver/storage module housing is surrounded with 4 inches of Johns-Manville ceraform insulation, limiting conduction losses to 3.7% of input power.

AIR BRAYTON SOLAR RECEIVER

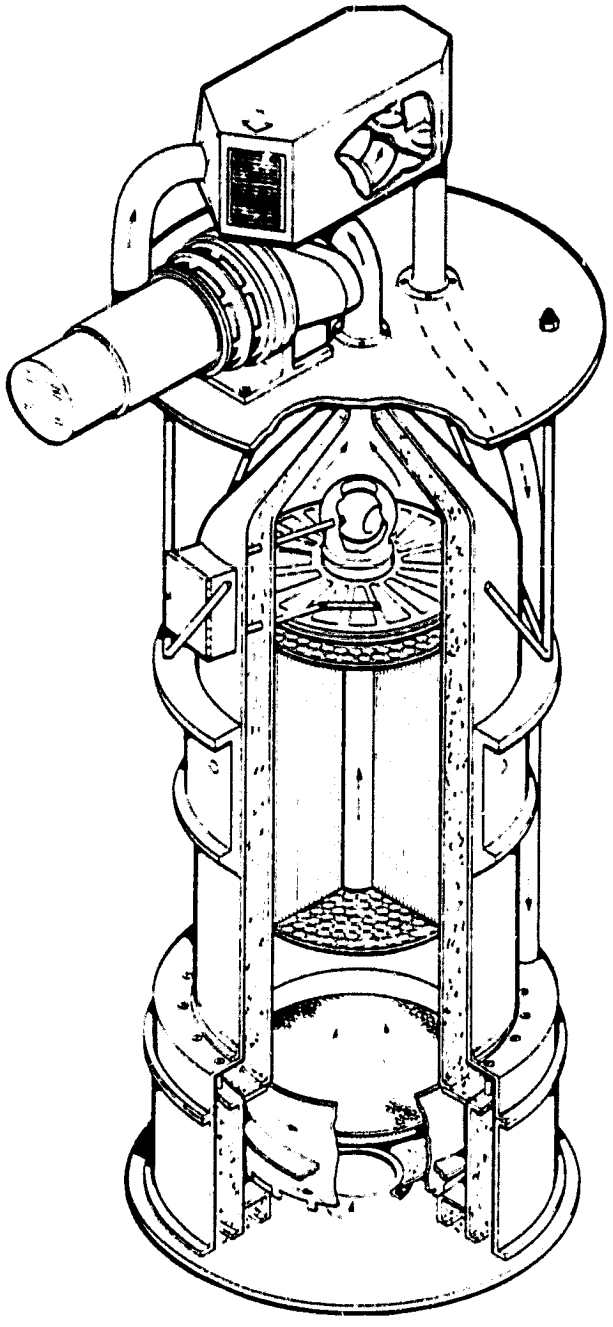

RECEIVER INLET SCROLL

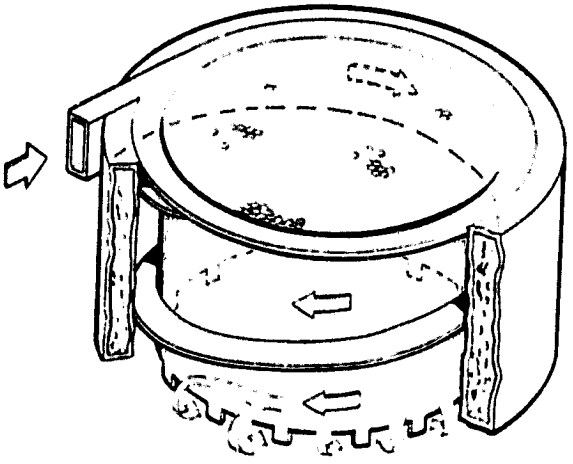

Figure 3-3. The Air Brayton Solar Receiver is integrated with the power conversion module. The inlet scroll is a critical design element.

The entire receiver cavity aperture is sealed with a quartz window to allow the receiver to be pressurized. Preheated air enters the receiver and is directed into a scroll of rectangular cross section, which is wrapped around the receiver housing. Previous receiver tests have shown that this inlet ducting design is critical to the stable operation and efficiency of the receiver. Initially, the air expands as it makes a complete revolution around the housing. This expansion recovers some of the pressure drop and serves to buffer entrance flow nonuniformities. During the second revolution, the air is forced into the receiver cavity through screened ports at the base of the receiver. After entering the receiver cavity, the air travels through a conicial set of screens before passing through the honeycomb matrix heat exchanger. These screens provide the pressure drop necessary to assure a uniform flow distribution through the matrix.

The heated air can be ducted either directly to the turbine inlet nozzle or through the storage medium to the turbine. Path selection will depend on the prevailing conditions during system operation. For example, if the storage is empty, then all the heated air is forced through the storage honeycomb until the storage is fully charged. If storage is fully charged, a residual air flow through the storage section replaces energy loss through wall conduction.

Two coupled valves, located at the top of the receiver/storage module, provide positive control of the flow path of the receiver outlet air. A ball valve at the top of the center duct controls the receiver outlet air routed to the turbine. The second valve, two

concentric flat plates with cut-outs like blades, controls the flow through the storage medium. The coupled operation of these two valves maintains a positive flow control during any mode of operation.

3.3 SYSTEM OPERATION

Based on the insolation data provided by JPL (Figure 3-4), we estimate that the turbine operation will start, under off design conditions, when the isolation level reached 0.6 kW/m^2. Before starting, the storage will be filled using the starter-driven compressor to circulate air through storage. In 45 minutes of operation, the storage medium will be fully charged at 1500^oF. Starting at 7 a.m., the system will then operate under off-design conditions. At 9:30 a.m., the insolation is sufficient to provide design output power. The system will operate at on-design conditions until about 2:30 p.m. During this time, if storage is required, it will be refilled as soon as full flux is available before resuming on-design operation. From 2:30 to 5:00 p.m., the unit will operate under off-design conditions. Finally, the storage tank will be used to shut down the system at 5:15 p.m.

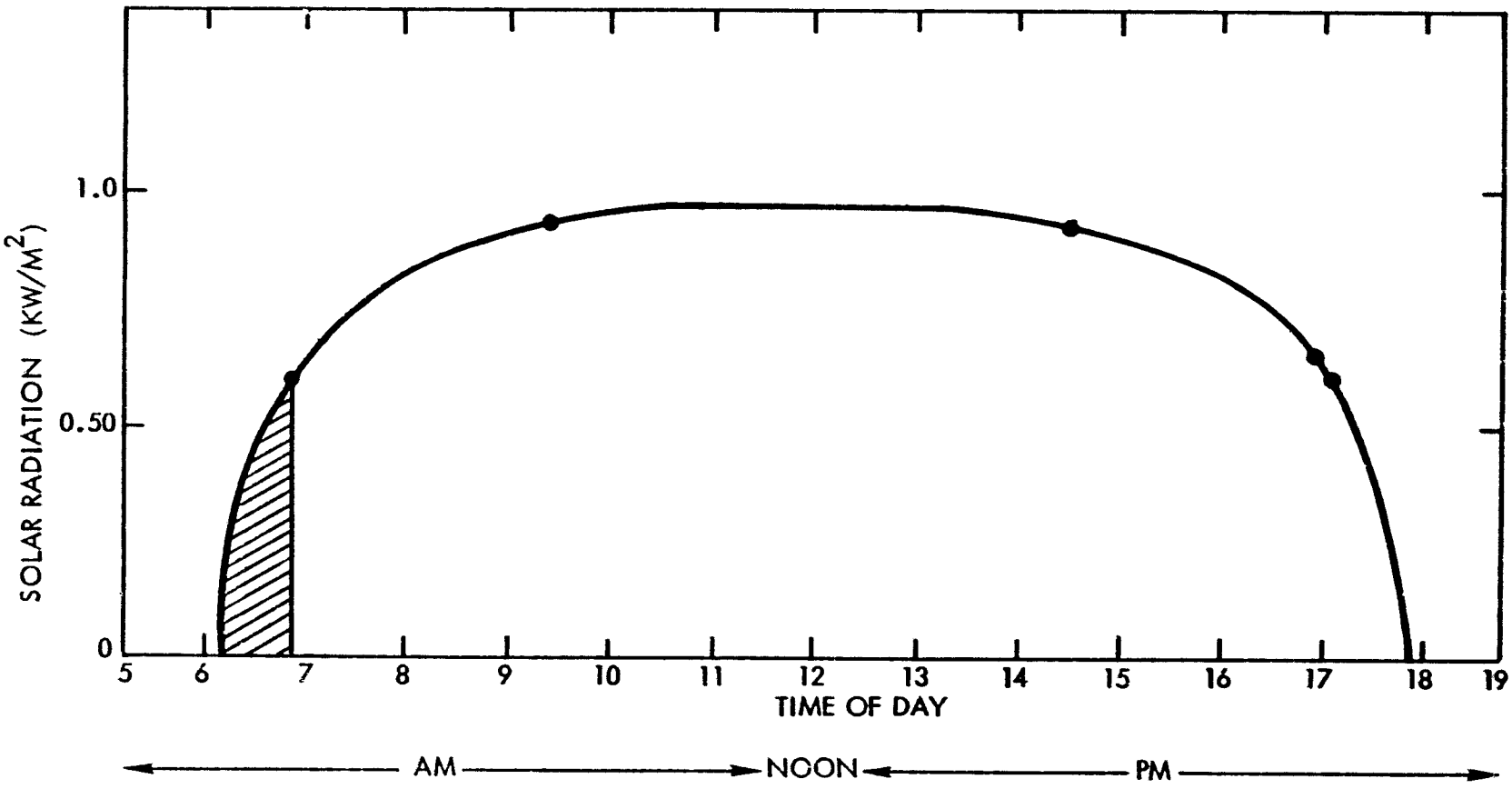

Figure 3-4. The Air Brayton Solar Receiver will be operational from 7:00 a.m. to 5:00 p.m. during an average sunny spring day.

SECTION 4

PARAMETRIC ANALYSES

A parametric analyses was conducted to study the merits of various receiver designs compatible with a point focusing system. The analysis covered the range of variables given by JPL as shown in Table 4-1. The results were used to select the best candidate for further detailed design.

As part of the parametric studies a detailed finite element analysis was done to characterize the thermal transfer problem. By solving the set of simultaneous equations, receiver efficiency, thermal profiles, and pressure drops were obtained with relative ease. All temperature dependent properties of the materials were taken into consideration, without compromising or relying on unnecessary assumptions. As a result of this analysis, a set of parametric curves were obtained that showed the relationships of the dependent and independent variables.

4.1 TYPES OF RECEIVERS ANALYZED

Two types of receivers were investigated (Figure 4-1); a honeycomb matrix receiver and tubed receiver. In the honeycomb receiver, solar energy is captured by a ceramic matrix located behind the focal plane. Preheated air circulates in the receiver cavity and is heated as it passes through the matrix. Two types of receiver operation were analyzed with the honeycomb design. The first involved

TABLE 4-1. SUPPLIED VARIABLES

Independent Variables:

Peak thermal power in (KWt)	50, 90, 150
Fluid outlet Temperature (^{o}F)	1000, 1300, 1500, 1600
Fluid Inlet Temperature (^{o}F)	1800, 1000, 1100, 1200
Fluid Inlet Pressure (Psig)	30, 45, 60, 75

Dependent Variables:

Receiver efficiency %

Pressure Drop Δp (psi)

Maximum cavity temperature (^{o}F)

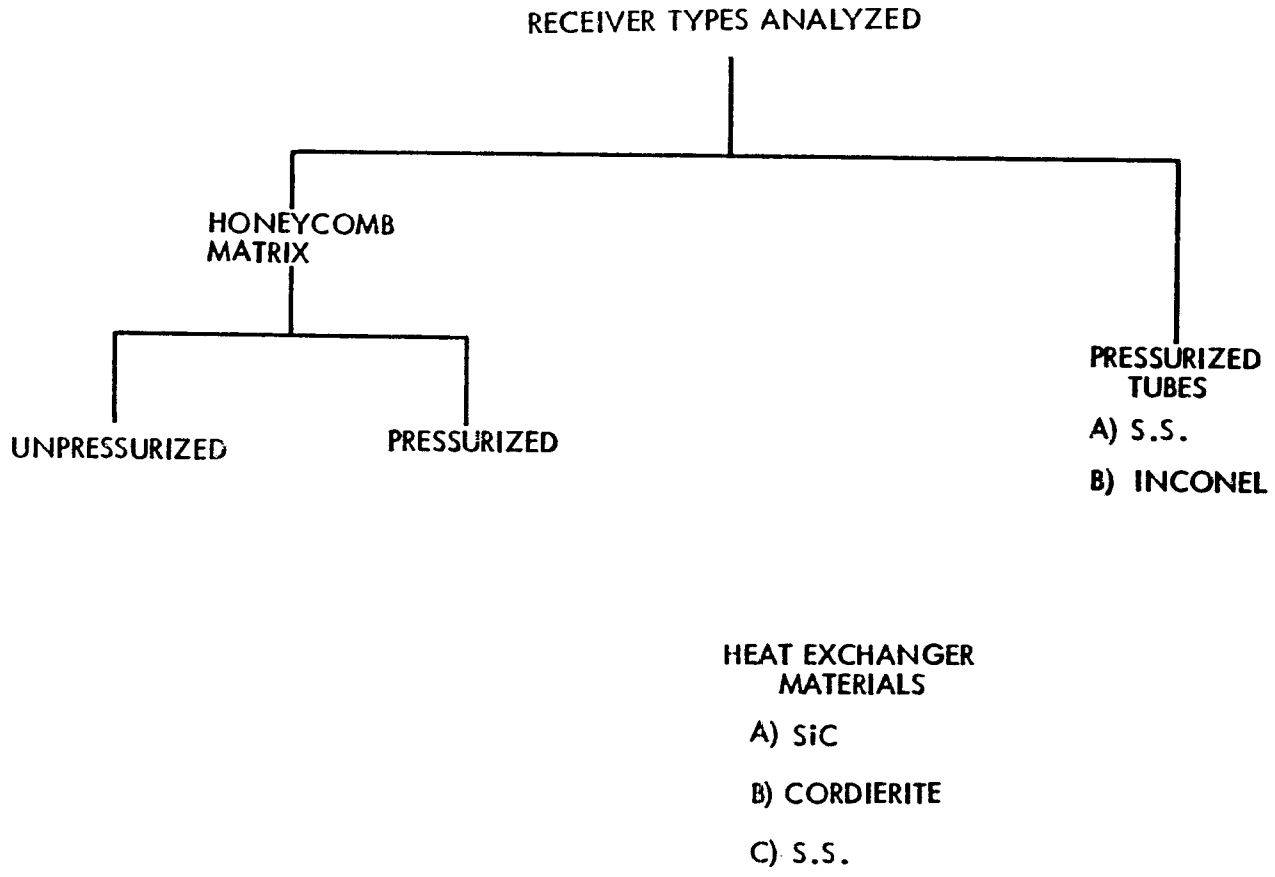

09018-10

Figure 4-1. Two types of receivers were analyzed; the honeycomb design was chosen for the ABSR application.

an unpressurized matrix receiver based on Sanders' own split cycle concept. The key feature of this concept is the ability to separate the solar collection cycle from the turbine cycle by using highly efficient sensible heat storage. This allows the user to schedule power output to meet demand without direct dependence upon instantaneous insolation. A high degree of flexibility in plant operation is obtained by allowing different rates of thermal energy collection and consumption.

Heated air leaving the receiver cavity through the outlet interconnect piping is routed to the top of the storage unit, is cooled as it passes through the storage causing a 1500^{0}F thermocline to propagate slowly through the stove and then returns to the solar receiver. When air leaving the bottom of the charging storage unit approaches 1500^{0}F, the unit is fully charged and is switched out of the energy collection subsystem loop.

The unpresssurized matrix receiver concept differs from competitive configuration in that it does not use the standard high pressure tube-boiler techniques, but captures and transfers heat at near-atmospheric pressures, using a material and configuration that is a highly efficient absorber of solar radiation. This matrix heat exchanger operates with very low pressure drop (less than 0.3 inch H_2O), thus reducing the air sealing requirements and permitting the components of the heat exchanger to be assembled loosely to allow for thermally-induced motions. Since the entire receiver operates at near

atmospheric pressure, safety hazards and the cost and weight of the pressure vessel are minimized.

The second matrix receiver is pressurized and has a quartz window installed at the aperture. It provides the pressure seal necessary for the receiver to operate based on the conventional open cycle recuperated Brayton engine. In operation, the receiver is mounted so that the window is located at the focal plane. Energy from the collector passes through the window and impinges on the ceramic matrix.

The flow distribution in the two types of receivers, using a honeycomb heat exchanger is the same. Therefore, the thermal and flow analysis for both types were carried as a parallel effort. The effect of the window and the corrected air properties were taken into account for the pressurized matrix receiver.

The matrix receiver has several important features. The window provides a pressure seal in a relatively cool region. All structural components are insulated from the high temperature gases allowing the use of conventional alloys and of thinner structural components. The honeycomb ceramic matrix has a low pressure drop, less than 0.3 inches H_2O, at design flow rates. This means that tight seals are not required at the heat exchanger and that the matrix components can be compliantly mounted to prevent buildup of thermal stresses.

Because of the clear separation of the structural and heat exchanger functions, each are independently optimized. Since there

are no large pressure drops across it, the heat exchanger matrix only requires the strength to support itself and can be selected for its optical absorptivity and heat transfer properties. Structural members, with the exception of the aperture window, need not have high heat transfer capability or special optical properties.

The parametric analysis of the honeycomb receivers was done for both the unpressurized and pressurized units. To conform to JPL's requirements, the receiver selected for the conceptual design study was the pressurized honeycomb receiver.

In addition to the honeycomb receivers, tubed receivers were also considered during the parametric study. In this receiver concept compressed air circulates through tubes lining the receiver cavity as shown in Figure 4-2. Solar radiation entering the cavity heats these tubes which then transfer the energy to the compressed air. There are spaces between adjacent tubes and an insulated reflecting surface is located behind each row of tubes. This configuration minimizes the circumferential temperature variation, and the radial thermal stresses in the tube walls. The turbine exhaust heat is recovered in a recuperator and waste heat is exhausted to the atmosphere.

4.2 RECEIVER MATERIALS

Two types of heat exchanger materials were investigated: (a) metallic and (b) ceramic. The maximum temperature limit of 1600^{o}F outlet air temperatures allows the use of metallic heat exchangers

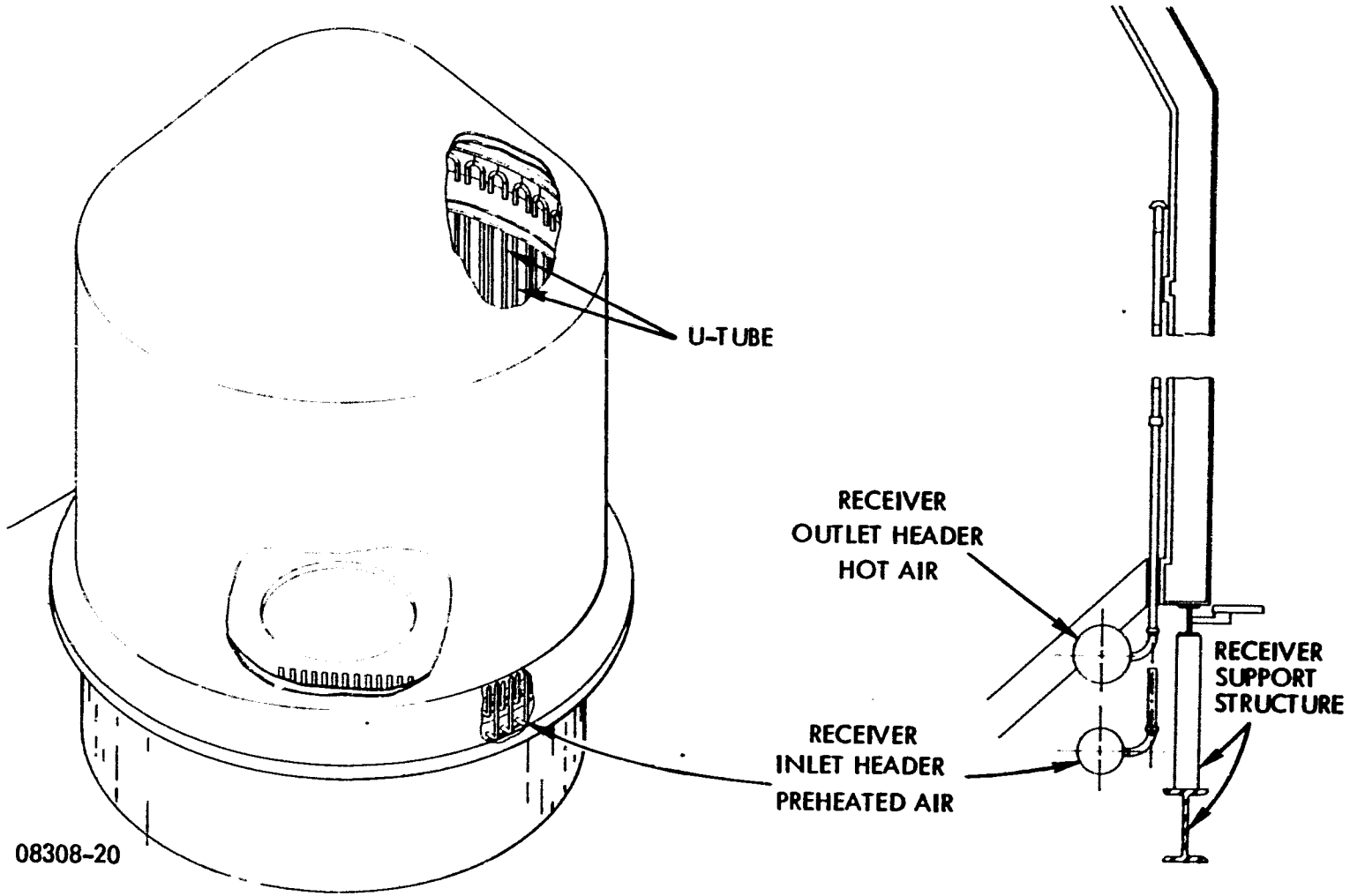

Figure 4-2. In the tube type receiver, compressed air circulates through tubes lining the cavity.

in the form of high nickel alloys. Ceramic heat exchangers, with their high temperature characteristics and low cost in high volume production, offer the best solution for the receiver heat exchanger.

Silicon carbide (SiC) honeycomb material was investigated for use as the matrix heat exchanger because of its good conductivity, high absorptivity, and its high temperature capability. An extensive effort was undertaken to investigate alternative ceramic materials such as alumina, Cordierite and Mullite. Although these materials have low absorptivity and, in some cases, low conductivity, they offer cost advantages for the ABSR receiver.

Insulation is an integral part of the receiver design. Johns-Manville ceraform insulation has been chosen as the candidate material because of its excellent insulation properties and low weight. The insulation, lining the interior of the receiver, minimizes conductive losses through the walls.

High temperature alloys, such as type 316 stainless steel and inconel 617, were considered for all receiver interior components. The max temperature that the alloys will experience, at the design point is 1700^{o}F. This temperature is well below the maximum operating range of 1900 - 2000^{o}F for these alloys. The exterior shell temperature was calculated to be 150 - 200^{o}F with four inches of Johns-Manville insulation; therefore, a low carbon steel pressure shell is used. Because of the low shell temperatures, a lightweight receiver can be designed within the ASME pressure vessel codes.

The properties of the heat exchanger materials, SiC, cordierite and stainless steel (SS), that were investigated during the parametric study are shown in Appendix A. The ceramics have high temperature capabilities, high conductivities, and a low coefficient of thermal expansion. These properties contribute to good heat transfer and to the life and reliability of the heat exchanger. In addition 316 stainless steel was considered since temperature levels under consideration did not exceed the limiting levels of 1900 - 2000^{o}F.

Figure 4-3 shows the flux distribution along a honeycomb tube for each of the three materials considered. With its high absorptivity and conductivity, SiC captures the largest fraction of energy at the front face of the honeycomb. In SS or cordierite the incoming flux penetrates the matrix to a greater depth before it is absorbed. As an example, all the incident energy was absorbed in 0.5 inch of SiC while 2.5 to 3 inch of cordierite was necesary to obtain the same effect. The low absorptivity of cordierite allows the energy to travel farther down the honeycomb tubes before it is firally captured. The SS exhibited characteristics in between the ceramics and required 1-1.5" of honeycomb tube length for energy capture.

4.3 SCALING

The aperture sizes for 50 KWt and 150 KWt receivers were scaled from the 90 kW baseline design. Factors that were used for scaling are shown below.

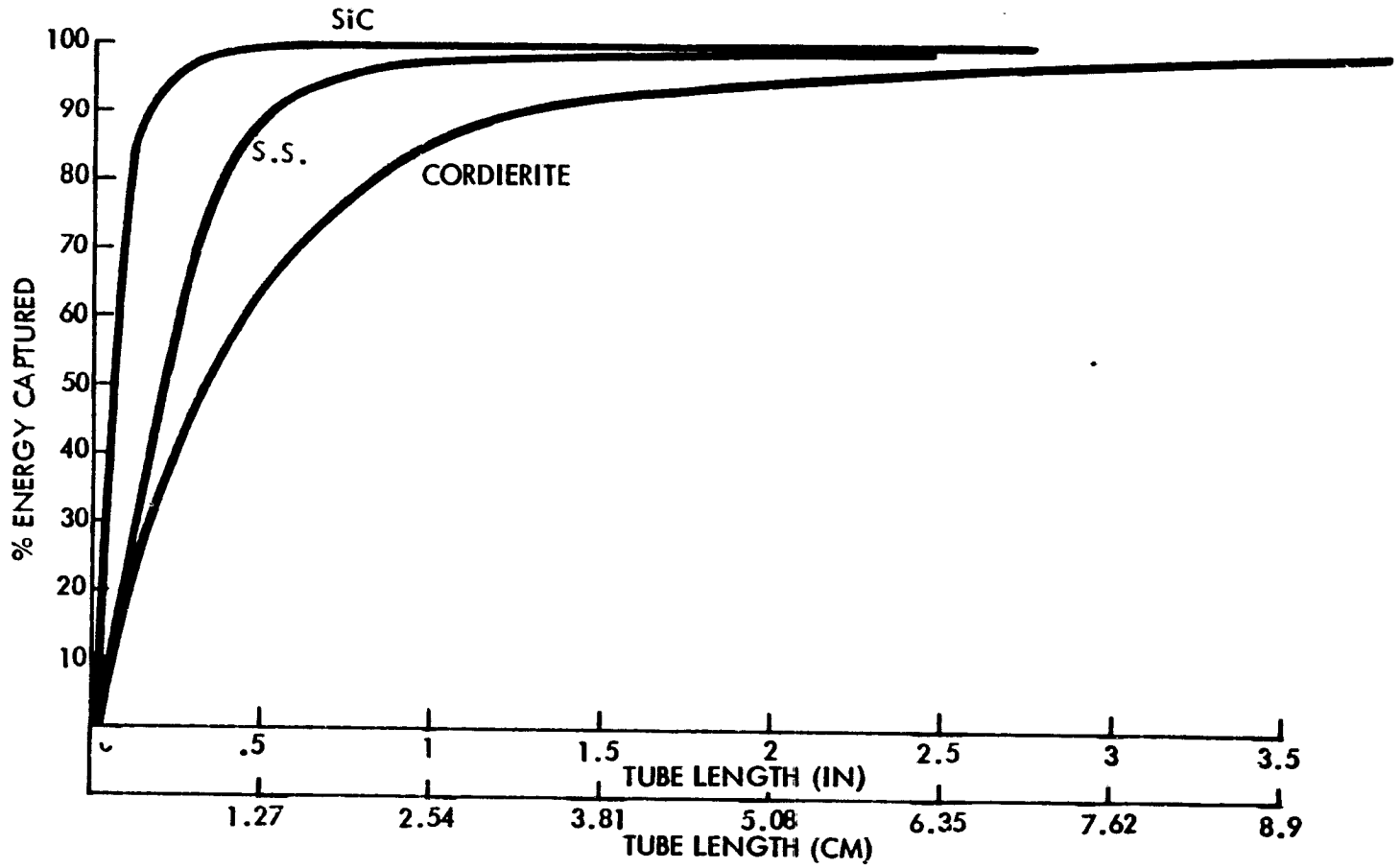

Figure 4-3. Energy capture along the honeycomb was compared for the three candidate materials.

Projected receiver efficiency	=	85%
Mirror reflectivity	=	86%
Solar constant	=	0.967 kW/m^2
Transmission of energy if window is used	=	92%
Receiver shadowing and ray misses	=	5%

The flux distribution for a 12m parabolic concentrator was given by JPL. The maximum energy available from this concentrator was calculated to be 90 KWt at the receiver aperture.

To determine the optimum aperture sizes for the different power levels, the flux data from the 12m concentrator was integrated, and the total energy into the cavity was calculated.

Input radiation into the receiver increases sharply with aperture diameter, but eventually levels out when all the available energy from the concentrator enters the cavity. This occurs when the sun spot, sun half angle and tracking errors are considered and a limiting aperture size is defined in terms of incident radiation. Any increase in aperture diameter beyond that, would permit negligible energy capture by the receiver heat exchanger. Therefore, the fractional energy capture is a function of concentrator and aperture diameters.

Reradiation is a function of aperture size and cavity temperature. For a very small aperture, reradiation is negligible. On the other hand, if aperture size increases disproportionately it would theoretically reradiate all of the captured energy. This suggests that there is an optimum aperture size, where input energy is maximized while reradiation is minimized. This is defined as collection efficiency and is shown by relating reradiation with energy capture in the following way:

$$\eta = 1 - \frac{\text{Reradiation}}{\text{Energy into receiver}}$$

In Figure 4-4, the fractional energy capture and reradiated are nondimensionalized with available energy from the concentrator. They are plotted against a normalized aperture with concentrator diameter. Finally, the collection efficiency curve is plotted to show the relative sensitivity of fractional captured and reradiated energy with aperture size.

The optimum aperture size is selected at the peak of the collection efficiency curve. By selecting a concentrator size, the aperture diameter can be simply calculated.

Table 4-2 was constructed based on Figure 4-4 and the receiver input power levels that were furnished by JPL. The scaling assumptions were used to determine the concentrator size for each power level. The aperture size was selected at the maximum collection efficiency. Finally, assuming an F/D of 0.6, the focal length of each concentrator was calculated.

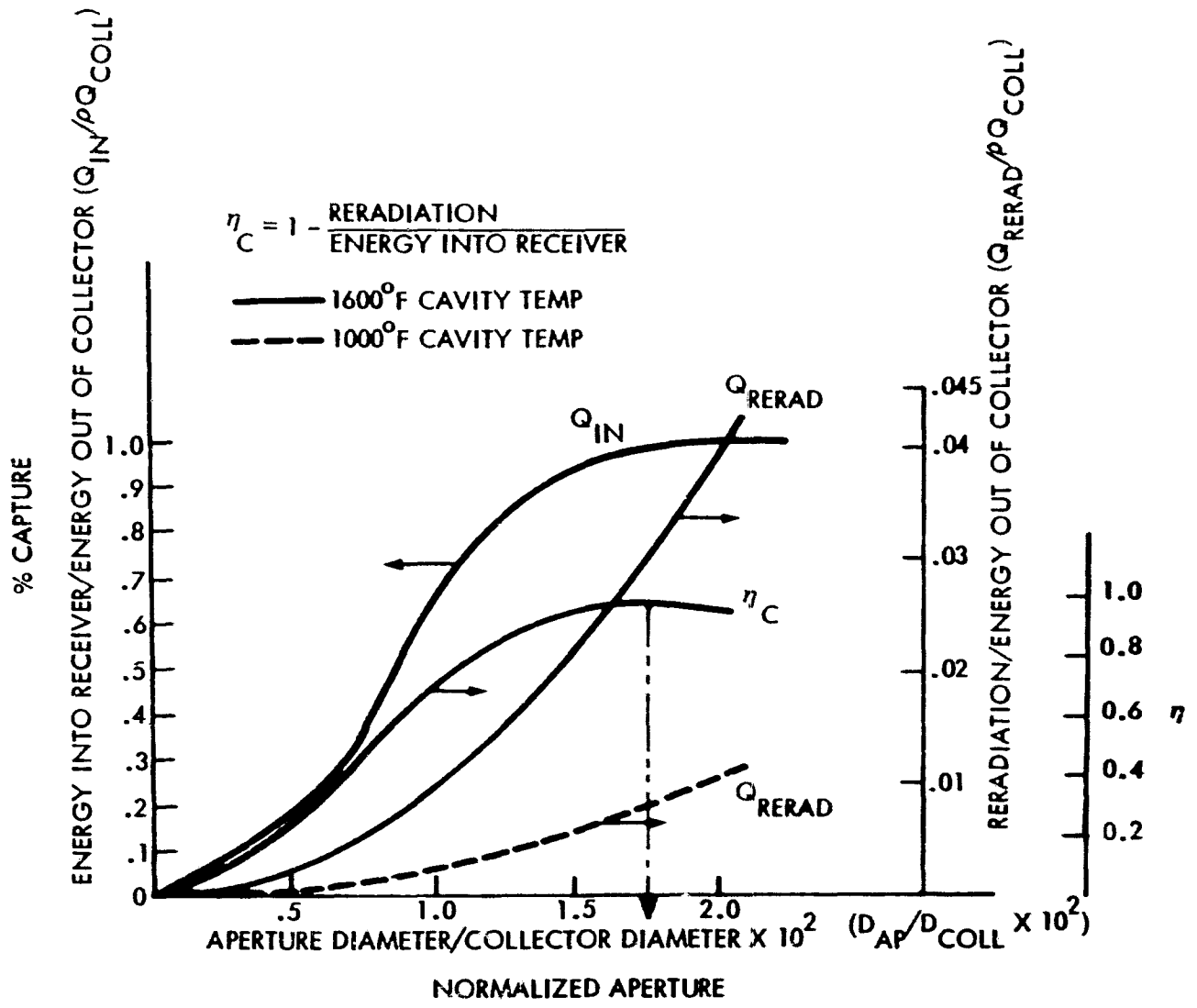

Figure 4-4. Energy capture efficiency (η_c) was calculated.

4.4 FLUX DISTRIBUTION

The receiver heat exchanger design was investigated to maximize the efficiency by capturing most of the flux directly on the heat exchanger. Figure 4-5 shows the orientation of both the honeycomb disk and tube heat exchangers.

The rays originating from the concentrator cross at the aperture and illuminate an area of the honeycomb disk. The image size of this area depends on the sun spot, sun half angle and tracking errors.

The honeycomb disk is located at the optimum distance behind the focal plane for efficient energy transfer into the air stream. Figure 4-6 shows the results of a parametric study of flux distribution on the honeycomb disk at various distances behind the focal plane. For all distance behind the focal plane the flux decreases toward the periphery. This effect is minimized when the disk is located far behind the aperture plane where the direct flux is minimum and most of the energy hits the matrix by diffuse radiation from the surrounding walls. At the other extreme, when the disk is located close to the focal plane, most of the direct flux is captured directly but with increased flux nonhomegeneity across the disk. The amount of reradiation from the cavity and hence receiver efficiency is dependent on the disk location. A matrix that is located close to the aperture reradiates more energy than a matrix located further back.

In the tube receiver, the best arrangement of the heat exchanger is along the cylindrical surface of the receiver. The tubes are exposed to incident flux and the manifolds are located at the base of

TABLE 4-2

SCALING OF COLLECTOR DIAMETER
AND APERTURE DIAMETER FOR VARIOUS
POWER LEVELS

Receiver input power	(KWt)	50	90	150
Collector diameter	(M)	8.75	11.73	15.15
Aperture diameter	(M)	.153	.205	.265
	(1N)	6.02	8.08	10.43
Focal length	(M)	5.25	7.04	9.1

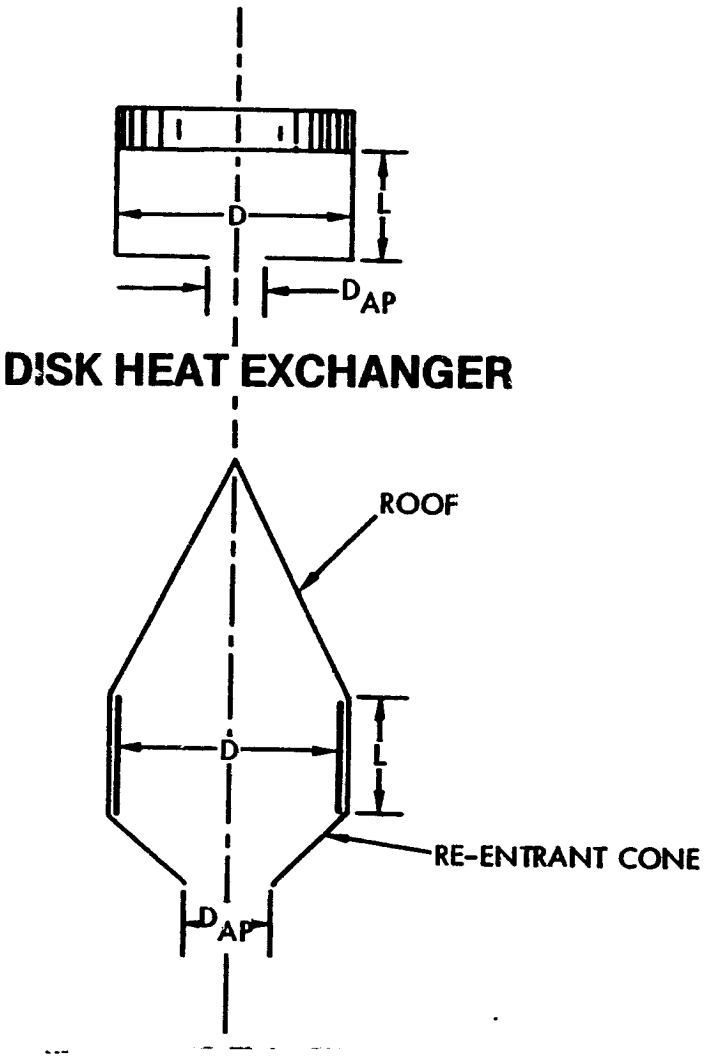

Figure 4-5. Both cylindrical and disk heat exchanger designs were evaluated.

APERTURE DIAMETER = 20.32 CM (8")
FOCAL LENGTH TO APERTURE = 7.2M
(23.62 FT)

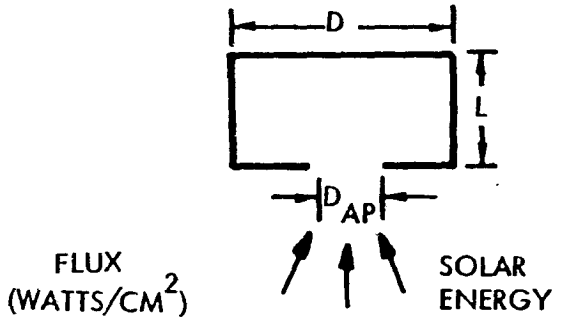

CURVE	L (CM)	L (IN)	% ENERGY DIRECTLY CAPTURED BY DISK
A	19.05	7.5	100
B	22.86	9	97.6
C	25.40	10	92.2
D	27.94	11	86.3
E	38.1	15	47.7

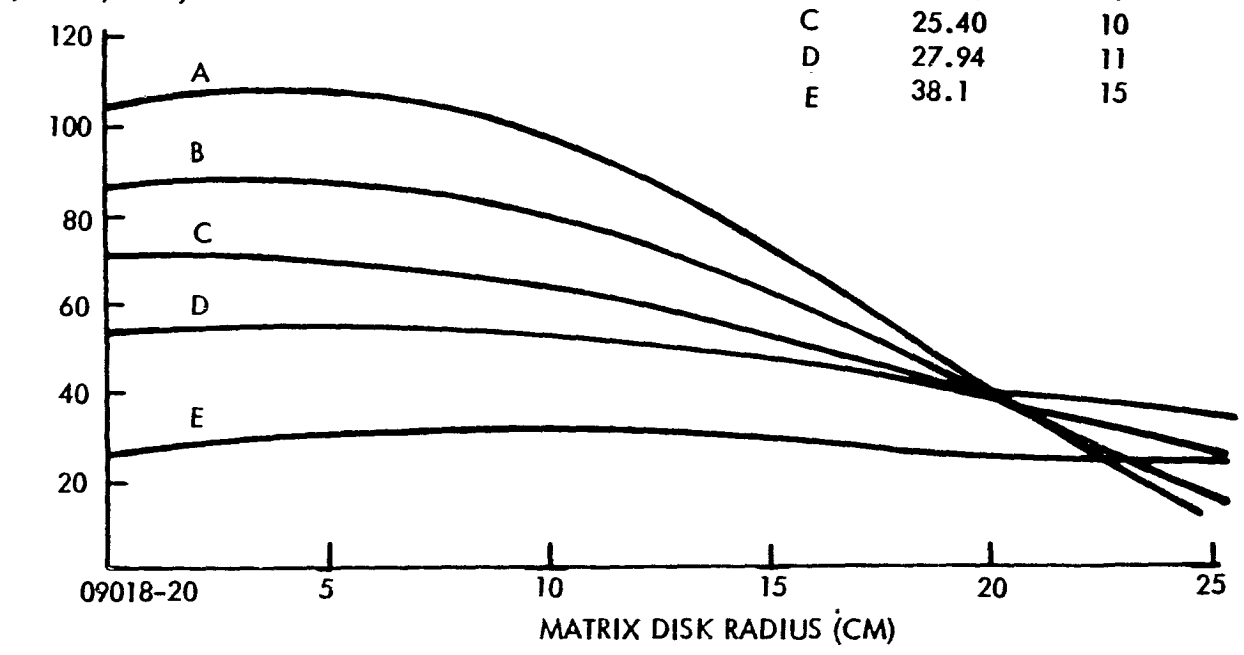

Figure 4-6. Flux distribution on the honeycomb disk was analyzed at various distances behind the focal plane.

the receiver, in a cool region, to protect the weld regions. In the best design of cylindrical tube heat exchanger, 50% of the direct rays entering the cavity do not hit the heat exchanger, but land on the roof of the receiver. Using a white surface for the roof, diffuse radiation is redirected back to the cylindrical section. A flat roofed receiver would increase chances of reradiation while a highly pitched roof is not very effective in reflecting back the energy. The analysis indicated that a roof and a reentrant cone of about 25^{o} to 30^{o} in half angle is optimum for redirecting the energy back on the heat exchanger.

The flux distribution along the cylindrical walls of the receiver is graphically presented in Figure 4-7. Based on 90 KWt receiver input power and the selected aperture size and receiver diameter, most of the direct flux is concentrated about the mid point of the receiver cylinder. With diffuse reflection and radiation from the reentrant cone and the roof, the flux becomes more uniform. The tube diameter, number and spacing is very critical in terms of obtaining uniform flux. The tubes must satisfy the heat transfer and pressure drop requirements, but, unlike honeycomb receivers, the circumferential temperature gradient around the tubes can cause failure and system shutdown. The spacing between tubes determines the amount of diffuse radiation from the receiver walls. Large spaces between tubes results in a large receiver diameter and hence greater obstruction losses. Whereas, with closely spaced tubes, circumferential temperature gradients can cause tube failures.

4.5 THERMAL PERFORMANCE

A finite element computer program was used to solve the heat balance equations that represent a receiver exposed to the given

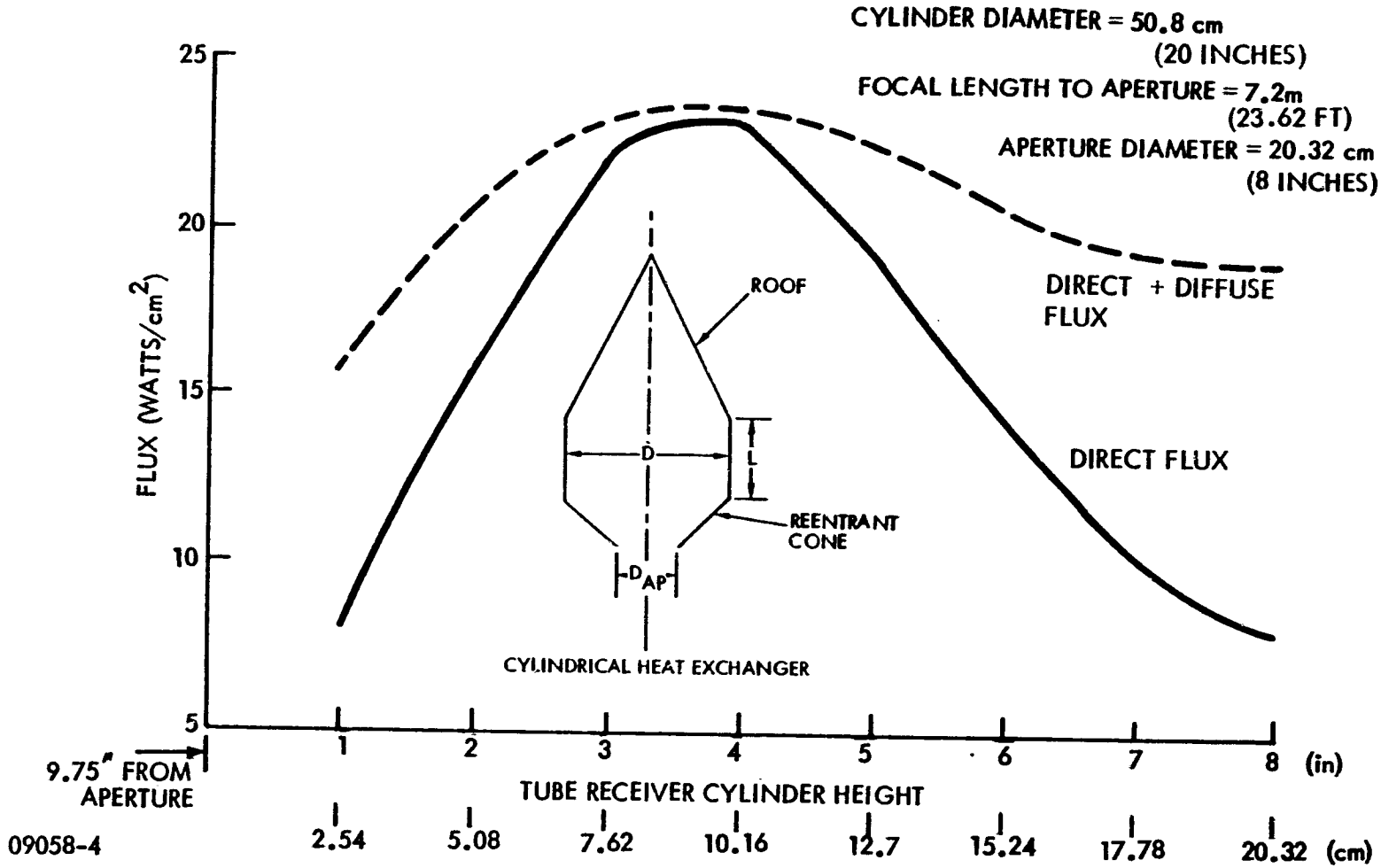

Figure 4-7. As shown in this graph of flux distribution along the cylindrical walls, most of the direct flux is concentrated about the mid-point of the receiver cylinder.

insolation conditions. This modeling technique accounted for a wide variety of conditions, including nonlinearities due to temperature dependent material properties. The resulting simulation provided insight into receiver characteristics such as energy collection efficiency, temperature profiles, airflow pressure drops, transient responses to fluctuations in insolation or airflows, etc.

The present model accounted for the heat transfer processes; i.e., conduction, convection, radiation, fluid flow and heat transport with appropriate weighting to represent the average tube within a honeycomb or tube heat exchanger. Insolation inputs were handled as heat sources located at several points along the tube axis. The intensity of each source is proportional to computed flux distribution.

In these studies, the airflows were selected to meet the outlet temperature requirements. Among parameters accounted for in the simulations are.

- Insolation
- Receiver aperture area
- Active honeycomb area
- Length of honeycomb tubes
- Diameter and wall thickness of these tubes
- Wall insulation
- Conductivity, density and heat capacities as function of temperature

In addition, the values of viscosity versus temperature for air as well as the smooth pipe relationship for the friction factor versus Reynolds number were specified. The relationship between Reynolds, Prandtl and Nusselt numbers was also evaluated in each segment of the model as appropriate to its temperature and flow conditions.

The prime results of the parametric study included

- Efficiency estimate
- Pressure drops
- Fluid outlet temperatures
- Maximum cavity temperatures
- Axial temperature profiles

After obtaining the steady state solutions, transient analyses were conducted to establish turn-on and turn-off procedures. In addition, the effects of concentrator shading due to cloud cover were investigated to determine adjustments to maintain rated receiver output temperatures.

Receivers were analyzed that would accept 50, 90 and 150 KWt of input power. Both unpressurized and pressurized matrix receivers were analyzed. Figure 4-8 shows the relationship between receiver inlet and outlet temperature and mass flow rates. In addition the effects of different power levels are related to system mass flow. For a given power level there is an inverse relationship between receiver mass flow and outlet temperature. This is due to the

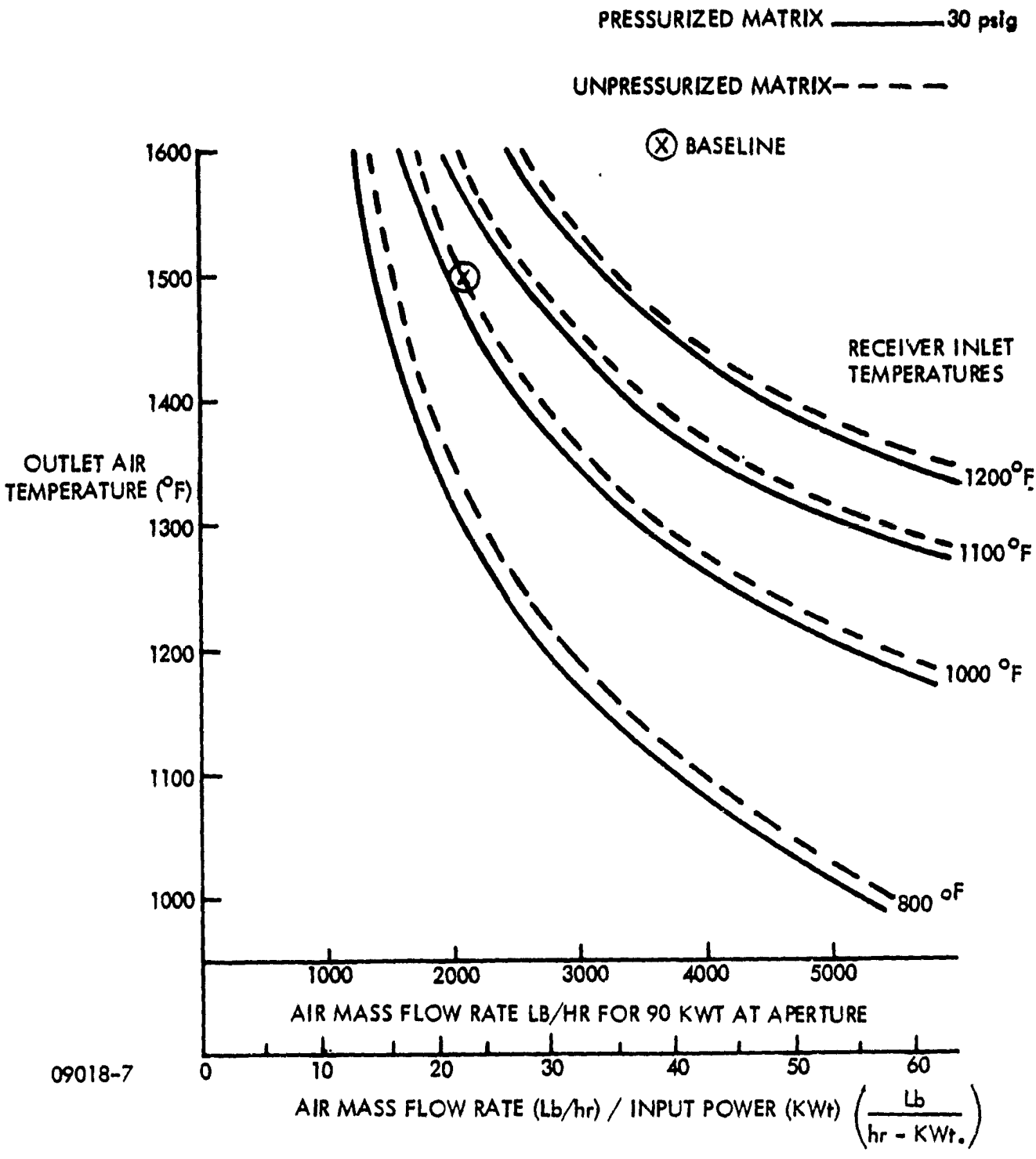

Figure 4-8. Both pressurized and unpressurized receiver design were analyzed to show the relationship between inlet and outlet temperatures and mass flow rates.

cooldown of the heat exchanger with increased mass flow. Therefore, for a constant temperature operation, the mass flow is a very effective way to control receiver output temperatures. Similarly, in order to maintain a fixed ΔT between receiver inlet and outlet temperatures, constant mass flow rates, and insolation must be maintained.

The effect of receiver pressurization was to decrease the outlet air temperature for a given mass flow. This effect is caused by an increase in friction pressure drop and the resulting change in air density which occurs when a pressurized receiver is compared with an unpressurized one.

The unpressurized receiver losses are reradiation, conduction, and convection, while the pressurized matrix has the added loss of transmission through the quartz window at the aperture but has no convective losses. Receiver efficiency drops with an increase in outlet temperature, Figure 4-9, mainly because of an increase in reradiation losses. Receiver inlet temperature plays a very minor role in the efficiency change. For constant receiver inlet temperature and input power, the flow rate is adjusted to follow changes in solar flux in order to maintain a constant output temperature. When inlet temperature is decreased, the average cavity temperature and reradiation drops, resulting in slightly higher efficiencies. The difference between the unpressurized and pressurized receiver efficiencies at a given temperature is due to the 8% transmission loss associated with the quartz window. This effect is to offset by a reduction in covection losses from the aperture. The convective loss is greatest when the sun is near the horizon.

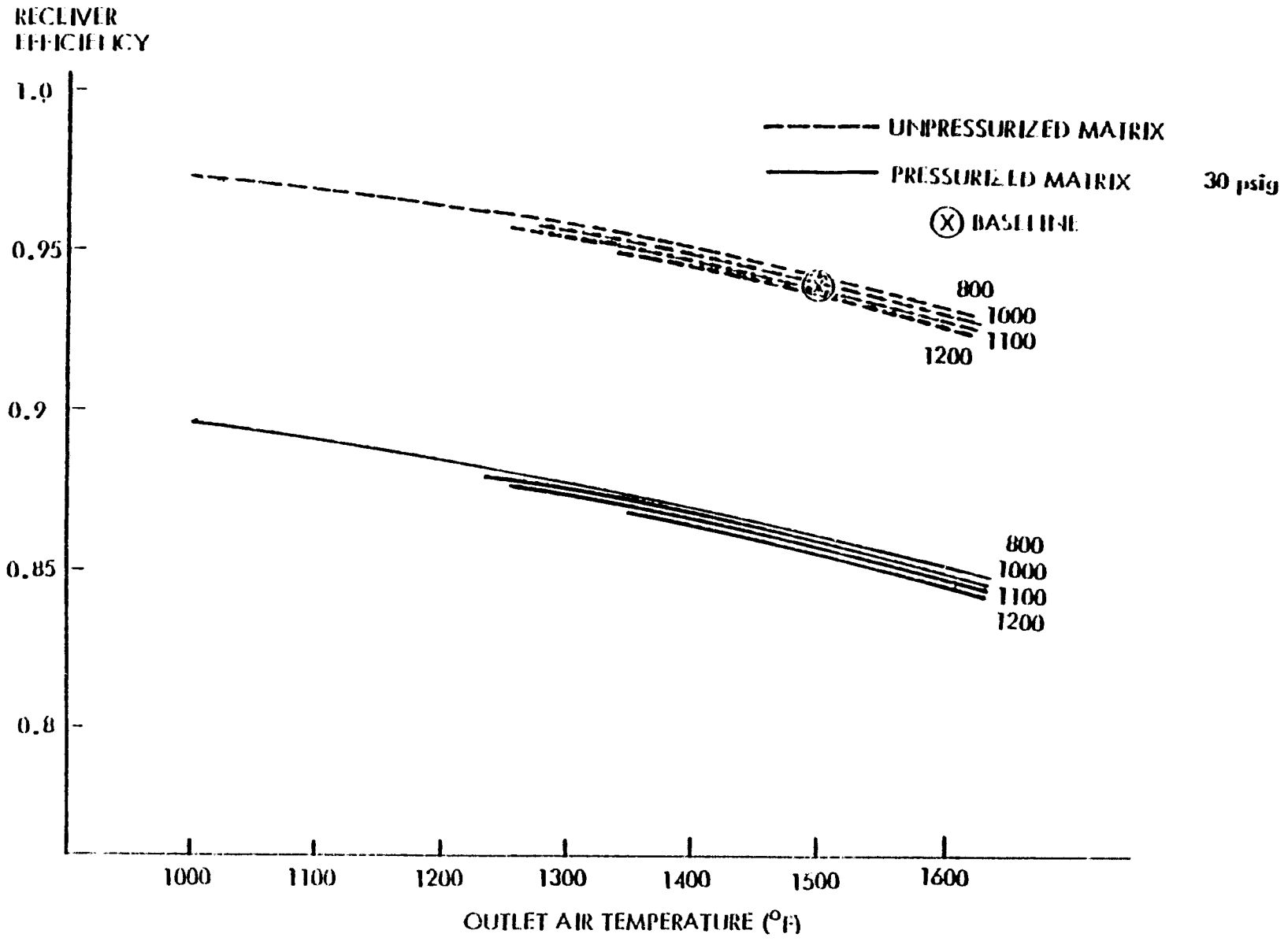

Figure 4-9. Receiver efficiency versus outlet air temperature is compared for both pressurized and unpressurized design.

The cavity ratio is defined as the projected heat exchanger area over the aperture area. Peak efficiencies are obtained at cavity ratio of 10 for 90 KWt input power (Figure 4-10). For low cavity ratios, the receiver temperature increases and the effect on reradiation lowers the efficiency. Similarly, as cavity ratio increases, the conduction losses dominate because of the increased surface area resulting in a decrease in receiver efficiency. Therefore, the ratio between matrix active area and aperture area is an optimum at approximately 10 if losses through the receiver are to be minimized.

A plot of tube receiver efficiency versus outlet air temperature, Figure 4-11, is similar to the unpressurized matrix receiver, Figure 4-9. Inlet air temperature has a slightly greater effect on the efficiency of the pressurized tube receiver compared with the unpressurized matrix receiver. This increase is due to the larger temperature rise in the tube walls.

Tube receivers are also sensitive to receiver diameter, Figure 4-12. For a given tube 0.30 inch in diameter and 8 inches long, the peak efficiency of 94% occurs for a receiver diameter of 35 inches. As receiver diameter is decreased from this optimum, reradiation losses dominate. Above this diameter conduction losses increase and cause a loss in efficiency.

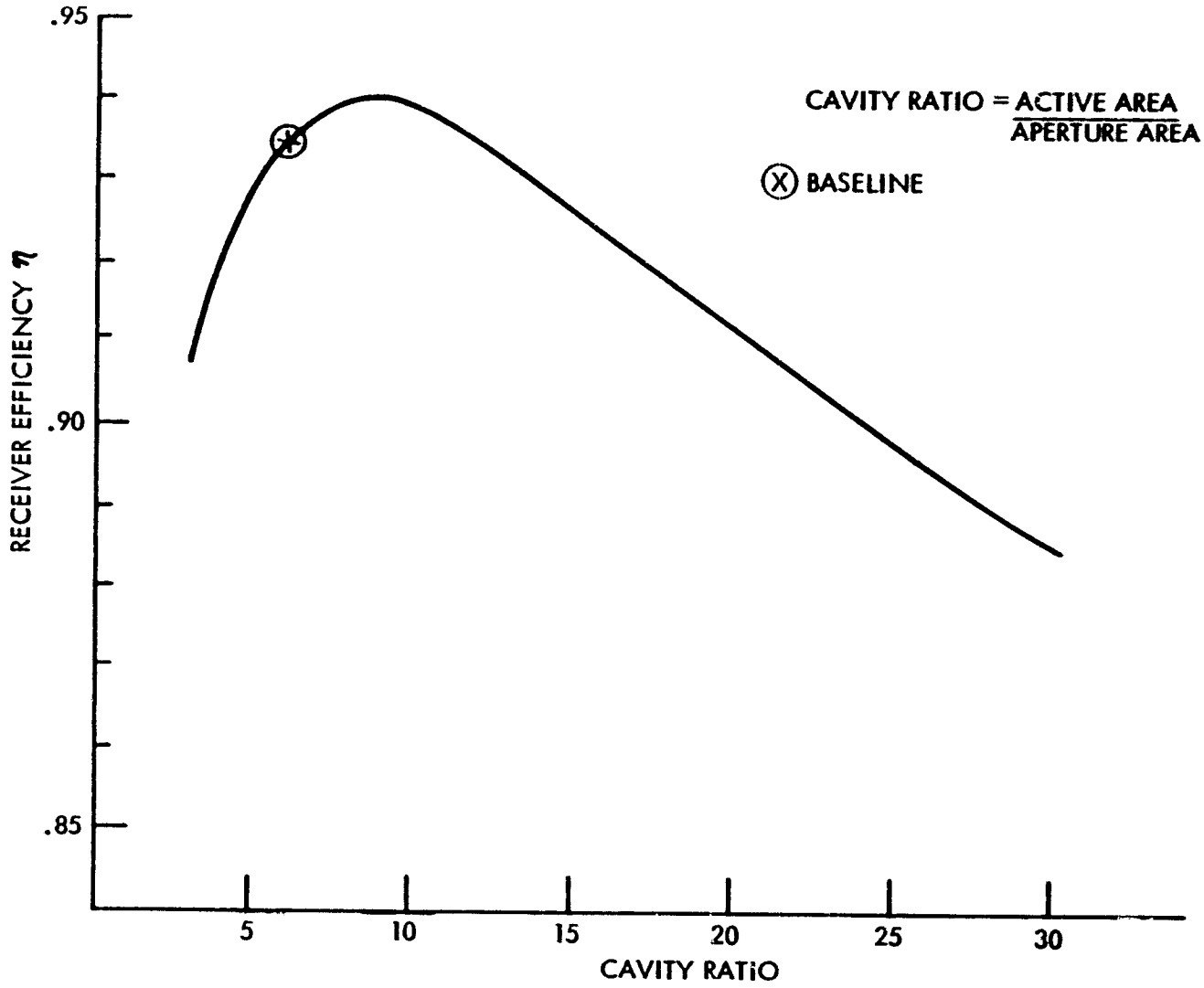

Figure 4-10. Receiver efficiency peaks at a matrix receiver cavity ratio of about 10.

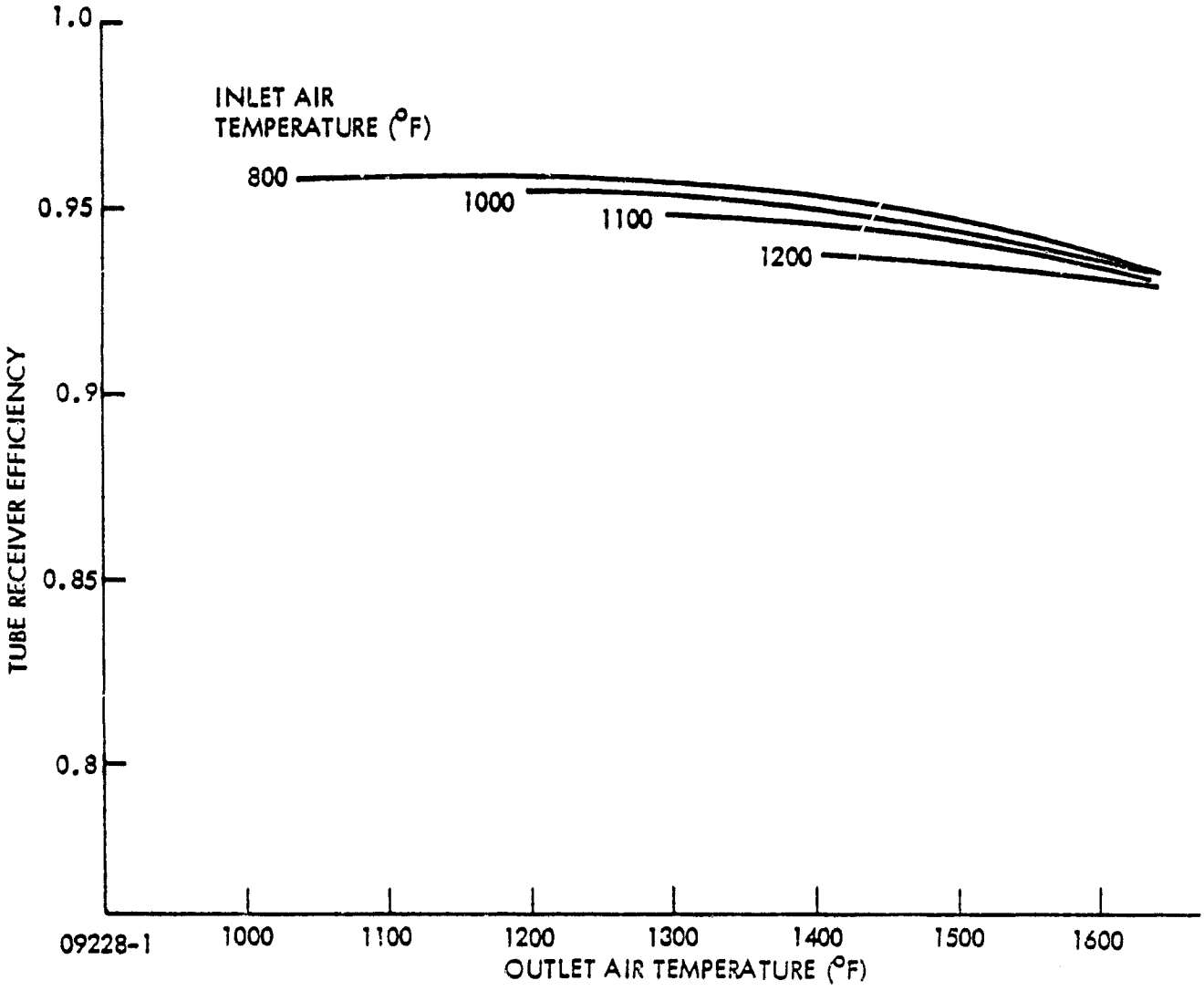

Figure 4-11. Tube Receiver Efficiency Versus Outlet Air Temperature.

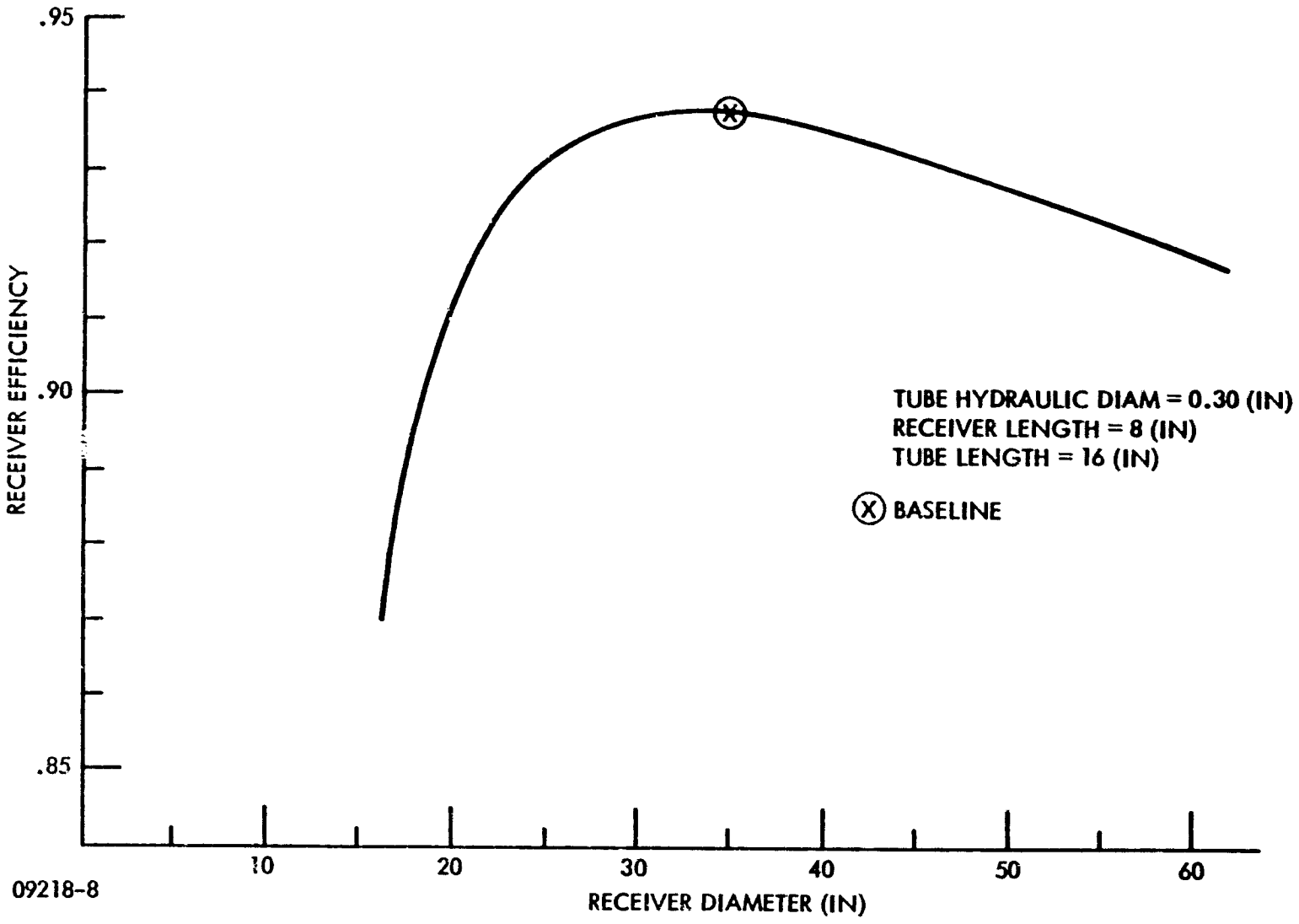

Figure 4-12. Cylindrical receiver efficiency peaks at a receiver diameter of 35 inches.

Another parameter which was optimized for the tube receiver was tube length, Figure 4-13. This analysis was conducted with the optimum receiver diameter and also included a penalty for pressure drop which results as tube length is increased. A peak efficiency of 94% occurred for tube lengths of 16 inches. For shorter lengths the cavity temperature increased causing in increase in reradiation loss because there was insufficient heat exchanger area available in the tubes. Longer tubes than 16 inches were penalized by the large pressure drops in the tubes.

Subsequent to the steady state analysis, a transient study was performed to measure the response of the heat exchanger to changes in insolation levels. Figure 4-14 shows the results of the transient analysis of the matrix receiver. Starting at an 800^{o}F receiver inlet temperature and design mass flow rate, the insolation level was instantaneously increased to design power. The receiver achieved equilibrium with the outlet air reaching 1080^{o}F in 24 minutes while the matrix equilibrated at 1900^{o}F. A cloud was simulated by cutting insolation and receiver mass flow such that the output temperature was maintained at the original level. Under receiver constant temperature operation a pyrehleliometer can provide advance notice of a reduction in insolation and, based on system time constant, the mass flow can be adjusted to eliminate the sharp change in output temperature. Finally, a shutdown was simulated where the insolation was cut but a residual mass flow maintained to cool down the cavity.

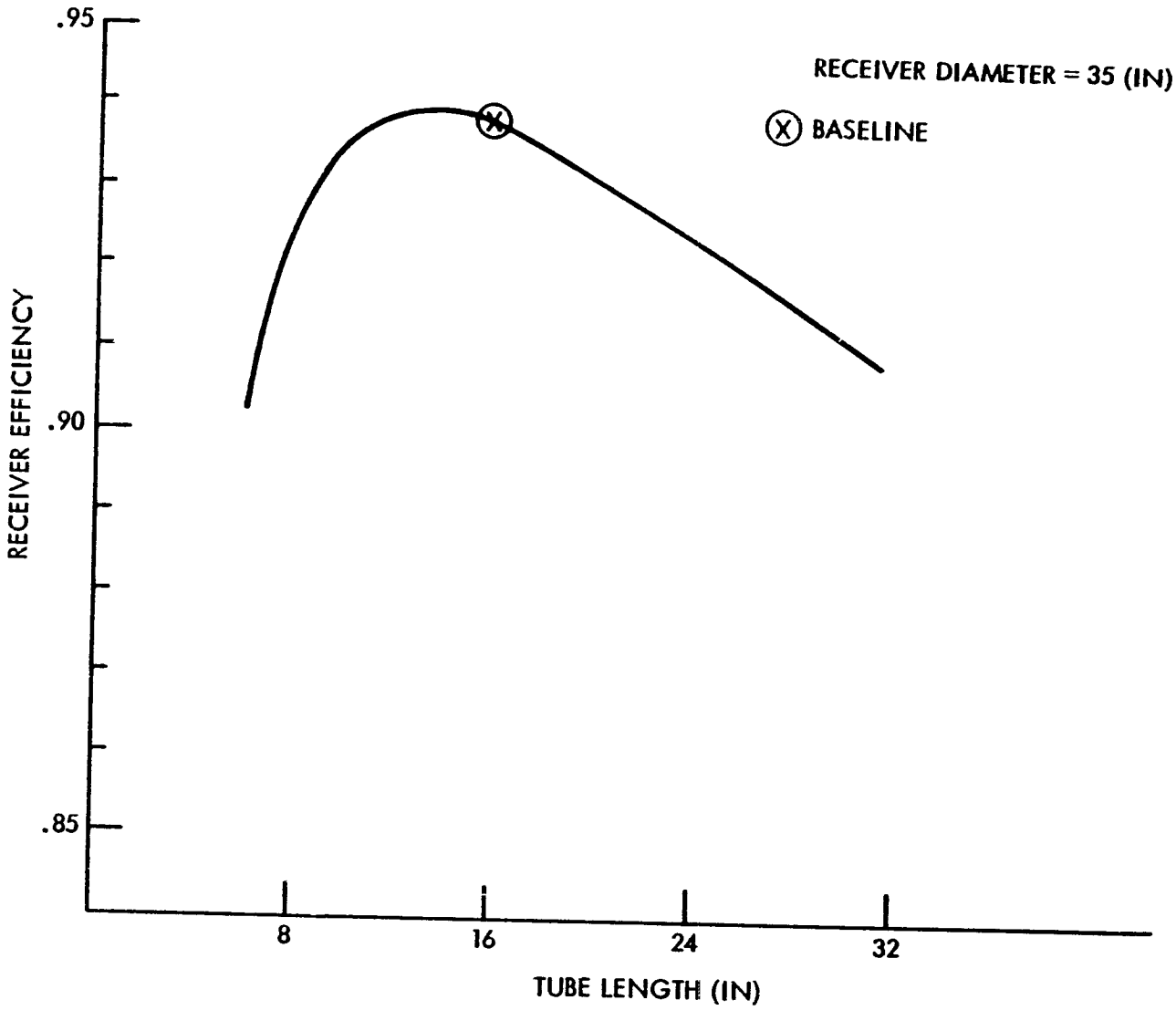

Figure 4-13. Cylindrical receiver efficiency versus tube length.

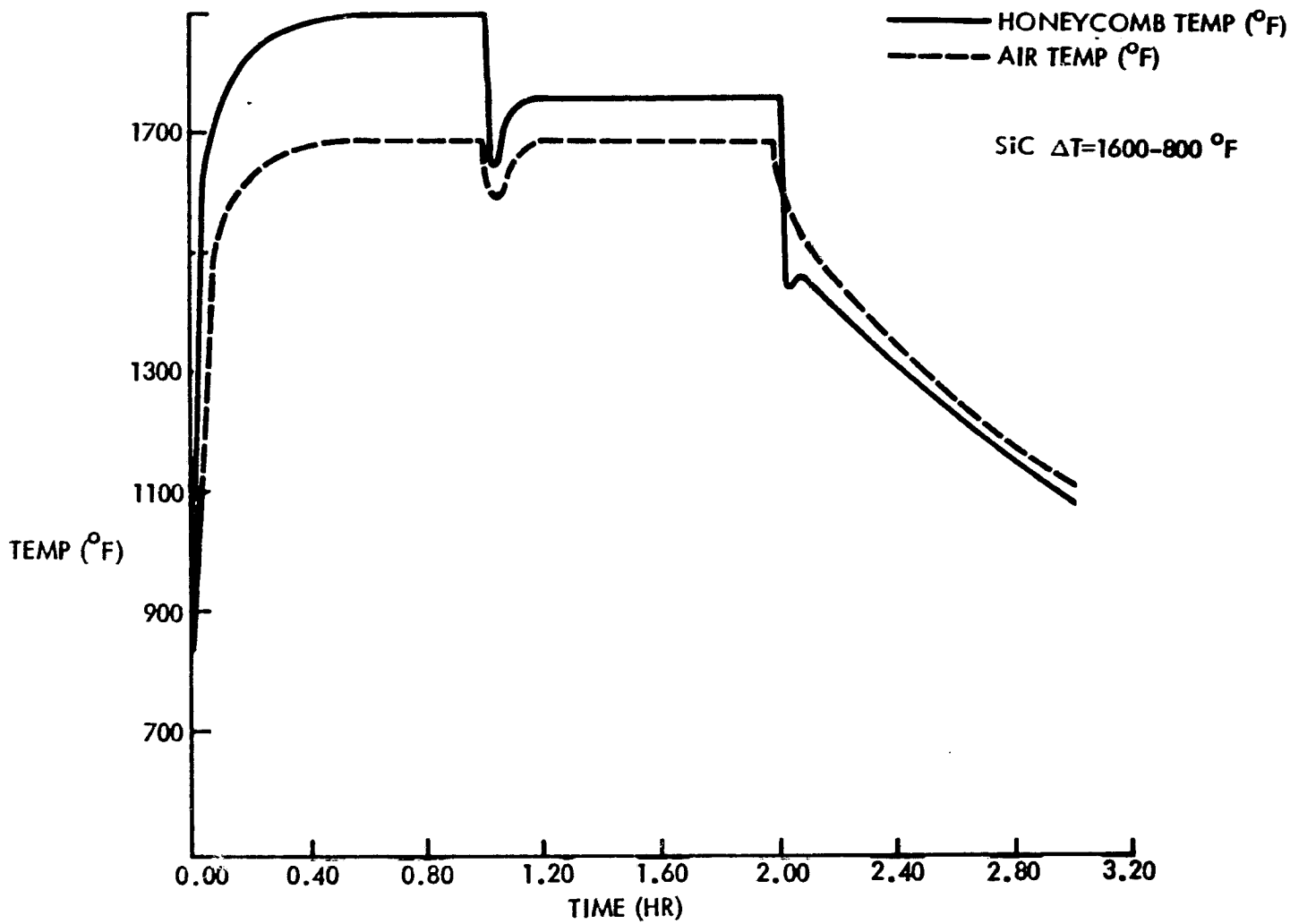

Figure 4-14. A transient analysis was performed on the matrix receiver.

4.6 PRESSURE DROPS

The finite element model solves for the pressure drops in the system along with the heat transfer analysis, taking into consideration the local temperatures. Flow velocities and Reynolds numbers are computed and, based on the flow regime, the frictional losses are tabulated at specified intervals.

During the parametric analysis, the pressure drops for the matrix heat exchangers were calculated as a function of receiver inlet and outlet air temperatures. A decrease in pressure drop occurs with outlet air temperatures, Figure 4-15. This is due to a reduction in the density of air with an increase in temperature. The pressure drops associated with the pressurized unit are lower than the unpressurized receiver because of the increased air density. For a given outlet air temperature, the pressure drop increases with receiver inlet temperature, Figure 4-15. This increase is due to the increased air velocity.

Figure 4-16 shows the pressure drops in the tube receivers under the same temperature conditions. In this case the pressure drops are 10 to 30 times more than in the matrix receivers. This is because small tube diameters and long tubes are necessary for the heat transfer process. This problem is entirely eliminated in honeycomb receivers, where the pressure drops are very small and the selection of honeycomb size is dependent only on the heat transfer characteristics desired.

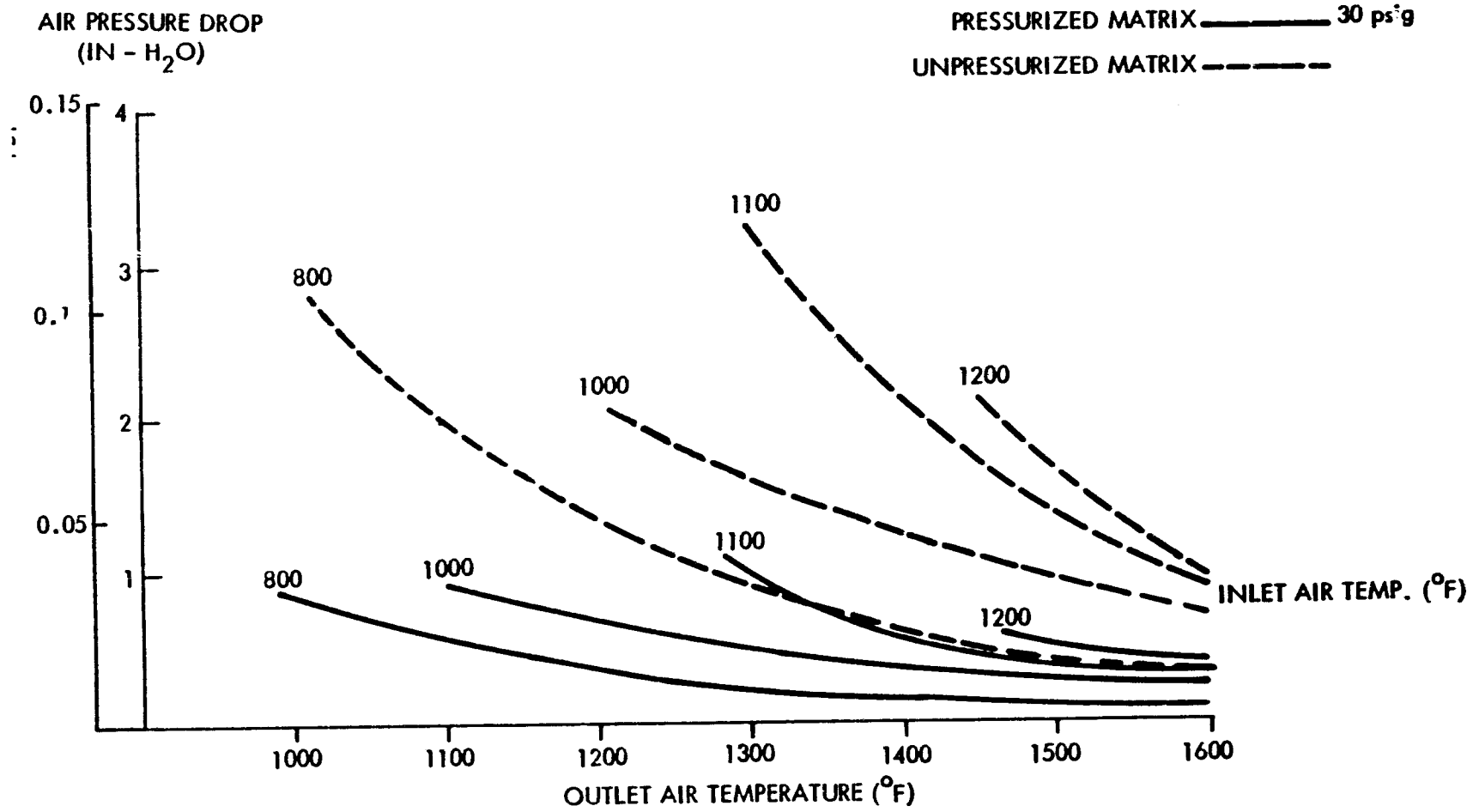

Figure 4-15. Air pressure drop was evaluated for four inlet air temperatures for pressurized and unpressurized design.

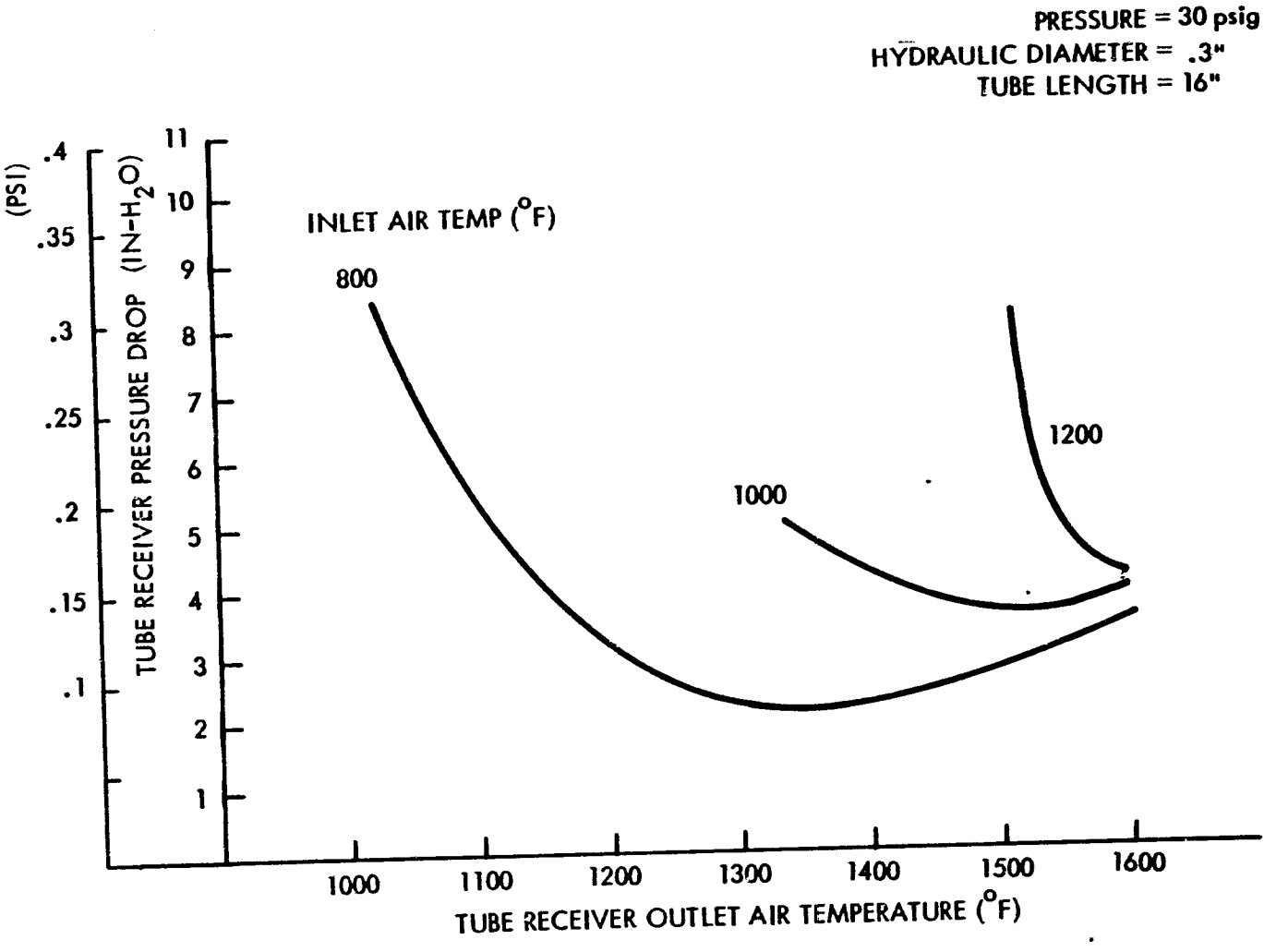

Figure 4-16. Tube receiver pressure drop was analyzed for three inlet air temperatures.

4.7 COMPARISON OF MATRIX AND TUBE RECEIVERS

Based on a detailed parametric study of the matrix honeycomb receivers (unpressurized and pressurized) as well as the pressurized tube receivers, the comparative value of each receiver, is outlined in Figure 4-17. From heat transfer considerations all three types exhibited performance adequate to meet the specified power conditions. The unpressurized matrix and tubed receivers do not need an aperture window since the former operates under atmospheric conditions and in the latter, the pressurized air is contained in the tubes lining the cavity wall. The pressurized matrix receivers require a quartz window at the aperture to maintain system pressure. In matrix type receivers, heat transfer occurs on a high surface area to volume ratio honeycomb that has direct incident solar radiation impinging on it. In flowing through the honeycomb the air absorbs thermal energy directly from the irradiated surface. In the tube receiver, heat transfer occurs across the tube wall to the air in the tubes.

The pumping power in matrix receivers is very low, 10 to 30 times lower than tube receivers. This is very important in the overall cycle efficiency calculation, since, for a low pressure ratio recuperated Brayton engine, the overall efficiency decreases sharply with an increase in system pressure drop.

The overall cycle efficiency of the unpressurized matrix receiver is best. It relies on transfering collected heat into a highly efficient sensible heat storage medium for use in the power generation

RECEIVER	HEAT TRANSFER	PUMPING POWER	RECEIVER EFFICIENCY AT 1500°F (%)	CYCLE EFFICIENCY (%)	MANUFAC-TURABILITY	CYCLIC THERMAL STRESS TOLERANCE	HOT SPOT TOLERANCE	SHARP EDGED CLOUD TOLERANCE	WEIGHT	RELATIVE RECEIVER COST
UNPRESSURIZED MATRIX	GOOD	LOW	94	25	BEST	GOOD	EXCELLENT	EXCELLENT	LIGHT	1
PRESSURIZED MATRIX	GOOD	LOW	86	21	GOOD	GOOD	GOOD	GOOD	MEDIUM	1.2
TUBE RECEIVER	GOOD	HIGH	94	20	DIFFICULT	POTENTIAL PROBLEM	POTENTIAL PROBLEM	GOOD	MEDIUM	2

Figure 4-17. The three types of receivers were compared for all relevant characteristics.

cycle. This is followed by the pressurized matrix that is placed in a conventional Brayton cycle. The low pressure drops associated with matrix receivers offer the advantage of high cycle efficiencies compared to tube receivers.

The manufacturability of the unpressurized matrix is easiest since it operates at atmospheric pressure, with no extraordinary precautions necessary to maintain system pressure and eliminate leakage. The pressurized matrix has the added sealing requirement for the aperture window. The manufacturability of the tube receiver is more difficult because the tube manifold must have individually rolled and welded tube attachments that increase the potential for failure.

Cyclic thermal stresses in the matrix receivers cause no problems in the design since the matrix is made of ceramic material and is supported in a compliant mounting structure. In the tube receivers, circumferential temperature gradients are a limiting factor in the selection of tube sizes and spacing. The low thermal stresses in matrix receivers minimizes the mechanical failures in the heat exchanger. In the event of cracking or hole obstruction the matrix receiver continues to operate with minor changes in performance. In a tube receiver, a crack or a weld failure results in loss of working fluid and eventual shutdown of the Air Brayton Solar Power System.

The ceramic honeycomb matrix is very tolerant of hot spots and variations in flux intensities across the matrix. Test results show that flux variations of 7 to 1 are tolerated in matrix receivers with no adverse effect. In tube type receivers variation of this magnitude will cause tube failures.

A sharp cloud obscuring the sun cuts the flux on the heat exchanger. Using the unpressurized receiver concept, the turbine is unaffected since the heat collection cycle is independent of the power generation. In a conventional Brayton cycle using a pressurized receiver, the response is immediate, but the use of a buffer storage system would assure continuous operation for a limited period.

The unpressurized matrix receiver has the lowest weight because it operates at atmospheric pressure and does not require a heavy pressure shell. The tube receiver and the pressurized matrix have approximately the same weight. The weight of the pressure shell in the pressurized matrix receiver offsets the weight of the manifolding in the tube receiver.

4.8 RECOMMENDED RECEIVER DESIGN

Based on the Parametric studies done for this contract the pressurized matrix receiver was selected for the conceptual design study because of the following reasons.

- High heat transfer efficiency
- Low heat exchanger pressure drops

- Low thermal stresses
- Tolerance to flux nonhomogeneities
- No convective loss at aperture
- Low production costs

On a production basis, the pressurized matrix receiver is the most cost effective. Its reliability, overall system efficiency, and compatibility with JPL's requirements make it the first choice for an early demonstration of a point focusing solar Brayton power system.

SECTION 5

RECEIVER CONCEPTUAL DESIGN

5.1 INTRODUCTION

Sanders has been designing solar receivers for over five years. During this period, an extensive background of experience and design capabilities has been developed. In particular, Sanders has developed an extensive software library for the calculations required in the deseign of efficient solar receivers. This fotware allows numerical solutions to a wide variety of thermal problems involving arbitrary combinations of conduction, convection, fluid heat transport and radiation. This numerical analysis is inherent in Sanders' design approach, has been proven reliable, and has been validated against experimental measurements on many occasions. The solution capabilities include nonlinearities (principally temperature dependences of material properties as well as those inherent in radiation), variation of friction factor with Reynolds' number, and variation of film heat transfer coefficient with Reynolds' and Prandtl numbers.

A distinctive feature of Sanders' analysis system is the extent to which is includes the fluid flow and pressure drop analysis along with the simultaneous associated heat transfer effects. Both steady state and transient solutions of a given physical system are available. This highly flexible system is readily applicable to solutions of a physical model at different levels of approximation, so that analysis complexity and cost can be traded off against required precision.

Sensitivity of solutions to hypothesized variations in both material properties and geometrical parameters can be performed with minimal difficulty.

The type of analysis made mossible with this system has facilitated rapid development of the receiver designs. In each case, a reasonable level of approximation for the end use was found. A variety of options was explored, with detailed analytical data identifying the design parameters leading the way to optimal values. This capability of adapting our analytical tools to the needs of the design process was especially effective in this receiver design which build on existing design and test experience.

The receiver/storage module layout is shown with the critical dimensions in drawing No 4019098, sheets 1 and 2 in the drawing package. The unit is cylindrically shaped, 40 inches in diameter, and 70 inches in height. The storage module is integrated with the receiver to minimize ducting losses and to present a single unit to interface with the power conversion unit. The receiver can easily be modified to eliminate storage, if desired, reducing system weight by 1/3.

Ceramic matrixes are used both for the heat exchanger and for storage. A Cordierite honeycomb of 2.6 inch thickness is sufficient to transfer the heat into the air stream in the receiver, and 18 inches of Mullite honeycomb will provide the 10 minute buffer storage. During cloud cover, the 10 minute buffer will be used to provide 1050^{o}F air to operate the engine (under off-design conditions) so that output does not fall below shutdown levels.

5.2 THERMAL DESIGN

5.2.1 Optical Design

The optical design of the receiver was configured to maximize receiver efficiency while minimizing costs. Where possible, at no increase in cost, the receiver design was arranged to provide maximum tolerance to variations in the specifications of the concentrator and of the power conversion unit.

5.2.1.1 Flux Distribution

Flux distribution at the 36 ft concentrator was specified by JPL as shown in Figure 5-1. Based on the size of the concentrator, a solar constant of 1 kW/m^2 and a mirror reflectivity of 0.9, the total energy incident at the aperture plane was calculated to be 85 KWt.

5.2.1.2 Aperture Size

To determine the optimum aperture size, the distribution at the focal plane shown in Figure 5-1 was integrated to determine the total radiation entering the aperture. Reradiation was assumed to occur at a cavity temperature of $1700^{o}F$. The resulting increase in reradiation with aperture radius is plotted in Figure 5-2.

The aperture size is selected at a point where the energy capture efficiency is insensitive to aperture opening. The aperture could be selected anywhere from 6 to 8 inches in diameter. An aperture diameter of 7.34 inches was chosen where capture efficiency is highest. Although the required window diameter of 8.5 inches is slightly more

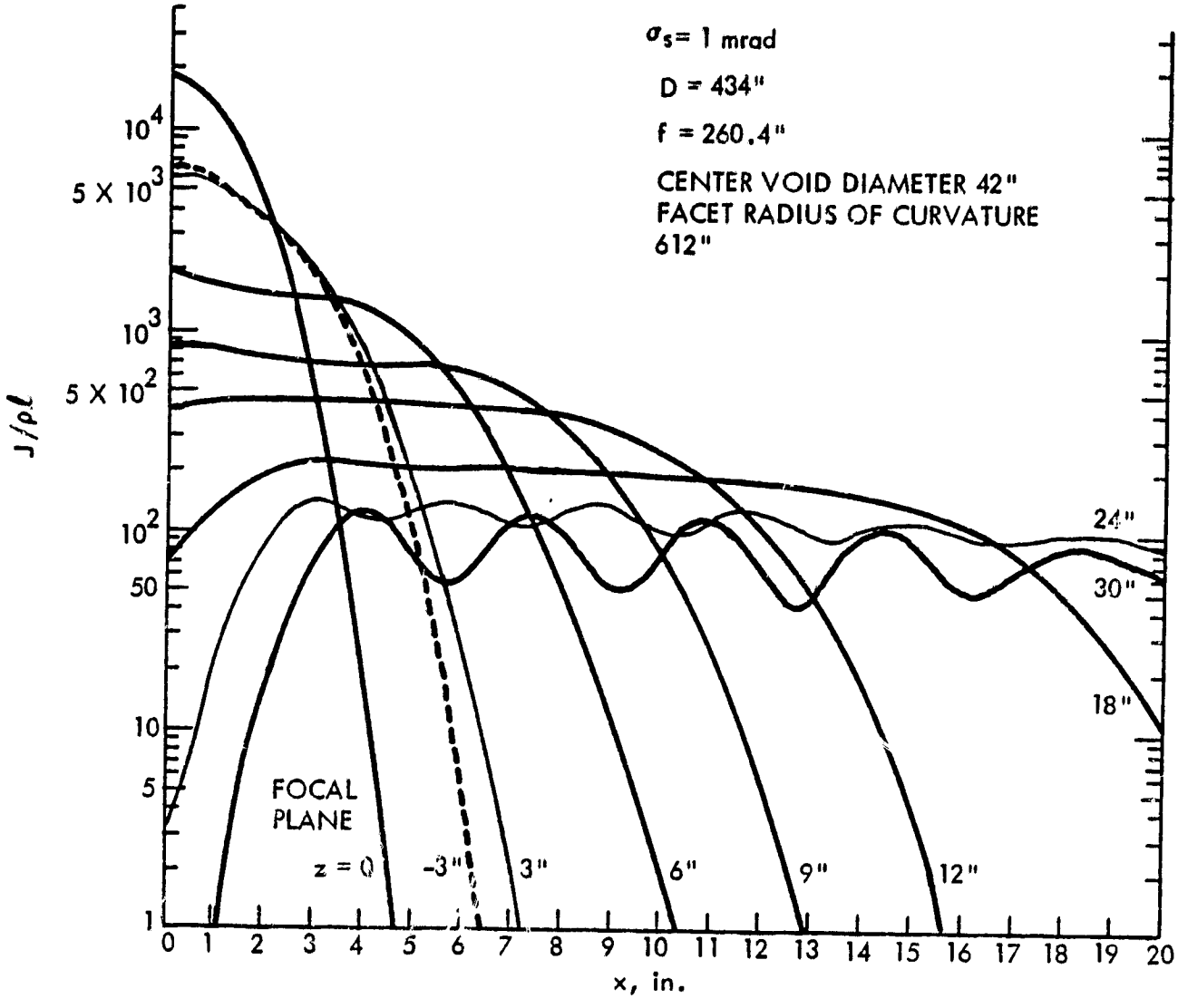

Figure 5-1. The flux distribution on the 36 foot diameter concentrator was specified by JPL.

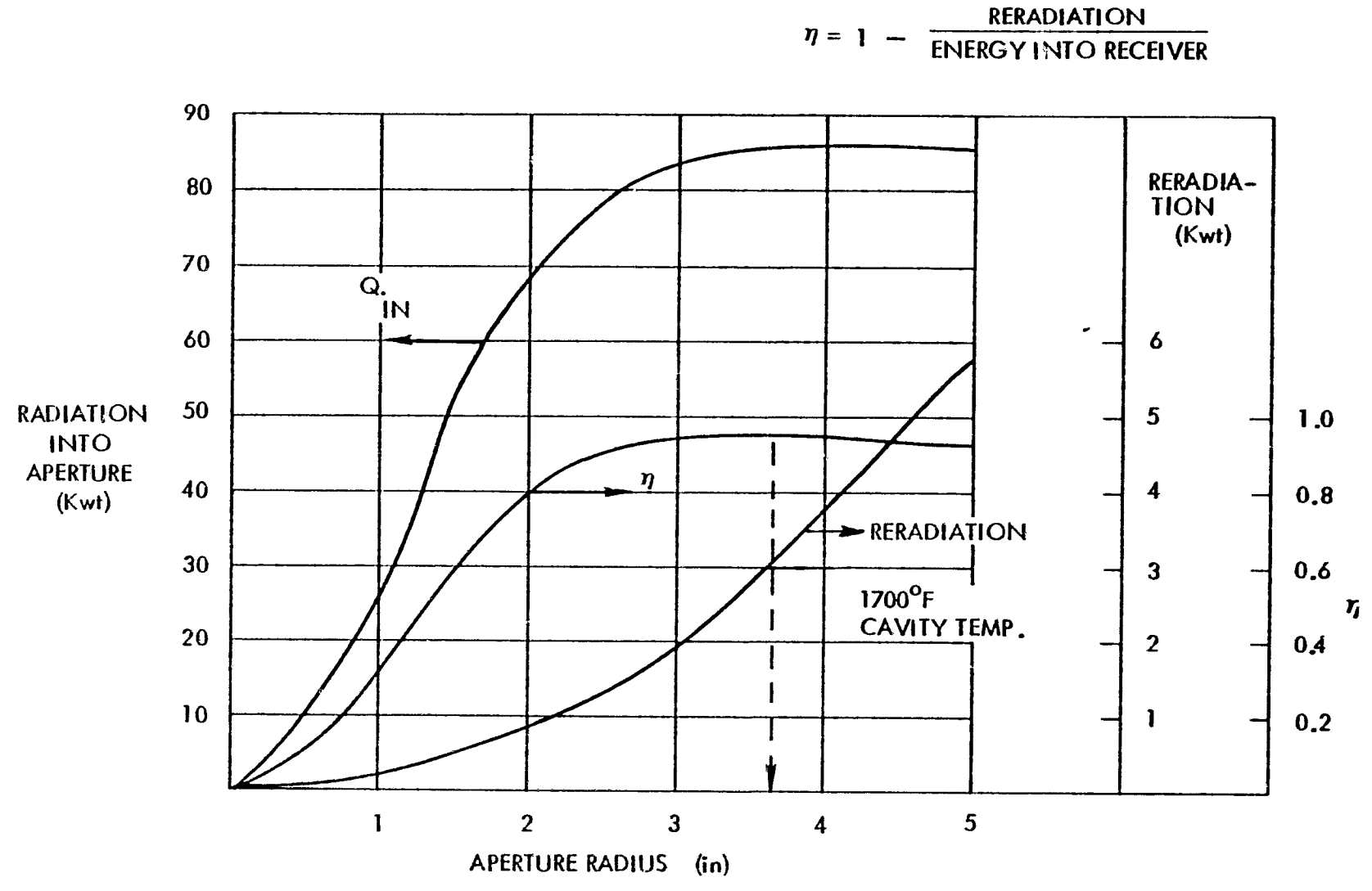

Figure 5-2. Reradiation increases with increasing aperture radius. The highest capture efficiency is at an aperture diameter of 7.34 inches.

expensive than the 6 inch window, it allows a greater tolerance to concentrator surface accuracy errors with no loss in receiver efficiency.

For a design pressure of 45 psi, Figure 5-3 shows the required thickness/diameter ratio for quartz window to be 0.073 or a thickness of 0.625 inch. Based on a tensile stress of 7000 psi, there is a safety factor of 7 in the design.

The percentage transmittance and transmission of the terrestial solar spectrum through GE Type 125 fused quartz are shown in Figure 5-4 as a function of window thickness. The transmission figures include absorption as well as reflections at two surfaces; the transmittance includes absorption effects only. These results are obtained by folding the solar spectrum against the properties of the window. A graph of transmittance of GE Type 125 quartz versus wavelength is shown in Figure 5-5. The window transmittance and transmission decrease with increasing window thickness. At the design conditions of 45 psi pressure, 8.5 inch diameter window of 0.625 inch thickness, the transmittance and transmission are shown to be 0.98 and 0.91, respectively.

To assure survival of the window, Sanders has investigated the heat balance under the required operating conditions. General Electric's test data indicates there is no significant change in transmittance at wavelengths below 4μ for temperatures up to the 2000^{o}F annealing point. In the infrared, where absorption is greater than .9 at room temperature, the spectral emissivity increases with temperature.

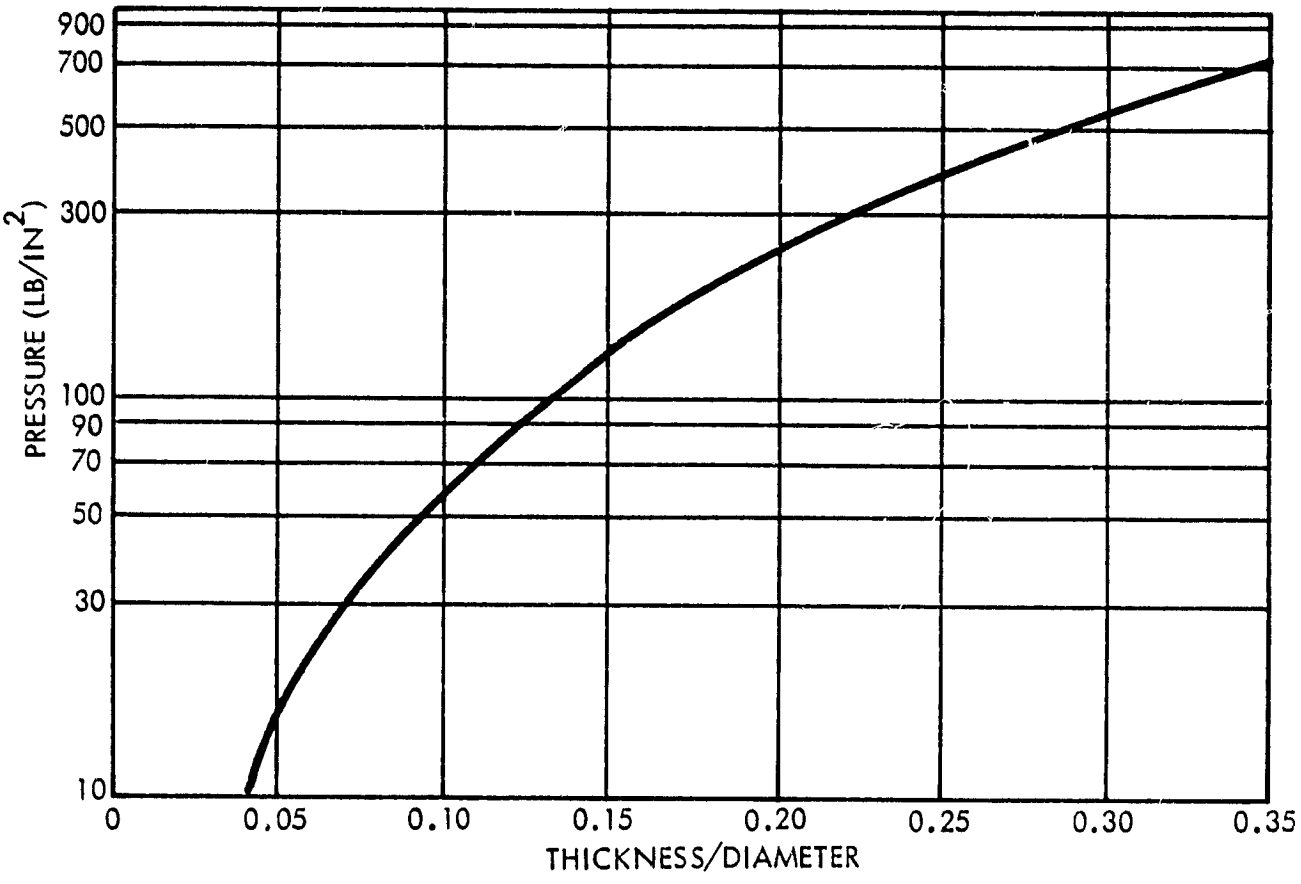

WICBO-030

Figure 5-3. Pressure vs thickness/diameter ratio is plotted for a quartz window clamped at the edges.

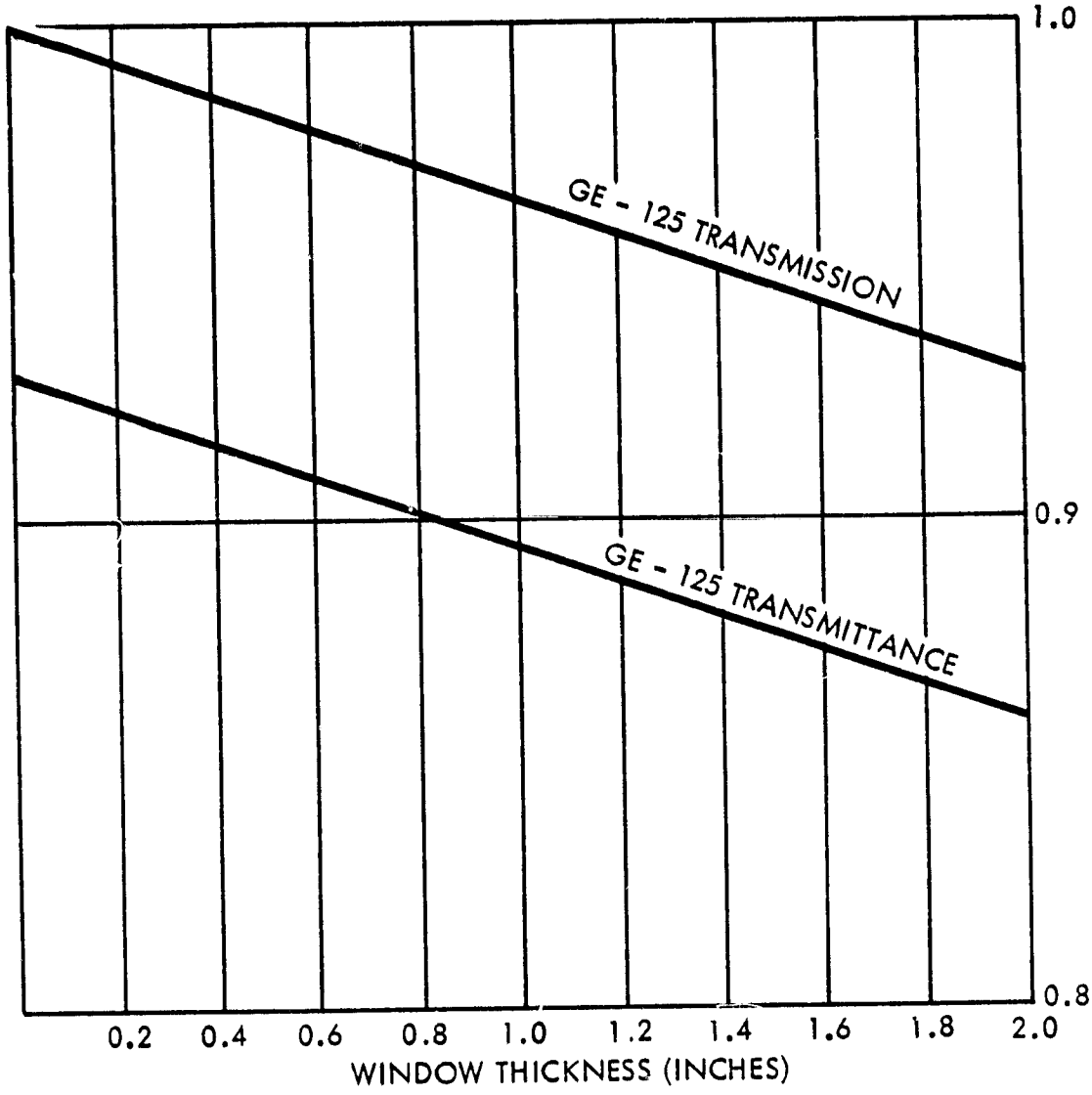

WICBO-029

Figure 5-4. Transmission values as a function of window thickness include absorption and 2-surface reflections; transmittance includes absorption only.

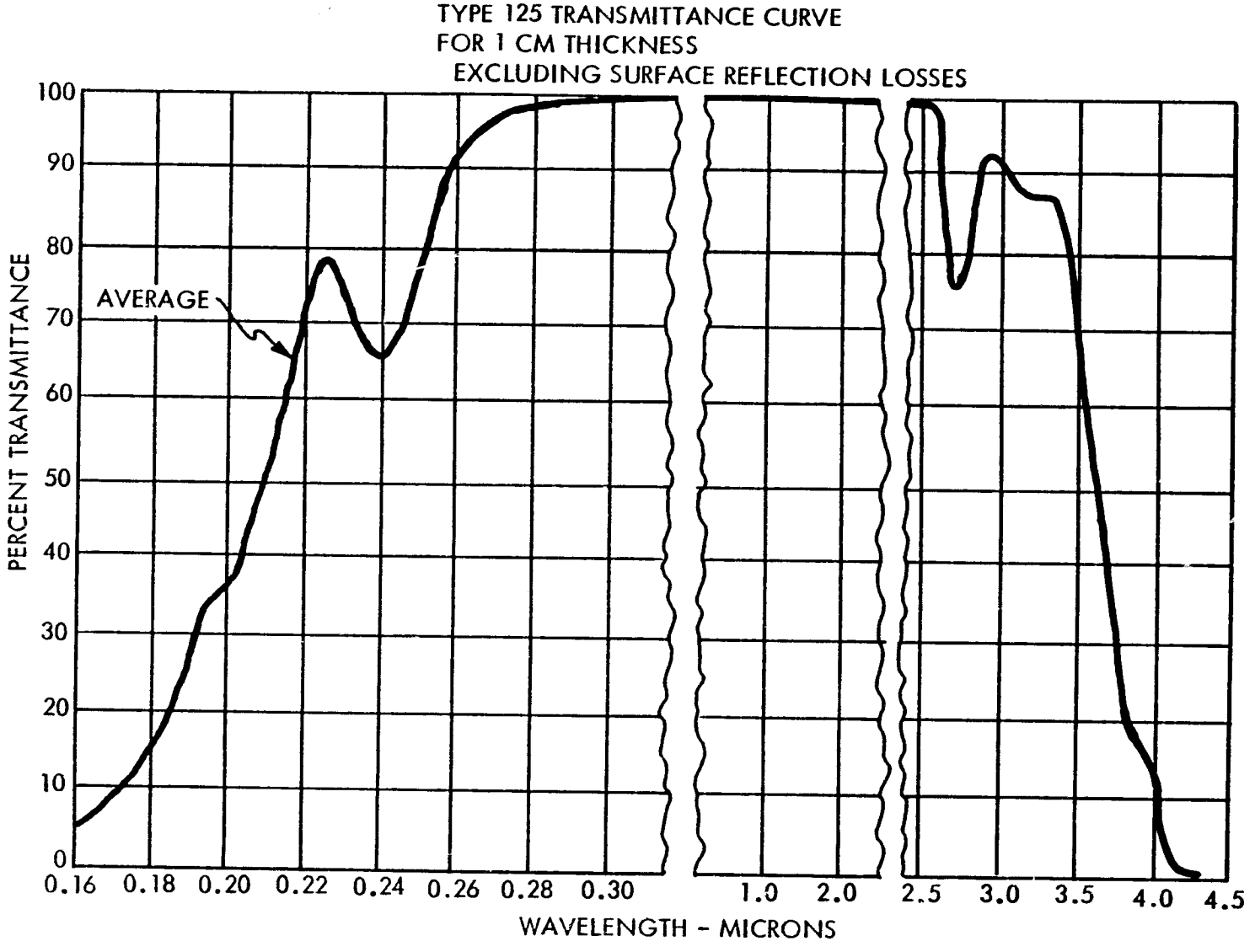

WICBO-031

Figure 5-5. The Spectral Transmittance of GE Type 125 quartz is plotted.

The receiver model was kept conservative in its treatment of the window by assuming total absorption of all energy reradiated from the matrix and cavity walls from 3.0 microns and up, giving it an average emissivity of 0.635. The actual figure for cold quartz, which absorbs from 4 microns and up, is somewhat smaller. With this higher emissivity the window temperature, 1034^{o}F is an overestimate, well below the 2000^{o}F annealing point.

To insure proper cooling for the window, Sanders plans to buffer the recuperator with 3% of the air flow and use this air to impingement cool the window. This cooling technique will maintain the window temperature below 1000^{o}F under all operating conditions. Temperatures, at the somewhat reduced flux levels (250 w/cm^{2}) encountered in the 10 kW receiver tests at White Sands approached 700^{o}F without cooling.

5.2.1.3 Matrix Location

After selecting the optimum aperture size, a parametric analysis was made to determine the matrix cross sectional area and the optimum location behind the aperture plane. The analysis showed that a 22 inch honeycomb disk would give sufficient surface area to ransfer the heat and meet the design goal of 1500^{o}F receiver outlet air temperature.

Sanders' computer flux mapping program was used to optimize the receiver efficiency, and, to the extent possible without decreasing efficiency, direct incident flux onto the disk. Figure 5-6 shows the results of the direct flux distribution versus matrix radius for the chosen location which is 11 inches behind the aperture plane. The calculated ratio of peak flux to minimum flux for the directly incident solar energy is 4:1. This is considered smaller than the ratio in the 10 KWt receiver which was successfully tested at White Sands. A ratio of 7:1 was measured in the 10 KWt receiver. Honeycomb matrix heat exchangers can withstand high flux nonuniformities due to their large flow area, whereas, in tube receivers such nonuniformities can result in local hot spots and tube failures.

5.2.2 Heat Transfer Characteristics

A computer model was developed by Sanders to solve the set of simultaneous heat balance equations that represent the receiver when it is exposed to a given insolation. All four modes of energy transport; i.e., radiation, conduction, convection and fluid flow, are modeled to obtain:

- Receiver efficiency
- Pressure drop
- Fluid outlet temperature
- Maximum cavity temperature
- Axial temperature profile in honeycomb tubes

DISK DIAM. = 55.88 cm (22")

APERTURE DIAM. = 18.64 cm (7.34")

FOCAL LENGTH TO APERTURE = 71 m = 21.65'

APERTURE TO MATRIX DISTANCE = 11 INCHES

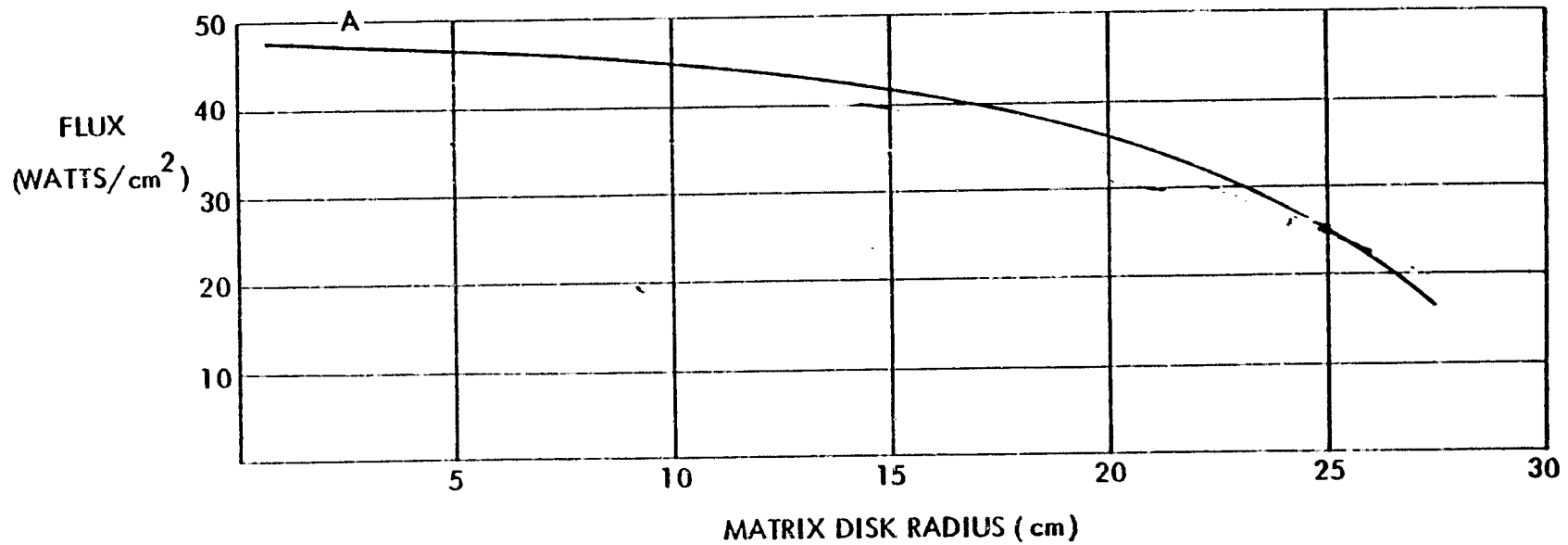

Figure 5-6. Flux distribution was plotted as a function of matrix radius.

Transient analyses were conducted after the steady state solutions were validated. The objective was to establish turn-on and turn-off procedures for the system by exploring the relation of stresses to the insolation and airflow levels from which a set of system operating constraints was established. In addition, the transient study is valuable in establishing the effects of cloud cover and determining systems operational strategies that are needed to maintain receiver outlet temperatures.

5.2.2.1 Pressure Drop

Every attempt was made to minimize pressure drops through the system to assure high cycle efficiency. The passageways and ducts were designed for minimum pressure drop. Sanders' analyses of the receiver matrix indicates a pressure drop in the order of 0.01 psi during operation at the design point. Figure 5-7 shows the behavior of the matrix pressure drop as a function of receiver outlet temperature. In a constant RPM system, the pressure drop is essentially constant when insolation drops from 100% to 60% level; whereas, in a constant turbine inlet temperature system, pressure drop decreases with insolation due to the large change in air flow rate.

Because of low air velocities in the matrix receiver, the pressure drop considerations become relatively unimportant compared to the heat transfer considerations. This is in sharp contrast to tube receivers, where pressure drops play a very important role in

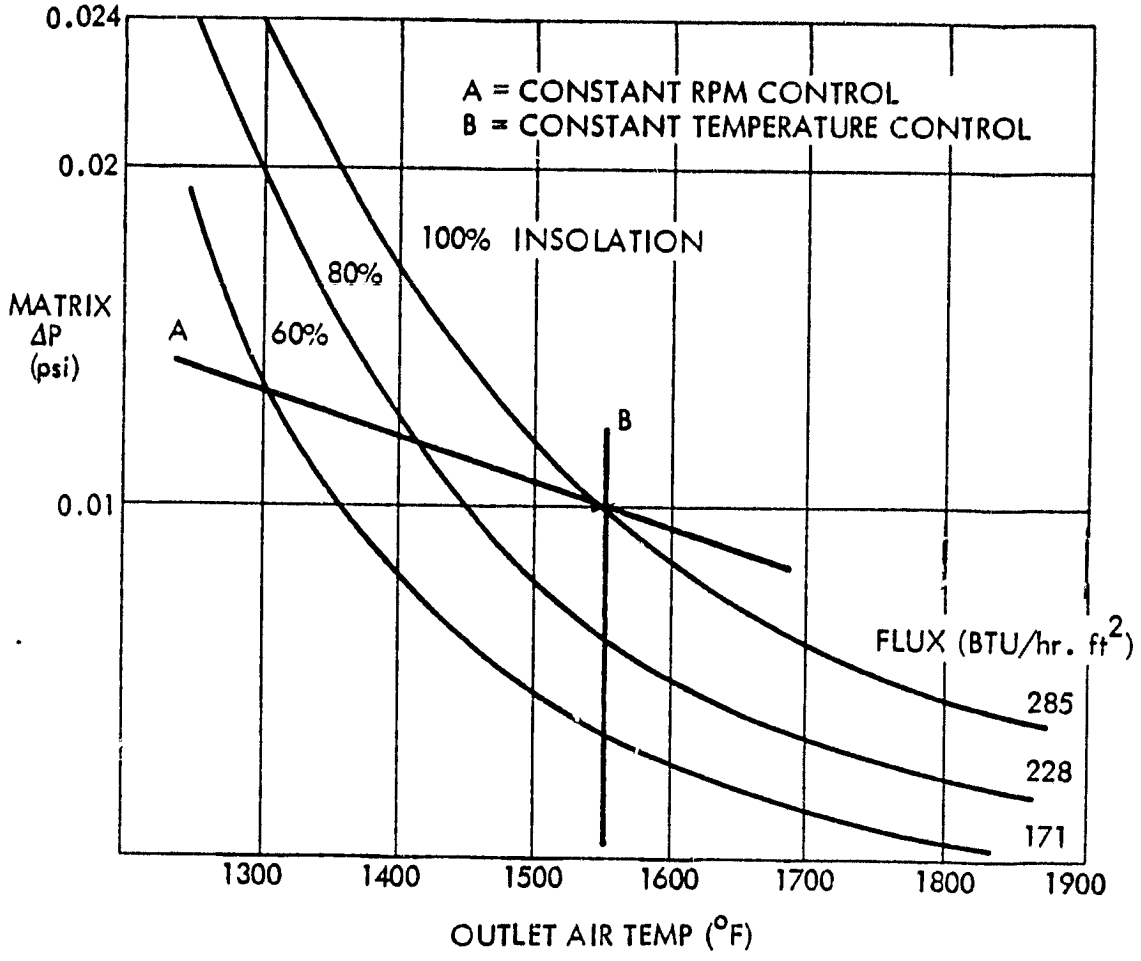

Figure 5-7. Matrix pressure drop is plotted as a function of receiver outlet temperature, showing the constant pressure drop in a constant RPM system when isolation drops from 100% to 60%.

selecting tube sizes; in many instances, forcing compromises in the selection of either heat transfer surface area or receiver size. The low pressure drops encountered in the matrix honeycomb heat exchanger provide added power conversion unit efficiency when compared to the pressure drops in tubed receivers.

Table 5-1 gives the pressure drop in the receiver components during operation at the design point and during operation from buffer storage. The pressure drop during buffer storage operation is greater because of the added drop encountered in the storage honeycomb and the receiver valve which will be 63% closed. In both modes of operation, the reciever/storage module pressure drop is well below the maximum allowable drop of 0.7 psi.

5.2.2.2 Honeycomb Temperature Profiles

Figure 5-8 shows the air temperature profile as it travels down the honeycomb tube, absorbing heat. Using a criterion of $20^{o}F$ difference between air outlet temperature and the back face of the matrix, a Cordierite thickness of 2.6 inches will provide the required heat transfer.

The effective cavity temperature has been calculated to be the average temperature of the receiver walls, including honeycomb, and is plotted versus outlet air temperature in Figure 5-9. The effective cavity temperature becomes important because it characterizes the amount of reradiated energy, and can be interpreted as the equivalent temperature of a blackbody occupying the aperture.

TABLE 5-1.

PRESSURE DROPS IN RECEIVER COMPONENTS

COMPONENT	DESIGN POINT OPERATION	BUFFER STORAGE OPERATION
HOT DUCT	0.065	0.033
COLD DUCT	0.066	0.066
INLET SCROLL	0.013	0.013
SCREEN	0.024	0.024
HEAT EXCHANGER MATRIX	0.012	0.012
STORAGE HONEYCOMB	0.007	0.175
RECEIVER VALVE	0.005	0.136
STORAGE VALVE	0.058	0.0023
TOTAL	0.25	0.461
MAXIMUM ALLOWABLE	0.7	0.7

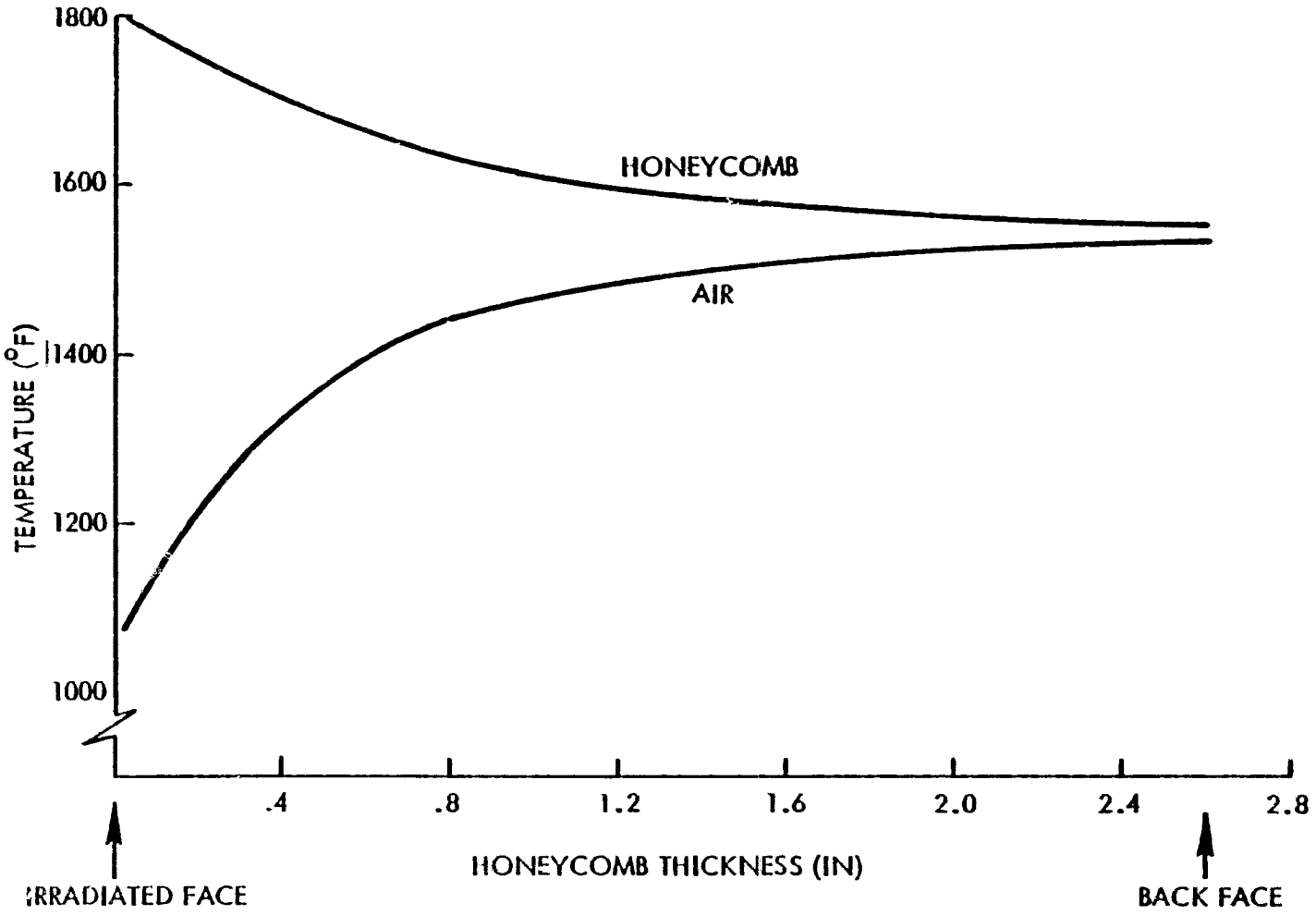

Figure 5-8. Air temperature increases as it travels down the honeycomb.

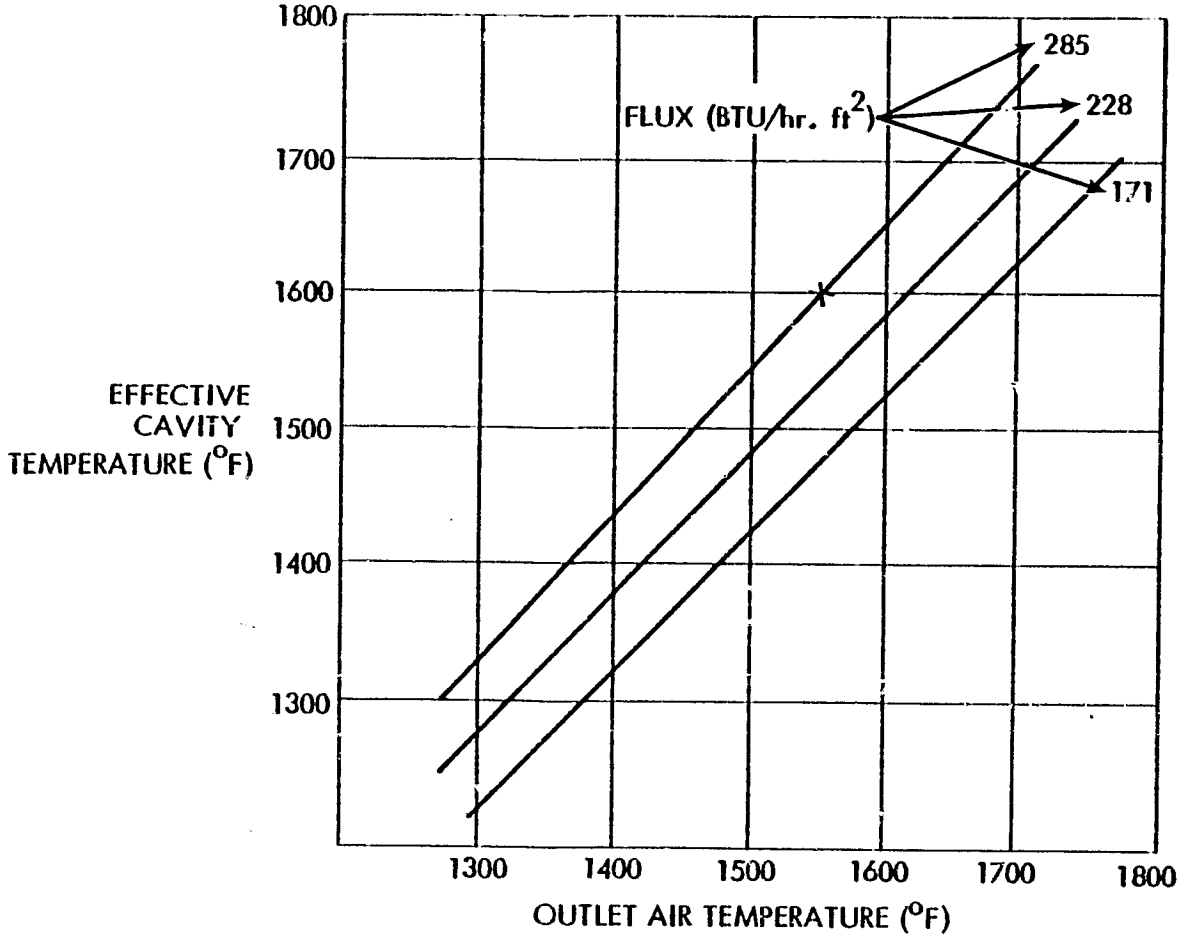

Figure 5-9. The effective cavity temperature characterizes the amount of reradiated energy.

The front face of the honeycomb matrix will be exposed to direct insolation; consequently, its temperature will be the maximum temperature in the cavity.

A feature of the honeycomb matrix heat exchanger is its ability to limit the difference between the peak temperature on the honeycomb and the air temperature. This, in turn, minimizes the reradiation effects.

5.2.2.3 Efficiency

The honeycomb matrix provides an efficient heat exchanger for the receiver. Because of its high heat exchanger surface area per unit volume, a matrix receiver can maintain low front surface heat exchanger temperatures and correspondingly low reradiation losses, and high efficiencies. This is in sharp contrast to tube receivers where surface area/unit volume is low. This results in larger tube receivers to accomplish the same amount of heat transfer. If receiver overall size is maintained, then tube size must decrease, resulting in higher receiver pressure drops. All these effects lower the overall cycle efficiency and cause a reduction in output power.

Sanders' analysis indicates a receiver efficiency of 0.86 at 1500^{o}F outlet air temperature at the rated mass flow of 0.533 lb/sec. Figure 5-10 shows air flow rate and receiver efficiency versus outlet air temperature at 100, 80 and 60% insolation levels. The receiver is at 1550^{o}F in order to have excess heat with which to compensate for heat losses due to conduction through the duct walls. This will

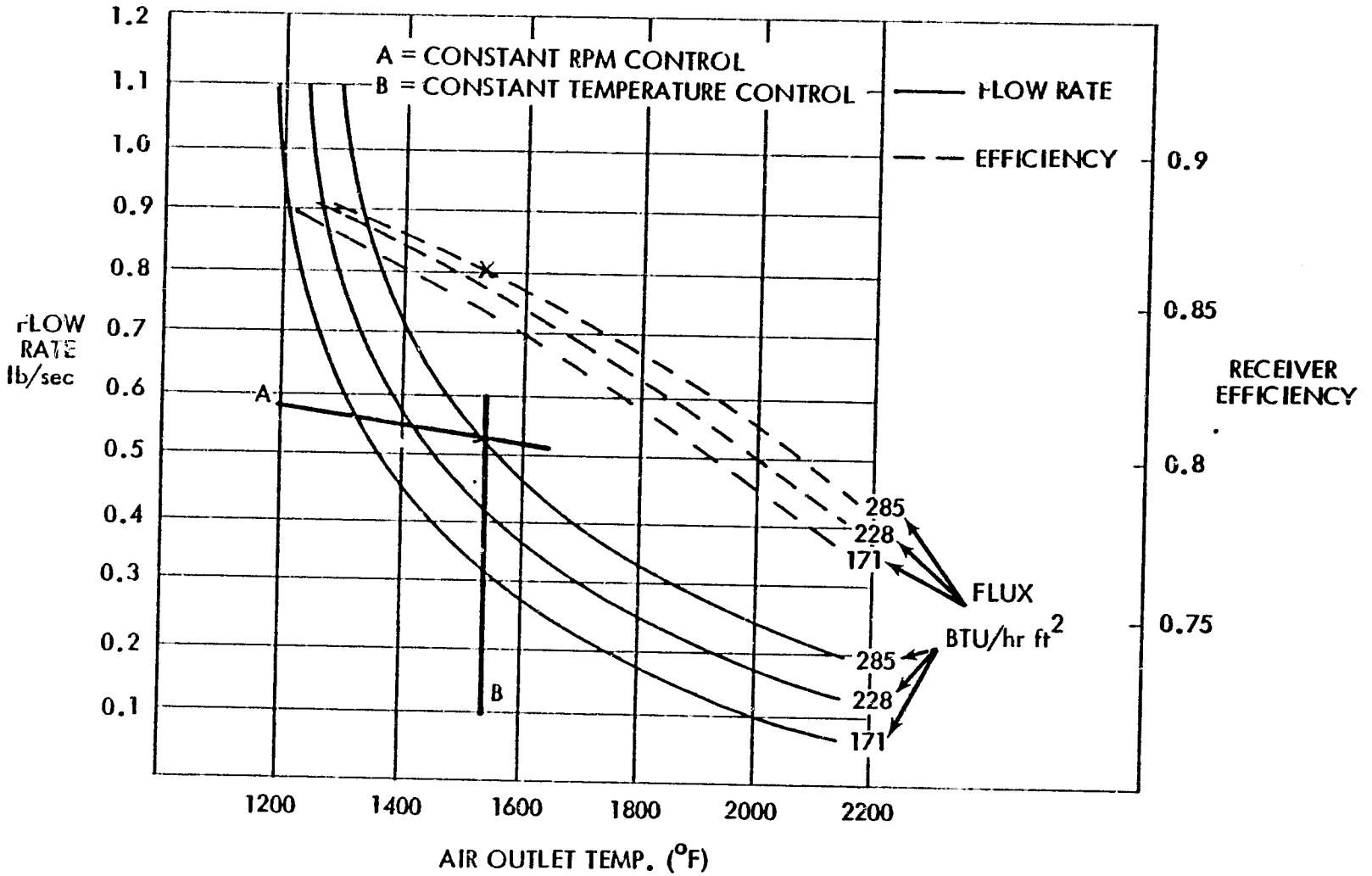

Figure 5-10. Flow rate and Receiver efficiency is plotted versus outlet air temperature.

ensure the ability to meet the turbine inlet temperature requirements. The receiver efficiency drops with an increase in outlet air temperature. This is mainly due to the increase in reradiation losses from the aperture. Curves A and B show the two modes of system control. For constant RPM operation, the receiver outlet temperature will drop with insolation and the flow rate will follow the characteristics shown by curve A.

5.2.3 Heat Loss Mechanisms

Five different energy loss mechanisms play an important part in evaluating the receiver performance:

- Conduction
- Convection
- Transmission
- Reradiation
- Pumping losses

5.2.3.1 Conduction

During normal receiver operation, the average internal temperature of 1500^{o}F dictated the specification of high temperature insulation material with low conductivity. Assuming a 150^{o}F external temperature, analyses indicate that 4 inches of Johns-Manville ceraform insulation would limit conduction losses to 3.7% of input power. Further increase in insulation thickness will add unnecessary weight without appreciably lowering the losses.

5.2.3.2 Transmission - Convection at Aperture

Sanders' solar receiver design uses a quartz window at the aperture to maintain the pressure in the cavity. Quartz is very efficient in transmission of ultraviolet and visible radiation, but there is a 4% loss of energy per face due to reflection. However, the sealed cavity design drastically reduced convective losses, thus offsetting reflection loss. Convection losses become important in both matrix and tube receivers where the aperture is open, especially in a dish tracking system when the sun is low and the receiver opening is nearly vertical. Under these conditions where the engine operates off design and all the available energy is required, the convective losses in an open system represent a greater percentage of losses than during design point operation. With a properly sealed window design, as demonstrated during the tests at White Sands on the Sanders 10 KWt receiver, convection losses are eliminated.

5.2.3.3 Radiation

Reradiation is a function of both the internal cavity temperature and the aperture size. The aperture size was optimized between incident energy and a nominal 1700°F reradiated cavity temperature as shown in Figure 5-2. In Figure 5-11, with an aperture diameter of 7.34 inches the reradiative losses are plotted as a function of effective cavity temperature for insolation levels of 100, 80 and 60%. For a given temperature, as insolation decreases the percentage reradiation losses

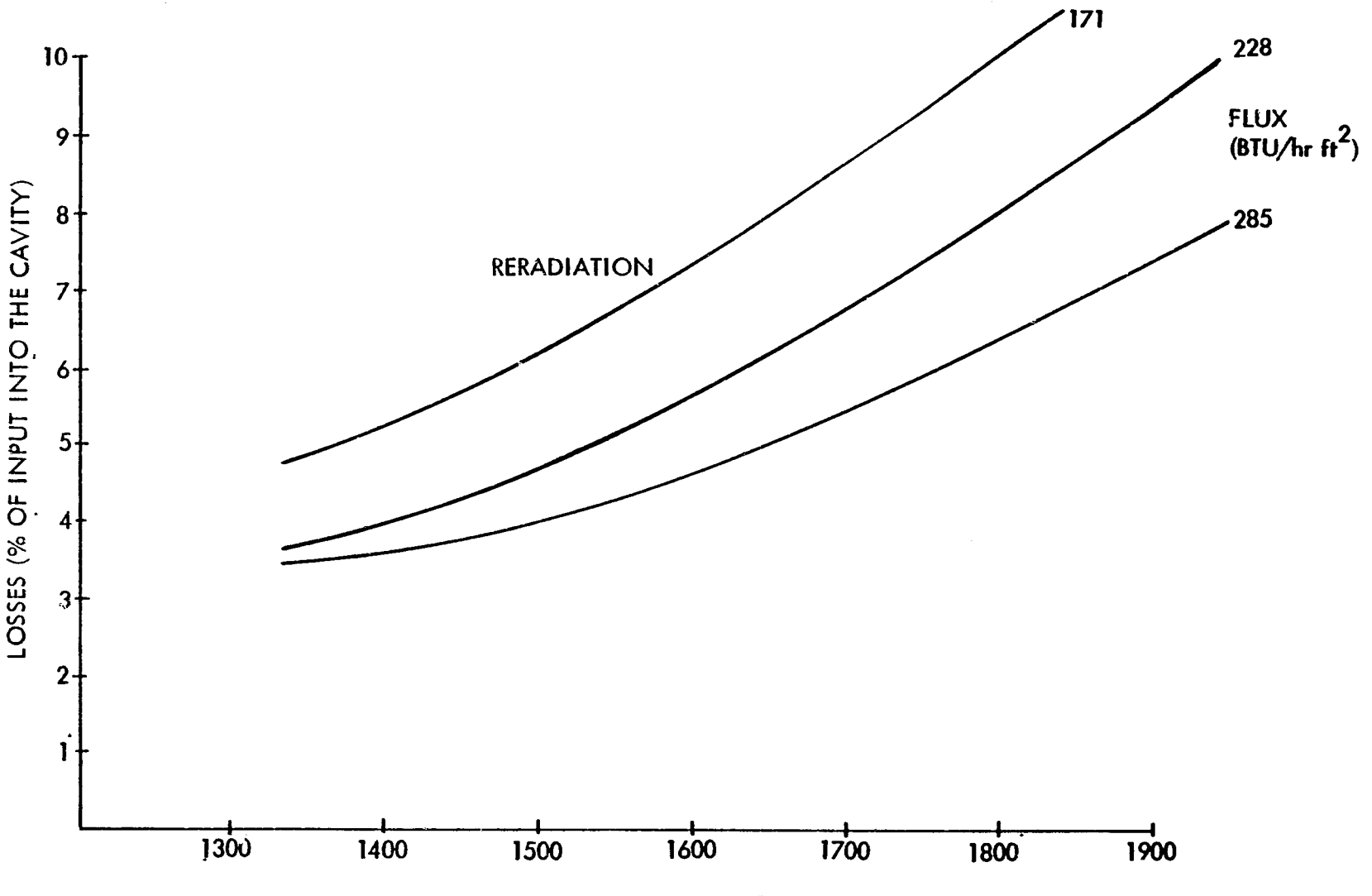

12078-31

Figure 5-11. Reradiation and conduction losses increase with cavity temperature.

will increase. At the design point, the reradiation losses total 4% of input power.

5.2.3.4 Pumping Losses

Pumping losses are associated with the frictional pressure drops throughout the system. Table 5-1 shows the pressure drops through the various components of the receiver/storage module when operating either at the design point or from the buffer storage. In either case, the total system pressure drop is below the maximum allowable drop as specified by JPL. This is accomplished with minimum ducting, smooth flow transitions, and a honeycomb matrix heat exchanger.

5.2.4 Buffer Storage

Sanders selected sensible heat storage for use in the proposed concept. This choice was based on two considerations. At the temperatures required for efficient Brayton engine operation, no other thermal storage concept investigated has reached a comparable state of development. In addition, a latent heat storage concept offers high risks in terms of eutectic containment at high temperatures. The sensible heat storage concept offered by Sanders is unique in that a thermal wavefront propagates down the storage container due to operation in a thermocline mode. This reduces the total storage system weight.

5.2.4.1 Storage Description

The common methods of storing thermal energy are difficult to use with heat engines because the temperature varies with the energy stored. We have found that such temperature variations are not required by any fundamental laws. The basic approach is to use a finely subdivided solid as the thermal storage medium, designed so that the heat transfer between air flowing through the structure and the solid material takes place with less "thermal impedance" than heat transfer along the airstream or through the solid.

If the solid is initially at a uniform low temperature (T_{MIN}) and air at a higher temperature (T_{MAX}) is introduced, the air has only to traverse a small distance before losing all its heat to the solid matrix near the inlet. It emerges at T_{MIN}. As airflow at T_{MAX} continues, heat is no longer transferred to the region near the inlet, which is already close to T_{MAX}; the heat is instead deposited in the adjacent matrix area, and is cooled to T_{MIN} in passing through the remaining matrix.

As this process continues, the matrix volume at T_{MAX} increases, and a "front" that separates the heated part from the cool part of the matrix propagates toward the outlet (at a speed much below the air velocity) until the entire matrix is at T_{MAX}. If flow continues, hot air emerges and thi energy is lost.

Reversal of the airflow, with air entering what was originally the outlet, causes a similar action in reverse. Heated air exits from what was originally the inlet, until the stored energy is depleted and all of the matrix is at T_{MIN}. Thus the temperatures in the matrix may be stratified, segregating the stored energy to one side of the stratification zone or thermocline.

This thermocline departs from ideality by occupying a finite zone in which the temperature varies smoothly between T_{MIN} and T_{MAX}. This zone enlarges with time but, with good design, occupies a relatively small fraction of the matrix. Thermocline details govern the efficiency with which stored energy may be extracted, however, the thermocline efficiency is better than with alternative thermal storage forms.

The segregation of stored energy in a volume that expands and contracts as energy is deposited and extracted is the ideal which the thermocline approaches. This natural thermal segregation mechanism was first discovered by Schumann[1] in 1929. Later studies have generalized this mechanism and have shown it to apply to gases as well as liquids, and to a variety of shapes of finely subdivided solids. Modeling studies and experiments conducted by Sanders have shown that, in honeycombs with cell diameters of the order of 0.1 inch and with solid fractions of 0.2 to 0.8, significant thermal segregation occurs with air at velocities in the 1 to 10 ft/sec range.

---

(1) T.E.W. Schumann, Heat Transfer: A Liquid Flowing Through a Porous Prism, J. Franklin Inst., Vol. 208, P. 405-16 (1929).

A major advantage of the honeycomb arrangement is that the pressure drops are reasonable for the required flow rates. For the receiver storage with a solid fraction (f)≈ 0.4, a diameter of 1.76 feet, and with adequate insulation, the thermocline spreads over several inches, and the pressure drop $(\Delta p/\Delta l)$ is given by:

$$\frac{\Delta p}{\Delta l} = \frac{\dot{m}}{A_{TOT}(1-f)} \frac{1}{p_o} (T_{MAX} + 460) \times 4.55 \times 10^{-6}$$

where

Δp = pressure drop (lb/ft^2)

Δl = length (ft)

p_o = absolute pressure (atm)

$\dot{m}$ = mass flow rate (lb/hr)

f = solid fraction

A_{TOT} = storage cross sectional area, total value (ft^2)

and

d_H = hydraulic diameter ≈ 0.003227 ft.

The sensible heat storage module integrated with the receiver design provides a 10 minute buffer to prevent the engine output power from dropping below shutdown levels during periods of insufficient insolation. A properly designed ceramic honeycomb matrix is very effective in generating a thermocline in the storage. Table 5-2 shows the characteristics of the Mullite honeycomb that will be the storage medium. A Mullite weight of 193 lb and overall dimensions of 1.76 ft

in diameter and 18 inches in height are used to achieve the 10 minute buffer storage.

TABLE 5-2

MULLITE HONEYCOMB CHARACTERISTICS

MATERIAL	MULLITE HONEYCOMB (CERAMIC)
REQUIRED MASS OF MULLITE	193 LB
HONEYCOMB SOLID FRACTION	0.4
HOLES/IN^2	400
STORAGE VOLUME	2.7 FT^3
STORAGE EQUIVALENT DIAMETER	1.76 FT
STORAGE HEIGHT	1.5 FT
REQUIRED ENERGY FOR 10 MINUTE BUFFER DURING STARTUP	21 KW-HR
REQUIRED ENERGY FOR 10 MINUTE BUFFER DURING OPERATION	10 KW-HR
STORAGE TEMPERATURE	1500^{o}F

5.2.4.2 Operation

Early in the morning, when the sun angle is low, it is not possible to operate the turbine until the insolation levels reach startup values. Under these low insolation conditions, storage charging is begun using the starter-driven compressor to circulate the air. Charging of the storage will begin at the threshold level where input power equals system losses. At the 0.1 kW/m^2 and zero air flow level,

the receiver matrix will reach 1500°F. Above this insolation level, the storage system can be charged.

The JPL furnished insolation data was integrated to determine the available energy. Figure 5-12 shows insolation and available energy versus time of day. By using the starter and compressor, and ramping the flow according to Figure 5-13, storage will be filled in 45 minutes. By this time, the insolation level will have reached 0.6 kW/m^2 and turbine operation can begin under off-design conditions.

If for any reason the storage is depleted during normal operation, it is refilled before resuming turbine operation. This can be done in 25 minutes with solar flux at design levels. Figure 5-14 shows the temperature profile with time. Note that the honeycomb output temperature reaches an equilibrium temperature of 1500°F at the design mass flow.

The storage, which is maintained at 1550°F, is used to prevent the turbine inlet temperature from falling below 1000°F. When receiver output temperature reaches 660°F, a turbine inlet temperature of 1000°F can be maintained by discharging the storage with an air mass flow of 0.24 lb/sec, and mixing it with the receiver outlet air. This combination of temperature and flow assures a 10 minute turbine operation at 1000°F from storage as shown by Figure 5-15.

Throughout the day, a leakage flow is provided to the storage to balance the conduction losses. During this time, the pressure

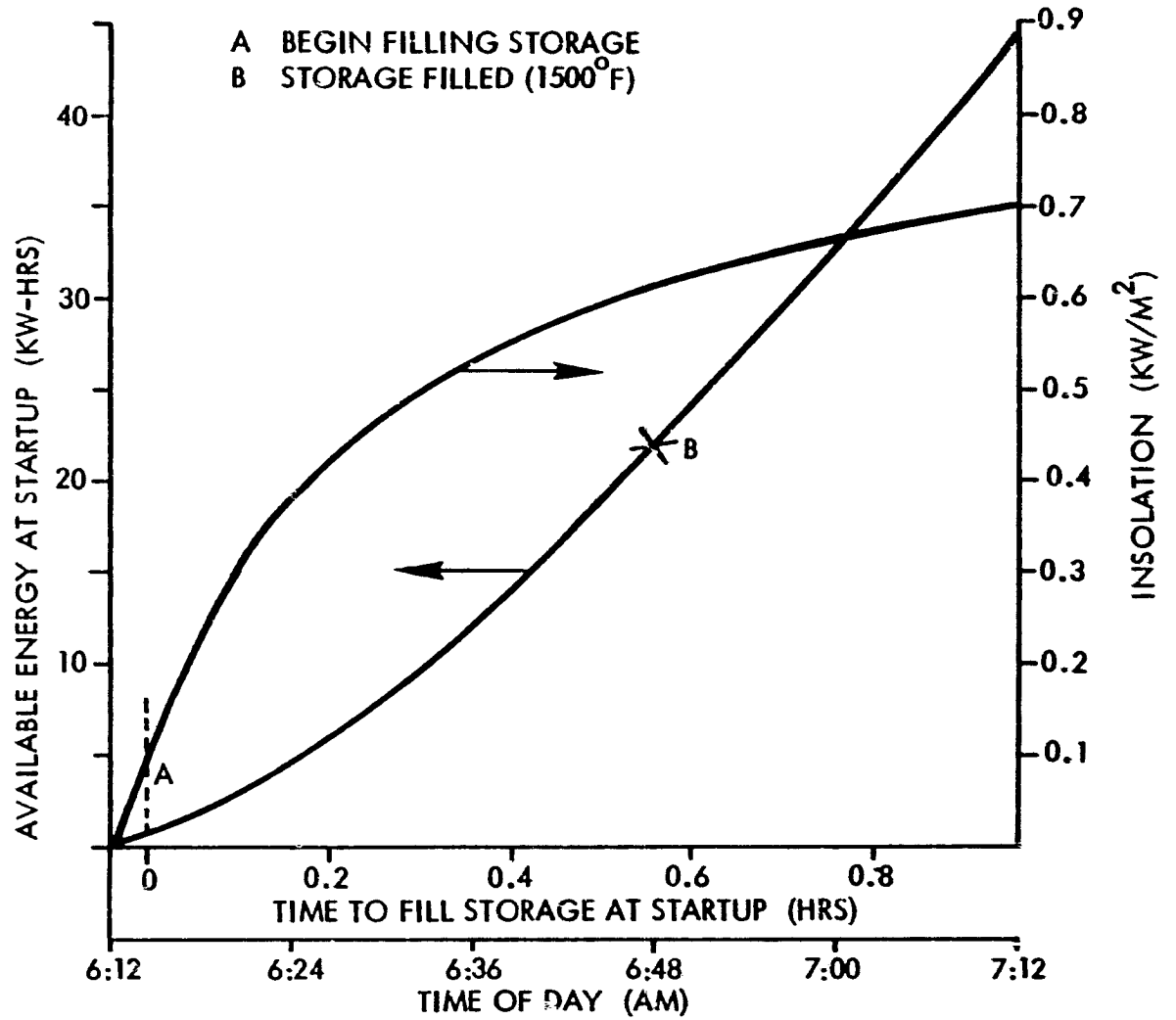

12078-24

Figure 5-12. As shown in this plot of storage capacity and insolation versus time of day, the storage system can begin charging when the insolation level reaches 0.1 kW/m^2.

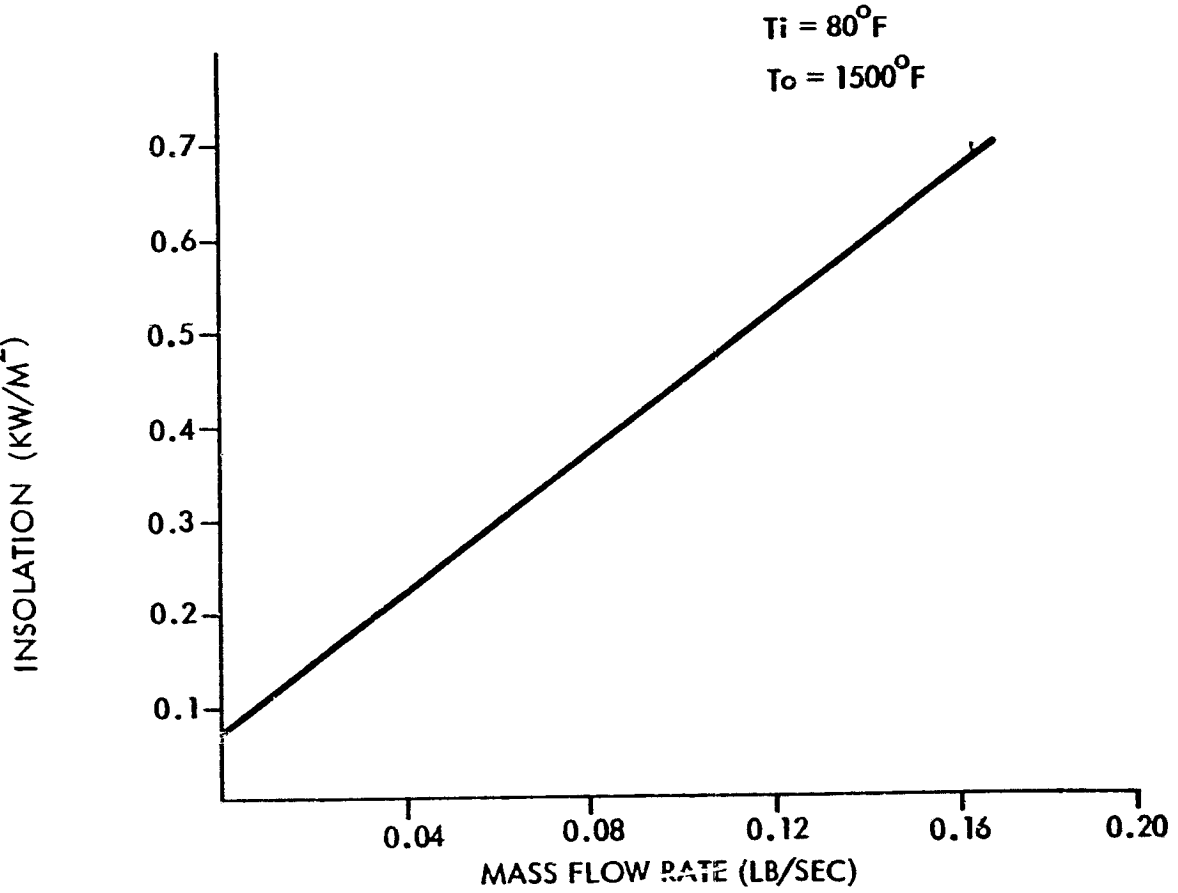

12078-15

Figure 5-13. By varying the mass flow as shown here, and using the starter and compressor, storage will be filled in 45 minutes.

AIR STREAM PROFILE
DURING STORAGE CHARGE

FLOW RATE THROUGH STORAGE = 0.533 LB/SEC.

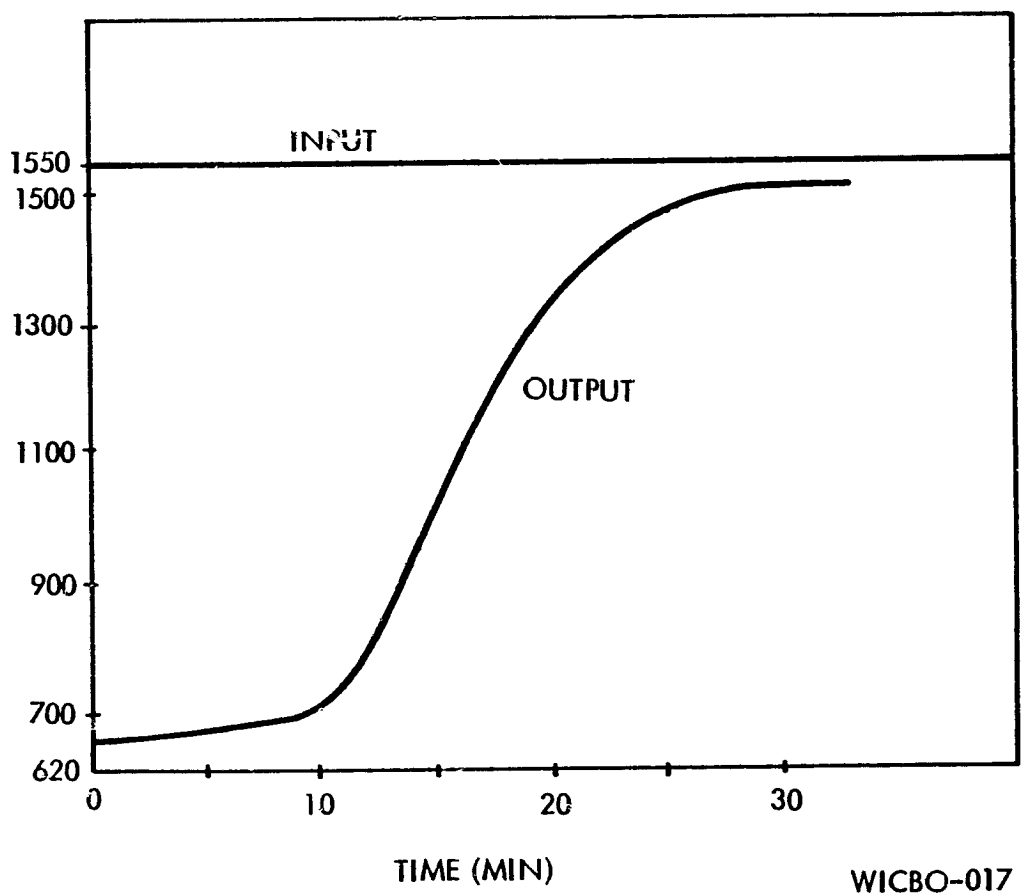

Figure 5-14. As the storage is charged, the output air stream temperature rises to 1500°F in approximately 25 minutes.

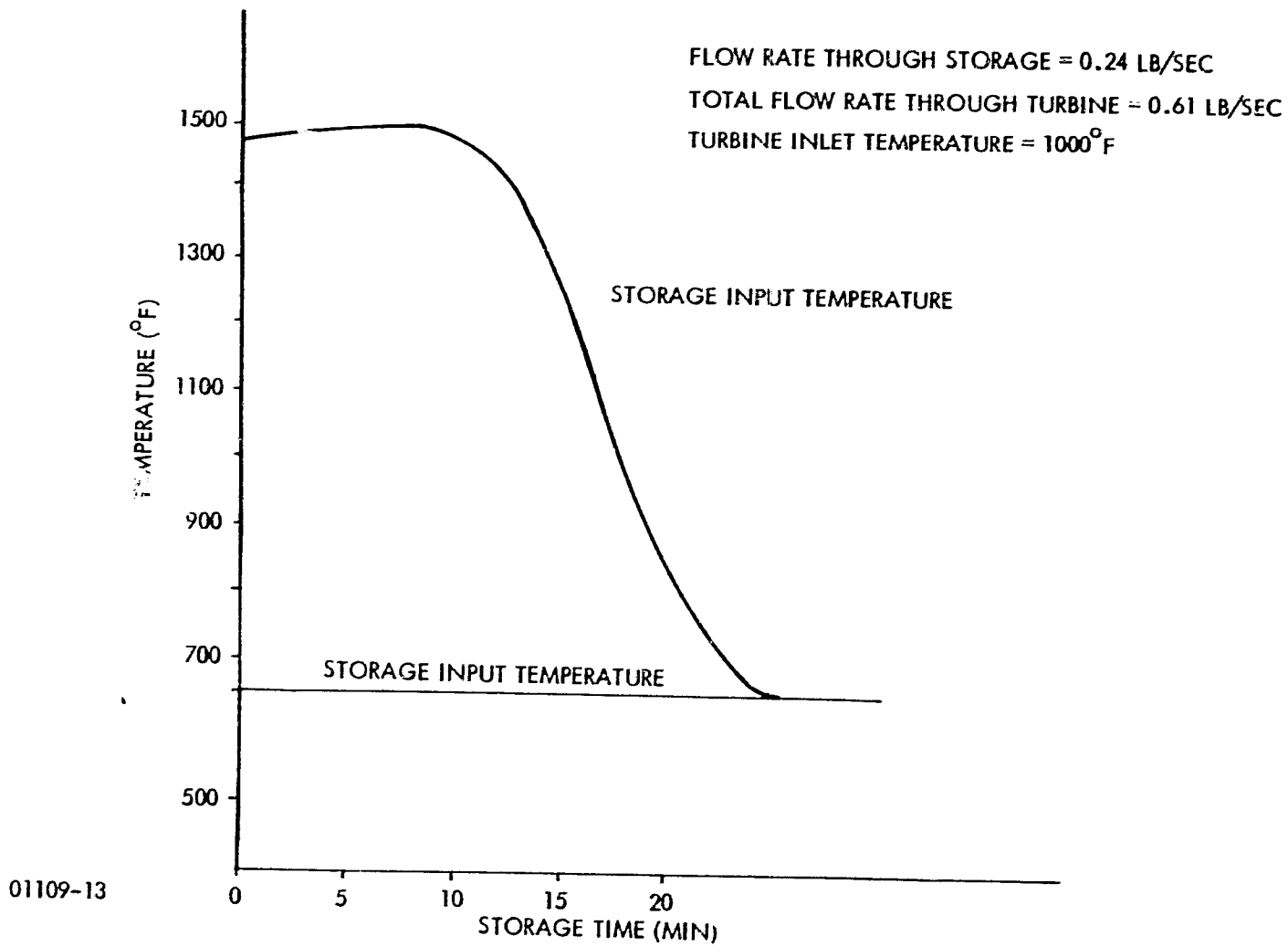

Figure 5-15. By mixing hot air from the stove (0.24 lb/sec) with receiver air at 660°F, a turbine inlet temperature of 1000°F can be maintained and can assure 10 minute turbine operation from storage.

drop in the storage is insignificant. However, during discharge the pressure drop suddenly increases as a result of increase in the mass flow rate through storage. Figure 5-16 shows this variation during charge and discharge. The pressure drop decreases during discharge because of the density change in the air.

5.2.4.3 Control

The storage operation is governed by the status of the turbine inlet temperature. When the turbine inlet temperature drops to 1000^{o}F, the storage valve is opened to increase the ratio of air flow through the Mullite. High temperature valves are used to modulate the flow directed to storage and the receiver outlet. These valves provide a positive flow control during system operation.

The receiver valve is a 4 inch butterfly valve with very low flow resistance. It has variable flow admission characteristics that allow mixing with storage air. The storage valve is basically composed of two flat plates with cutouts. The bottom plate is stationary while the top one rotates to various angles to allow a predetermined amount of air to go through the storage. Table 5-3 shows the valve positions during normal daily operation. These position depend on the prevailing conditions and will be controlled by commands generated from the central processor.

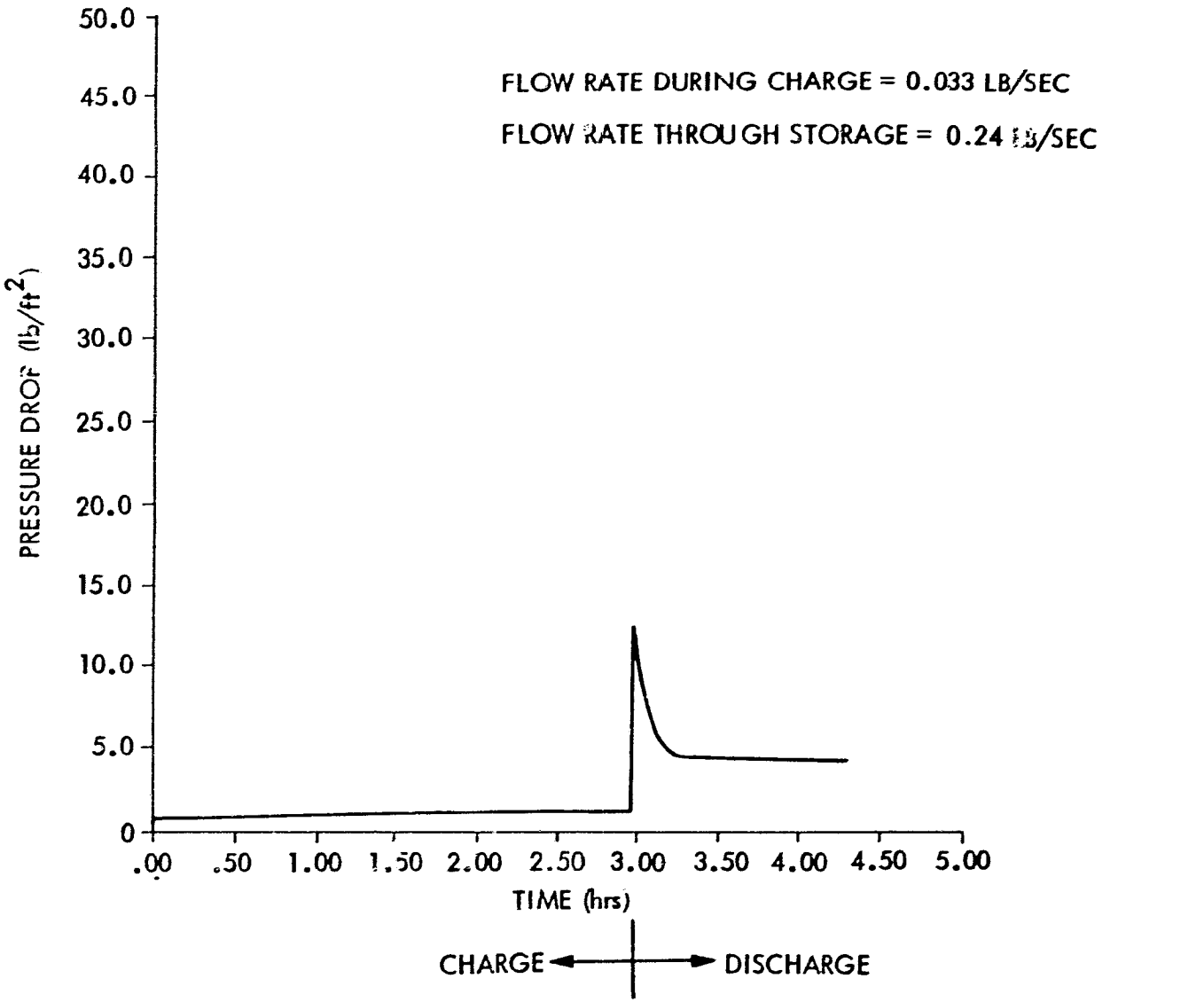

Figure 5-16. During stove discharge, pressure drop in storage suddenly increases as a result of the increase in mass flow rate. The pressure drop then decreases during discharge because the air density changes.

TABLE 5-3. VALVE POSITIONS DURING NORMAL DAILY OPERATION

	RECEIVER VALVE	STORAGE VALVE
STARTUP 6:15 - 6:48 AM	CLOSED	OPEN
ENGINE OFF DESIGN OPERATION 7 - 9:30 AM	OPEN	CLOSED
DESIGN OPERATION 9:30 AM - 2:30 PM	OPEN	2% OPEN
OFF DESIGN OPERATION 2:30 - 4:50 PM	OPEN	CLOSED
STORAGE DISCHARGE 4:50 - 5:00 PM	60% OPEN	40% OPEN
STORAGE CHARGE DURING NORMAL OPERATION	CLOSED	OPEN

5.2.5 Structural Design

To assure trouble-free, reliable service, a considerable effort was expended in the design of the receiver to assure its ability to withstand the structural, thermal, and pressure loads. A finite element analysis was made to determine the stresses which would result from thermal loads on the receiver heat exchanger matrix. Furthermore, ASME boiler codes were used to specify the shell thicknesses.

5.2.5.1 Pressurized Receiver

The Sanders concept uses a matrix heat exchanger in a pressurized cavity. To maintain the pressure, a fused quartz window is installed at the aperture. Fused quartz is commercially available and has a high transmissivity (0.99) for the ultraviolet and visible radiation spectrum. In addition, it has low infrared absorptance (out to 3.6μ). However, a 4% reflection loss occurs at each face of the quartz window.

Quartz is very strong in compression, in excess of 14,000 psi, and its tensile properties are greatly influenced by the degree of surface flaws or discontinuities. For good surface quality, tensile strength is in excess of 6,962 psi. In practice, a design safety factor of 7 is used in calculating maximum stress.

Based on the calculated stresses, for a safety factor of 7, a 7.34 inch diameter by 0.625 inch thick quartz window is required for

a 45 psi system pressure. The quartz itself is surrounded by high temperature gasketing capable of withstanding 2300°F. The gasketing provides a compliant surface and follows any thermal expansions encountered during normal daily operation. A bolt flange fastens the gasketing material and window to the aperture plate.

The operating pressure of 35 psia necessitates the use of ASME boiler codes in designing the various components of the receiver housing. Table 5-4 shows the housing components, the temperature and pressure conditions, and the estimated thicknesses based on the codes. The pressure housing, a 1/16 inch thick carbon steel shell, will be maintained at a low temperature by the 4 inch thick insulation.

5.2.5.2 Stress Analysis

Computerized structural programs have been extensively developed by Sanders using finite element analysis techniques. Critical system subcomponents were investigated, including:

- Honeycomb panels
- Structural components
- Matrix support for the honeycomb

These subcomponents were studied thermally for both steady state and transient conditions, and structurally for both static and dynamic loading. A scoping technique was used to analyze the honeycomb matrix

TABLE 5-4. ASME PRESSURE VESSEL CODES
(Structural Considerations)

	INTERNAL SHELLS	EXTERNAL SHELL	FLANGES		DUCTS	APERTURE PLATE
			HOT	COLD		
TEMPERATURE (^{o}F)	1500	200	1500	200	1500	200
PRESSURE (PSI)	45	45	45	45	45	45
MATERIAL	316 L STAINLESS STEEL	CARBON STEEL	S.S	C.S	316 L	CARBON STEEL
THICKNESS	1/16	1/16	3/16	3/16	1/16	1/4

microscopically, considering isotropic properties. The results of the microscopic studies were then applied to microscopic studies of the honeycomb matrix. In addition, Sanders' computational capability with coupled thermal and structural analysis aided the design of the matrix support structure.

A detailed finite element model was exercised to study the stresses resulting in the matrix heat exchanger based on the temperature profile developed in Figure 5-8. Figure 5-17 shows the honeycomb panel, with tube outlined detailed in with the coordinate axis as defined in the analyses. Since each tube of the honeycomb is part of the overall structure, the edges were constrained to be straight line. The edges AA', BB', CC', and DD' were allowed to move with thermal expansion but still retain their straight line shape.

The results of the analyses on silicon carbide (SiC), Cordierite and Mullite are shown in Figure 5-18. Originally, 1.8 inch of SiC was investigated as the receiver heat exchanger thickness. The margin of safety was not sufficient to warrant acceptance of the design. Due to the high absorptivity of SiC, the thickness of the disk was reduced to 1.3 inches without degrading the required heat transfer characteristics. As a result, an adequate safety factor was developed.

The higher cost of 22 inch SiC disks in limited production quantities, resulted in a decision to use Cordierite as the heat

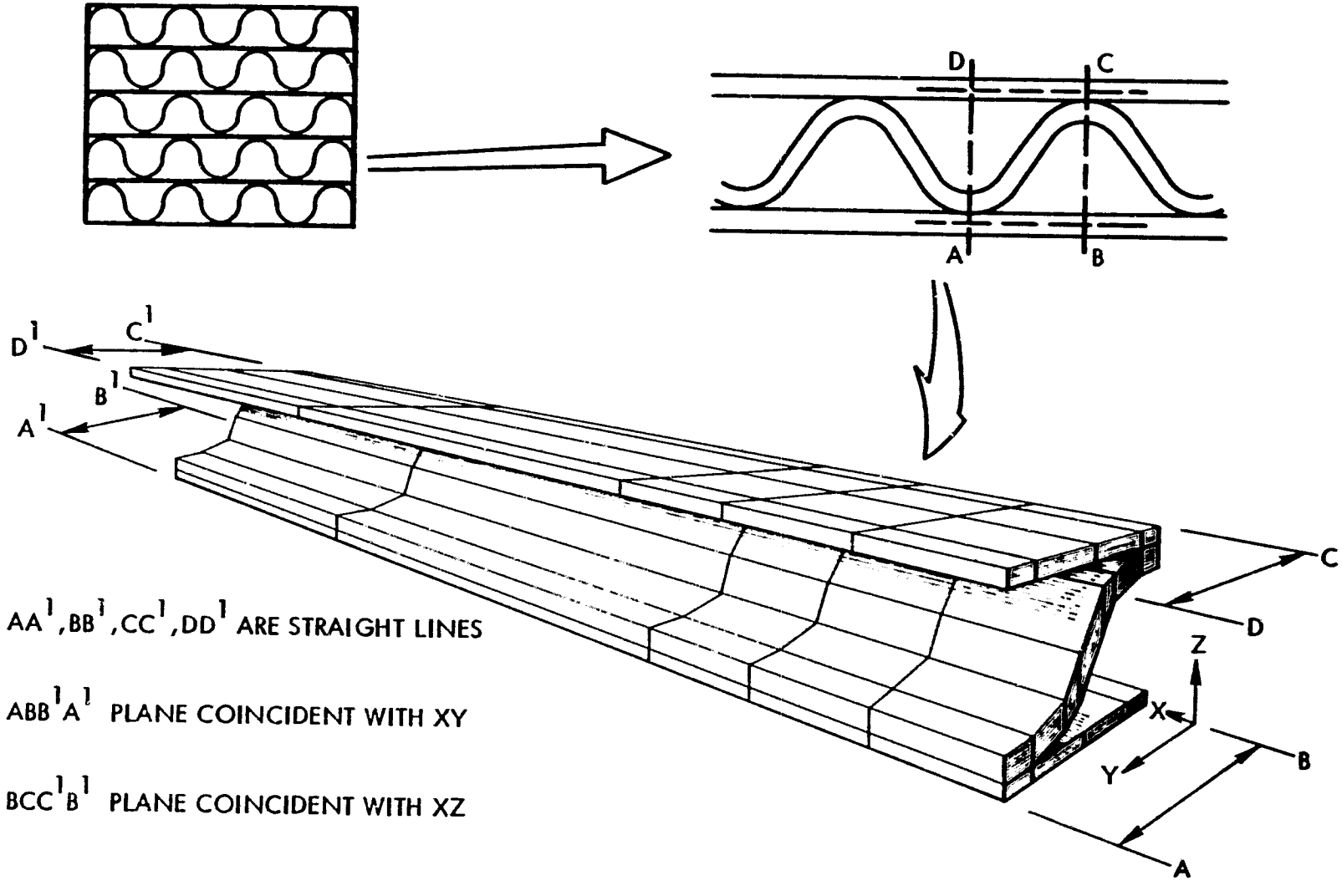

12078-66

Figure 5-17. This detailed, 75 element finite element model was used to study the stresses in the matrix heat

MATERIAL	SiC - 1.8"	SiC - 1.3"	CORDIERITE - 1.3"	MULLITE - 1.3"
EFFECTIVE STRESS (psi)	28.K	20.K	220	690
SAFETY FACTOR	.96	1.8	13.	22.
MAXIMUM SHEAR (psi)	14.K	10.K	120	360

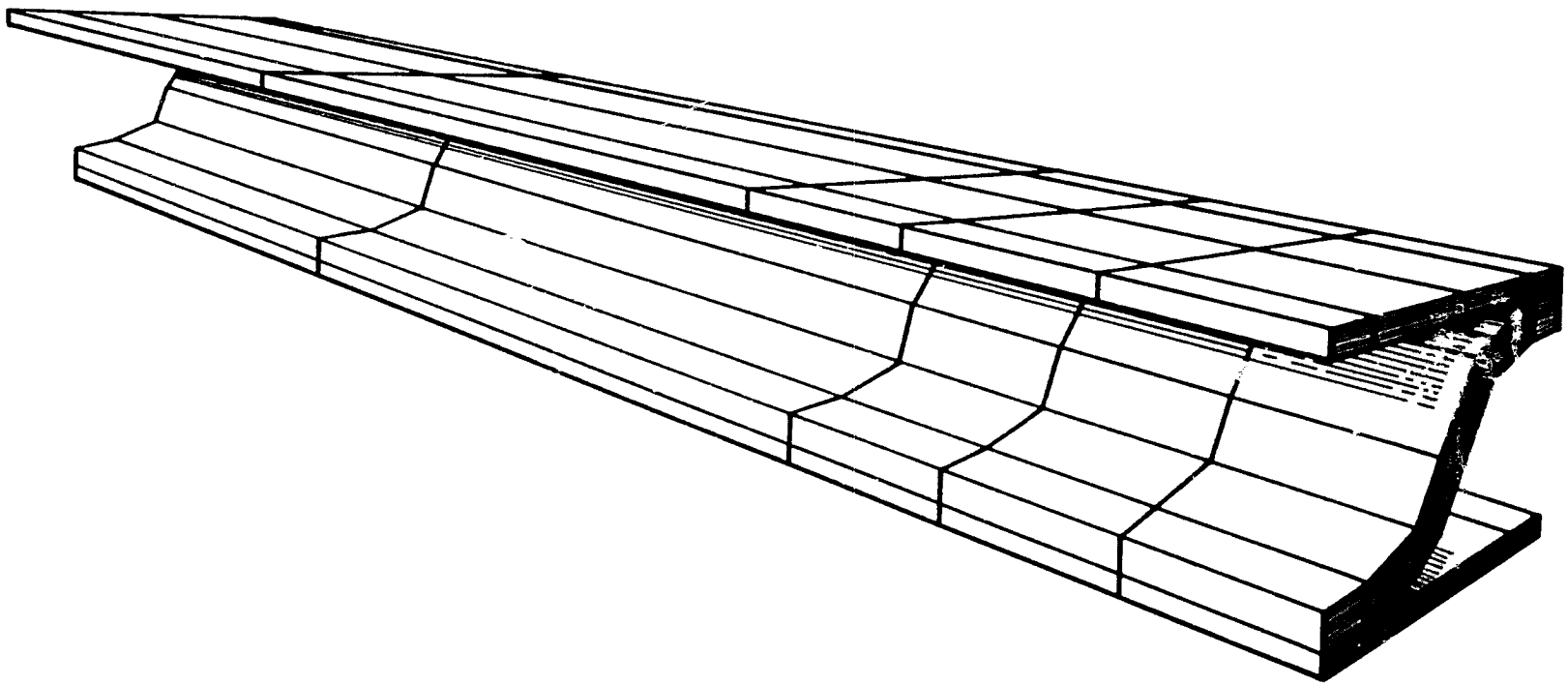

12078-65

Figure 5-18. Nominal, operating honeycomb stresses, safety factor and shear were developed for SiC, Cordierite and Mullite.

exchanger material for the near term application. Due to its low absorptivity (0.4), the Cordierite thickness required is twice that of SiC. Therefore, two disks, each 1.3 inch thick, will be mounted in close proximity to satisfy the thermal requirements. Sanders' analysis of the stresses on a 1.3 inch thick disk show a safety factor of 13.

Stresses on Mullite were also investigated since it is used for the storage material. Here again, because of its low thermal coefficient of expansion, the stress was very low.

5.2.5.3 Materials

Materials were specified throughout the design that were compatible with the high temperature environment. Table 5-5 shows the various components and the materials used for their design. All the internal components are made of ceramic and 316 stainless steel and will survive to 1900^{o}F. The pressure shell is designed with carbon steel and 4 inches of internal insulation. This is a considerably thinner shell than would be required with external insulation.

Cordierite and Mullite are used for the heat exchanger and storage materials. These ceramic materials can withstand temperatures higher than the system will encounter during normal operation.

TABLE 5-5. CHARACTERISTICS OF RECEIVER MATERIALS

COMPONENT	MATERIAL	LIMIT (°F)	DESIGN/CONDITIONS (°F)
HEAT EXCHANGER	CORDIERITE	2300	1700
INTERNAL SHELLS	STAINLESS STEEL	1900	1600
EXTERNAL SHELLS	CARBON STEEL	1200	200
INSULATION	CERAFORM	2300	1600
DUCTS	STAINLESS STEEL	1900	1600
VALVES	STAINLESS STEEL	1900	1550
STORAGE MEDIUM	MULLITE	2500	1550

5.2.5.4 Codes

ASME boiler and pressure vessel codes, Section VIII, Div. I, were used to design the outside shell, aperture plate, the flanges and the ducts. The design pressure for these components was 45 psia. Use of the ASME codes does not appear to impact the cost or weight of the unit.

5.2.5.5 System Weight and Volume Estimates

Throughout the design, a conscious effort was made to minimize receiver/storage weight. Table 5-6 shows the breakdown of weights and volume estimates of the three main components of the point focusing system. Working within a 1100 lb constraint in total component weight, the receiver/storage module of 580 lb accounts for slightly more than 1/2 the system weight. If storage is eliminated, then system weight is reduced by 380 lb. The C.G. of the unit was calculated to be at 4.1 feet behind the aperture plane where the mounting ring would be located.

The projected area of obscuration is estimated to be 12.56 ft^2. Based on a 36 foot concentrator, this translates into a 1.23% obscuration of the concentrator area.

TABLE 5-6. WEIGHT AND VOLUME

	RECEIVER	STORAGE	RECEIVER/STORAGE MODULE	POWER GENERATION MODULE	TOTAL SYSTEM
WEIGHT (LBS)	200	380	580	500	1080
OVERALL DIMENSIONS	3.33' DIAM × 2.66'	2.66' DIAM 3.34	3' DIAM 6	3.33' DIAM × 2.66'	3.15 DIAM × 8.66
VOLUME Ft^3	23.16	18.6	42	23	65

SYSTEM C.G. FROM APERTURE PLATE = 4.1 Ft CONCENTRATOR AREA = 1018 Ft^2

OBSTRUCTION AREA = 12.56 Ft^2 BLOCKAGE = 1.23%

5.2.6 System Operation

5.2.6.1 Design Point Operation

The Air Brayton Solar Reciever will operate on-design under the conditions specified in the cycle schematic of Figure 2-2. Preheated air at 1050°F is fed to the receiver and heated with incident radiation to the turbine inlet condition of 1500°F. The 1177°F turbine exhaust is cooled in the recuperator with the compressor air and exhausted to the atmosphere at 400°F. Component efficiencies were provided by JPL as shown in Table 2-8. The calculated receiver efficiency of 86% has been added to the table. Cycle analysis

TABLE 2-8. COMPONENT EFFICIENCIES

CONCENTRATOR	$\rho = 0.9$
RECEIVER	$\eta_{REC} = 0.866$
RECUPERATOR	$\eta_{RCPR} = 0.865$
COMPRESSOR	$\eta_C = 0.796$
TURBINE	$\eta_t = 0.872$
GEAR BOX	$\eta_G = 0.96$
MECHANICAL (COMPRESSOR & TURBINE)	$\eta_{mt} = \eta_{mc} = 0.95$
ALTERNATOR	$\eta_A = 0.88$

indicates a system thermal efficiency of 30% and overall efficiency of 21% with a resulting power output of 17 KWe.

5.2.6.2 Off-Design Operation

A constant RPM control has been selected as the most viable mode of operation for the Air Brayton Solar Receiver. To study the effect of off-design operation, cycle calculations at various turbine inlet temperatures and pressure ratios were carried out. Figure 5-19 shows the results plotted as a function of overall cycle efficiency. For constant RPM control the turbine inlet temperature falls with insolation, while maintaining overall pressure ratio. For example, when the turbine inlet temperature drops from 1500°F to 1300°F at a pressure ratio of 2.5, the overall efficiency drops from 0.21 to 0.18.

Figure 5-20 relates the turbine inlet temperature to the heat rate in the airstream. These results at various insolation levels were obtained from the receiver efficiency calculations of Figure 5-17. The constant RPM control necessitates that the engine follow the characteristics shown in Figure 5-20. As insolation drops, so will the turbine inlet temperature. Figure 5-21 plots the turbine input power, output power, flow rate and overall efficiency versus turbine inlet temperature. Overall efficiency drops as turbine inlet temperature is decreased due to increased losses. This brings the turbine to shutdown levels at 1000°F turbine inelt temperatures.

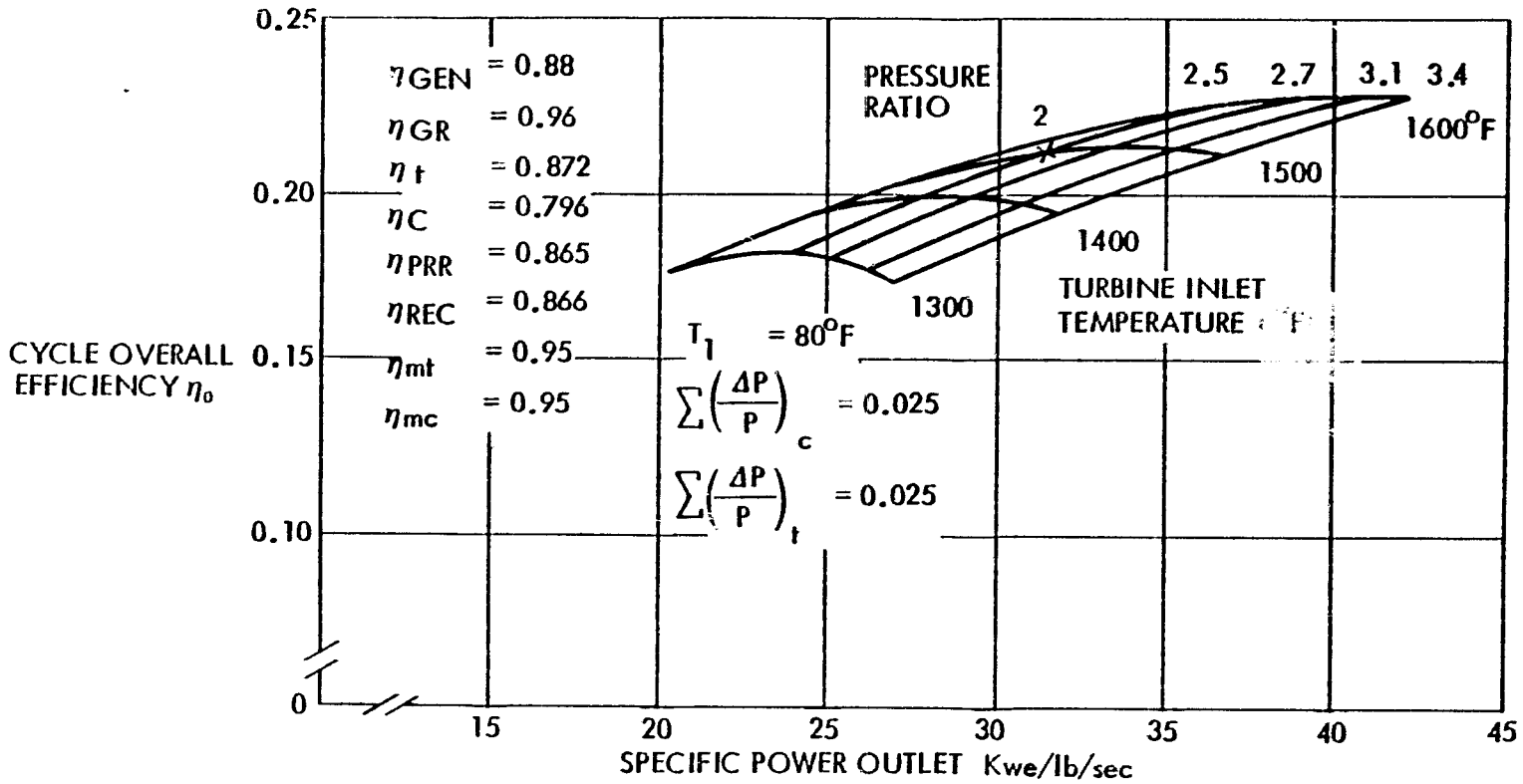

11288-10

Figure 5-19. Engine characteristics were evaluated at various turbine inlet conditions.

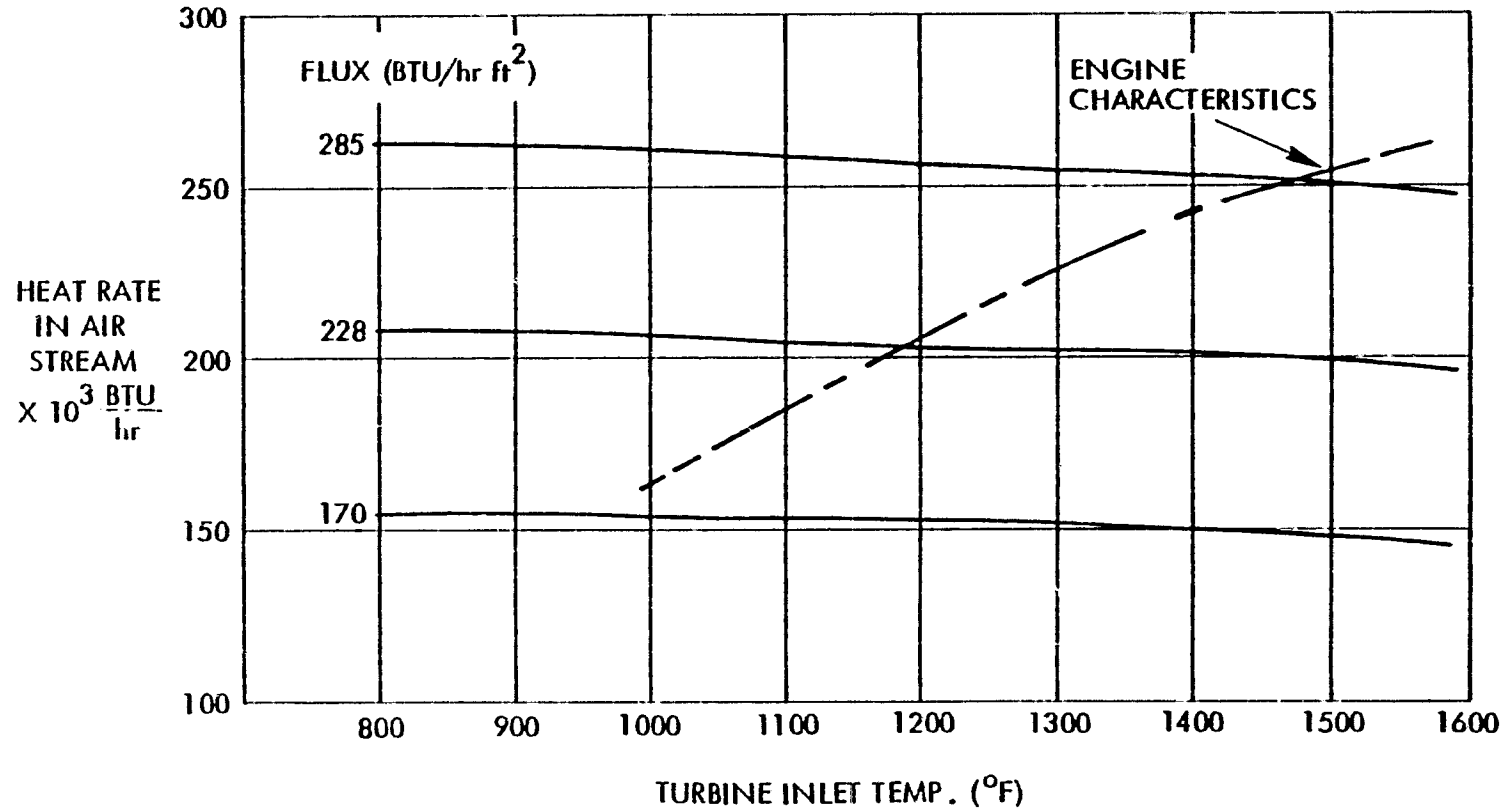

11288-11

Figure 5-20. With a constant RPM control, the turbine inlet temperature must drop as the insolation drops.

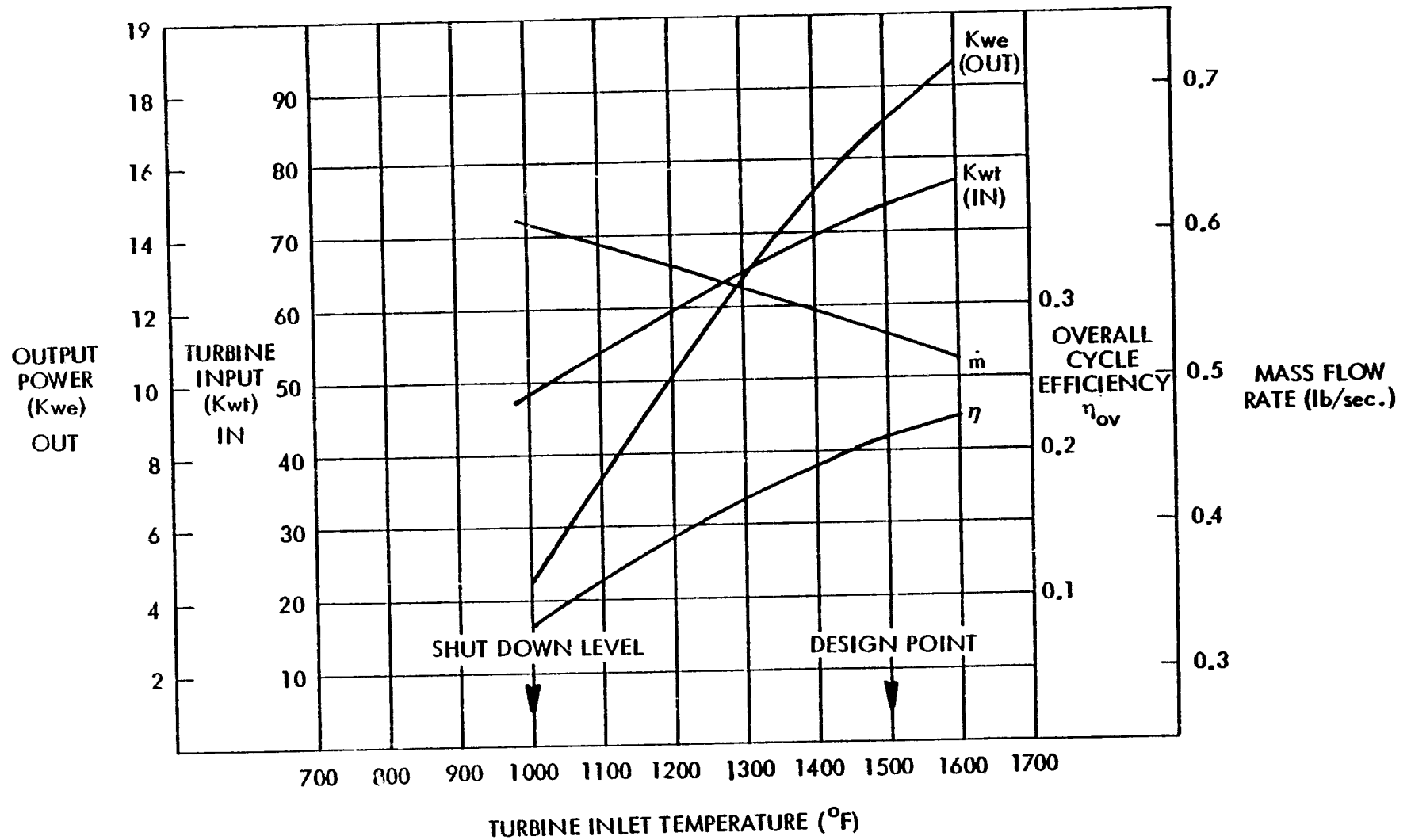

11288-12

Figure 5-21. System parameters are plotted against turbine inlet temperature.

Based on turbine operating characteristics, the output power is related to the solar flux as shown in Figure 5-22. When the flux reaches 60% of the full value the system will be shut down.

5.2.6.3 Start-up/Shut-down

The receiver response to startup and shutdown, Figure 5-23, has been investigated based on the assumed boundary conditions on receiver inlet temperature, flow rate, and input power. Ramping these three variables from an initial state to design conditions, the response of the matrix heat exchanger rises in a ramp and establishes steady state equilibrium in 15 minutes. At the end of one hour of operation, system shutdown was simulated by ramping down all three variables. The receiver outlet air temperature responded by decreasing below 1500^{o}F in 10 minutes due to the removal of solar insolation on the matrix. Subsequently, the slope of the response is less severe because, in the absence of direct insolation, the receiver matrix has a different time constant.

5.2.6.4 Control System

The control system of the ABSR is envisioned as in Figure 5-24 to have a microprocessor into which monitored data will be fed. Subsequently, a specific control action will be initiated depending on the prevailing conditions.

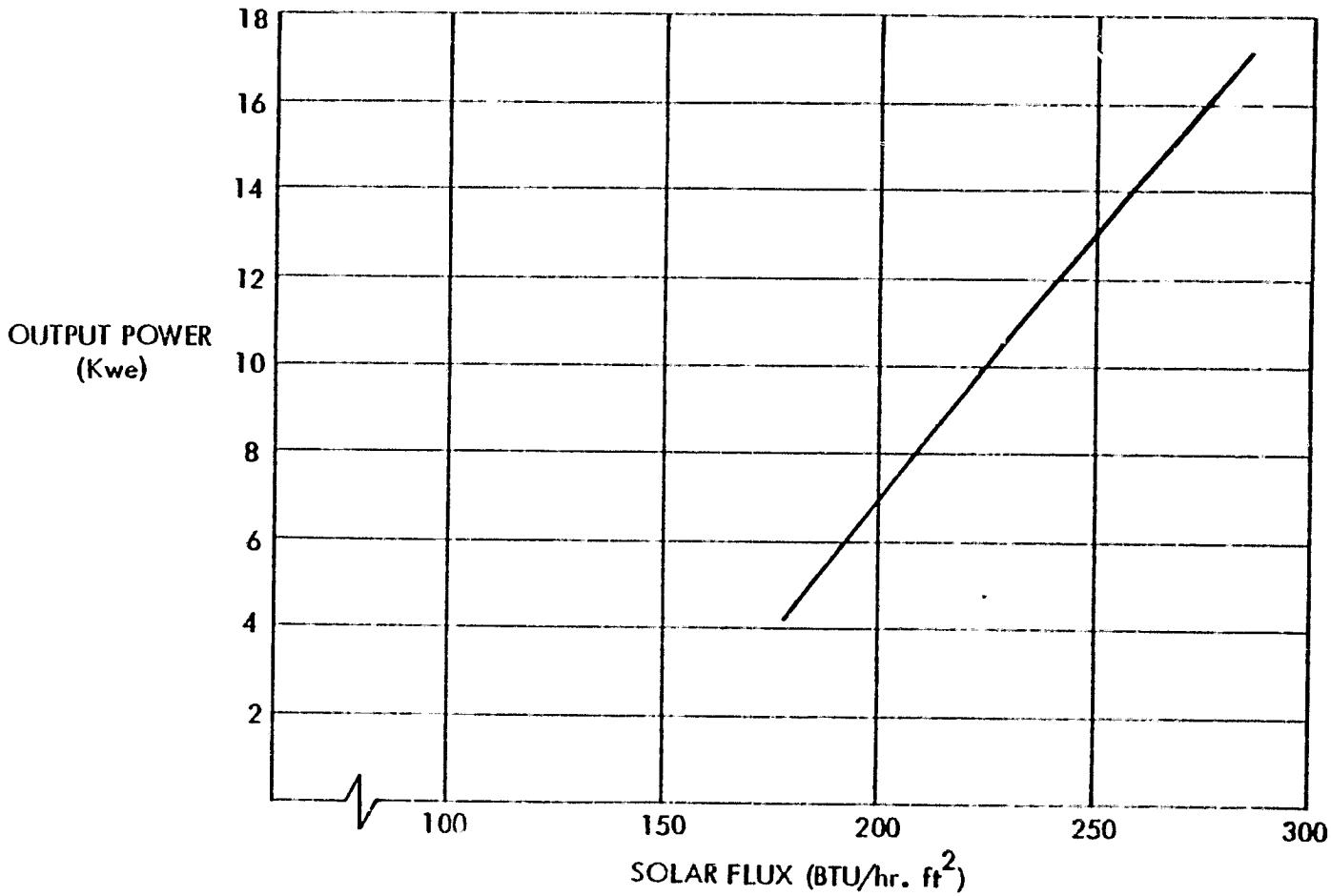

11288-13

Figure 5-22. System output increases nearly linearly with increased solar flux.

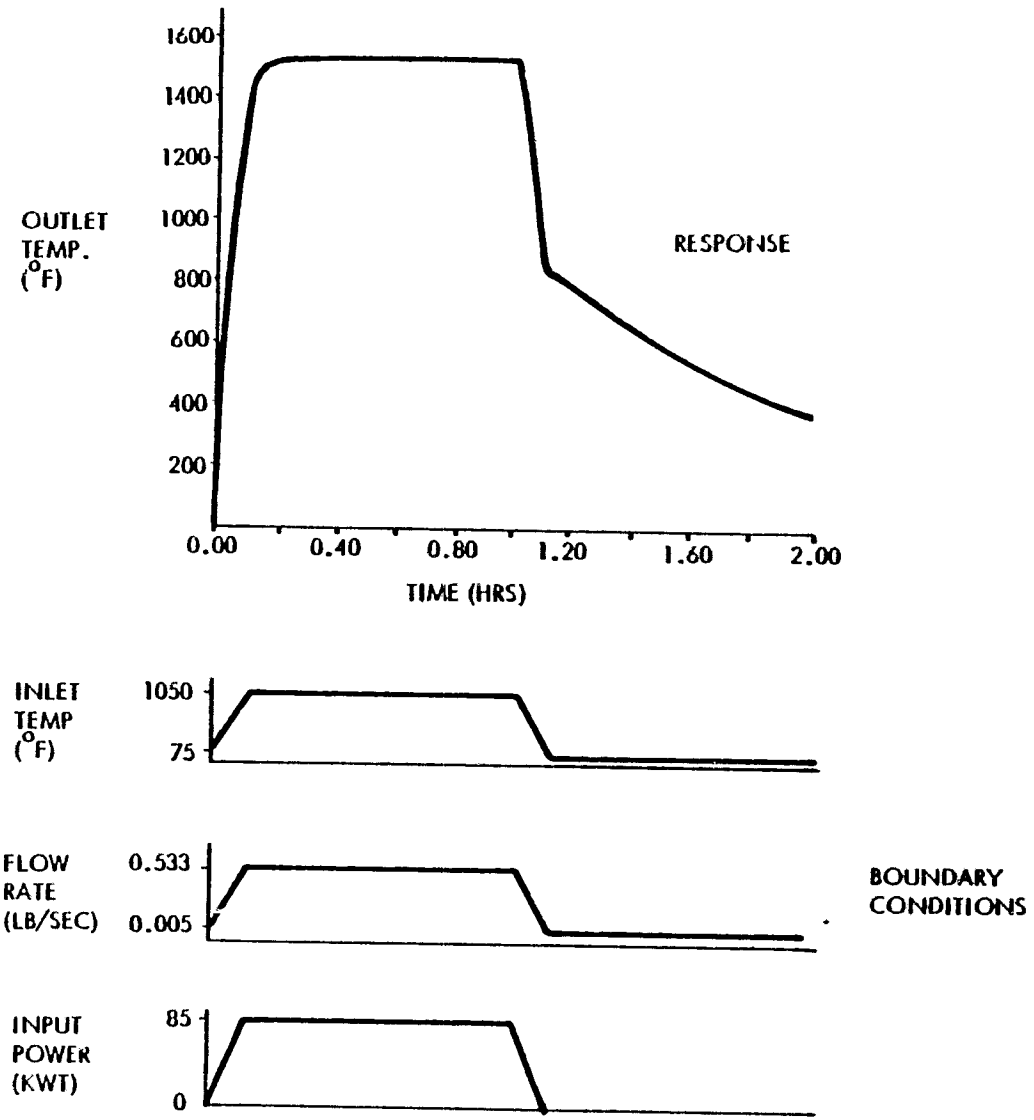

12078-27

Figure 5-23. Receiver response to start-up and shut-down was investigated based on receiver inlet temperature, flow rate and input power.

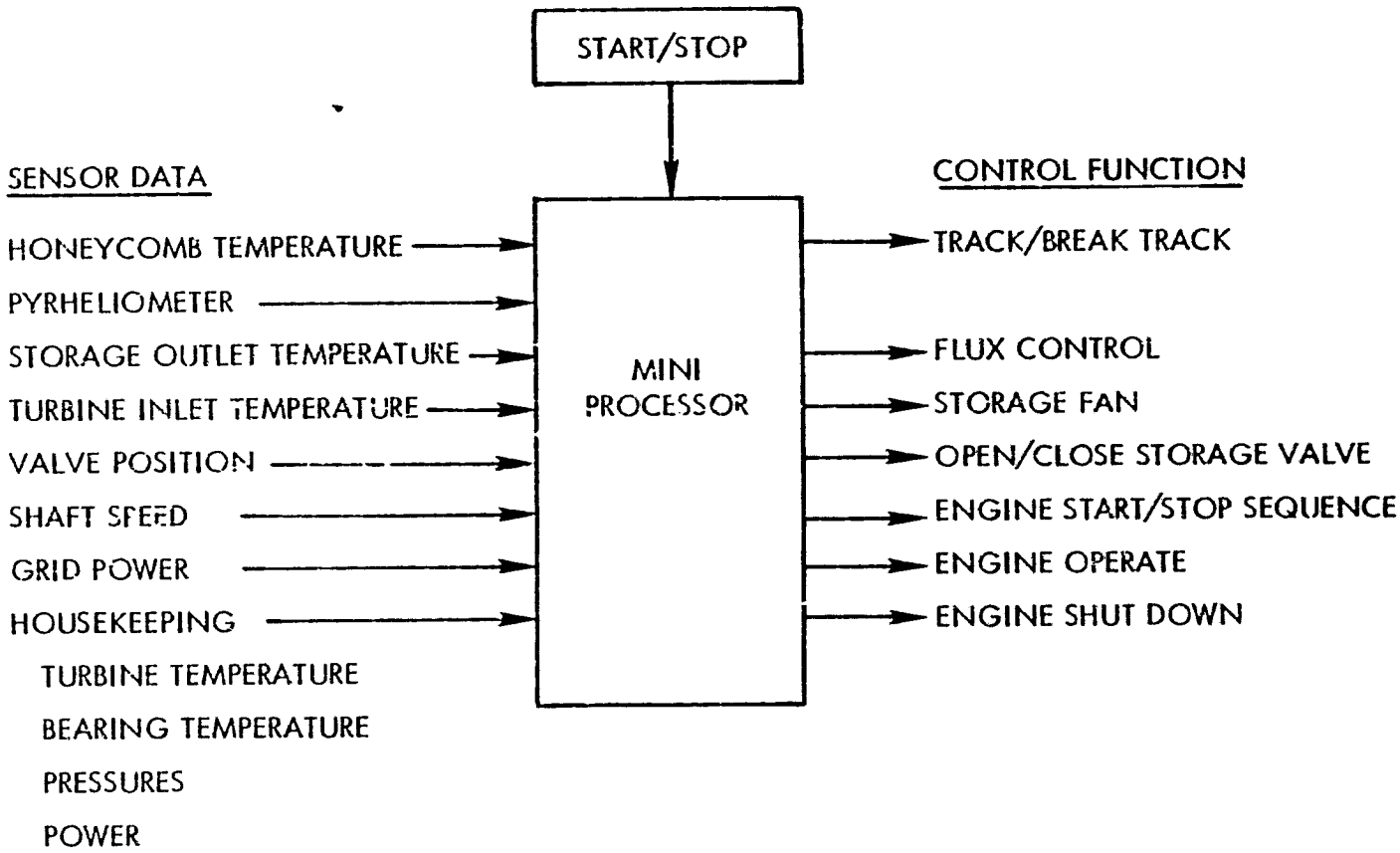

12148-3

Figure 5-24. A miniprocessor will form the heart of the ABSR control system.

Critical component temperatures and pressures will be monitored to initiate a given control fucntion and to assure the reliable operation of the unit. For example, receiver honeycomb and turbine inlet temperature data will determine how the flow will be apportioned between receiver and storage. In addition, this temperature information is important to initiate start-up and shutdown procedures and to initiate safety shutdowns. Turbine shaft speed data should be monitored to assure a constant RPM throughout the operation.

During start-up, the equipment will be powered up and collector tracking will commence after a "ready" signal. At the beginning of the day, the starter-driven compressor will fill the storage to 1500^{o}F temperature. Subsequently, the engine will be started. Once engine RPM reaches the synchronous speed and the generator is properly phased, the unit is connected to the load circuit. When cloud cover drops receiver outlet temperatures to 1000^{o}F, storage is activated by splitting the flow maintaining 1000^{o}F at the turbine inlet. By appropriate flow mixing, the 10 minute buffer prevents the engine from falling below shutdown levels. Once the storage has been exhausted, it is filled, as soon as there is sufficient insolation, prior to restarting the engine. A 5 minute engine shutdown is initiated at the end of the day when insolation is no longer sufficient to operate the unit.

Emergency shutdown is initiated when over-temperature or overpressurization is detected. In this case, the concentrator must break-track or air must bypass the recuperator.

5.2.7 Safety

To assure personnel safety, the system is designed in accordance with the appropriate safety codes. The receiver, for example, is designed to satisfy ASME boiler code requirements because it is pressurized to 35 psia in operation. Electrical controls for the receiver valve operation and for the instrumentation lines are wired in accordance with NEMA standards.

The system, presumably, will be capable of fully automatic and unattended operation.

Thermocouples (face, inlet, cavity, storage and outlet) are provided to monitor system performance and provide inputs to the system control (microprocessor). Receiver face temperatures will be used to correct tracking errors. Inlet and outlet pressures provide flow measurement and monitor system performance. Pressure fluctuations characteristic of compressor stall or turbine malfunction will signal the tracking to slew off-sun and would initiate the system shutdown sequence.

Passive radiation shields and sacrificial insulation protection on the receiver front face will withstand full sun in the event of tracker failure. After correction of the tracker malfunctions, the face insulation is replaced if excessive ablation has occurred. However, natural convection and radiation cooling of the front face shields will minimize the frequency of replacement; replacement of these parts should be required only after several tracker failures.

In addition, unlike the tube receiver heat exchanger where a single tube failure would shut down the entire unit, using the honeycomb matrix a trouble-free operation is assured even if many of the holes are plugged or cracked. This flexibility along with its high performance capability makes the ceramic matrix heat exchanger superior in Air Brayton Solar Receiver applications.

5.2.8 System Specifications

A set of system specifications was provided by JPL. Table 5-8 shows the efficiencies of the components to be used with the ABSR. The calculated receiver design operating conditions were used to formulate specifications, Table 5-9, for the receiver design.

Cycle calculations performed using a computer model were used to specify the design and off-design operational conditions. Based on the calculations, a 0.30 thermal efficiency was obtained from the system with 0.21 overall efficiency. This resulted in output power of 17 KWe.

5.2.9 System Performance

Figure 5-25 illustrates the system performance using a staircase chart to demonstrate the effect of each component on the efficiency of the point focusing system. Assuming peak insolation incident at a 36 ft concentrator, the maximum available power corresponds to 85 KWt. After deducting shading and blocking losses of 1.2%, the available energy decreases to 93.86 KWt. An average concentrator reflectivity of 0.9 has been assumed in the design. This reduces the power available at the aperture to 84.47 KWt.

TABLE 5-8. GIVEN SYSTEM SPECIFICATIONS

ELECTRIC POWER OUT	$P_{OUT} = 16.75$ KWE
EFFICIENCIES	
COMPRESSOR	$\eta_C = 0.796$
TURBINE	$\eta_T = 0.872$
RECUPERATOR	$\eta_{RCPR} = 0.865$
GEAR BOX	$\eta_G = 0.96$
MECHANICAL	$\eta_{MT} = \eta_{MC} = 0.95$
ALTERNATOR	$\eta_A = 0.88$
SYSTEM DATA	
PRESSURE DROP IN RECUPERATOR	$\frac{\Delta P}{P} = .06$
AIR MASS FLOW RATE	$\dot{m} = 0.533$ LB/SEC
SYSTEM PRESSURE RATIO	$P_R = 2.5$
TURBINE INLET TEMPERATURE	1500°F
RECEIVER INLET TEMPERATURE	1050°F
PEAK HEAT RATE OF APERTURE	35 KWT
TURBINE EXHAUST/RECUPERATOR INLET TEMPERATURE	1185°F

TABLE 5-9. SYSTEM SPECIFICATIONS

RECEIVER	
APERTURE DIAMETER	7.34 IN
APERTURE AREA	42.31 IN^2
CAVITY DIAMETER	22 IN
ABSORPTIVITY OF MATRIX	0.2
RECEIVER EFFICIENCY	86%
SYSTEM	
ELECTRIC POWER OUT	17 KWE
CYCLE THERMAL EFFICIENCY	30%
OVERALL SYSTEM EFFICIENCY	21%

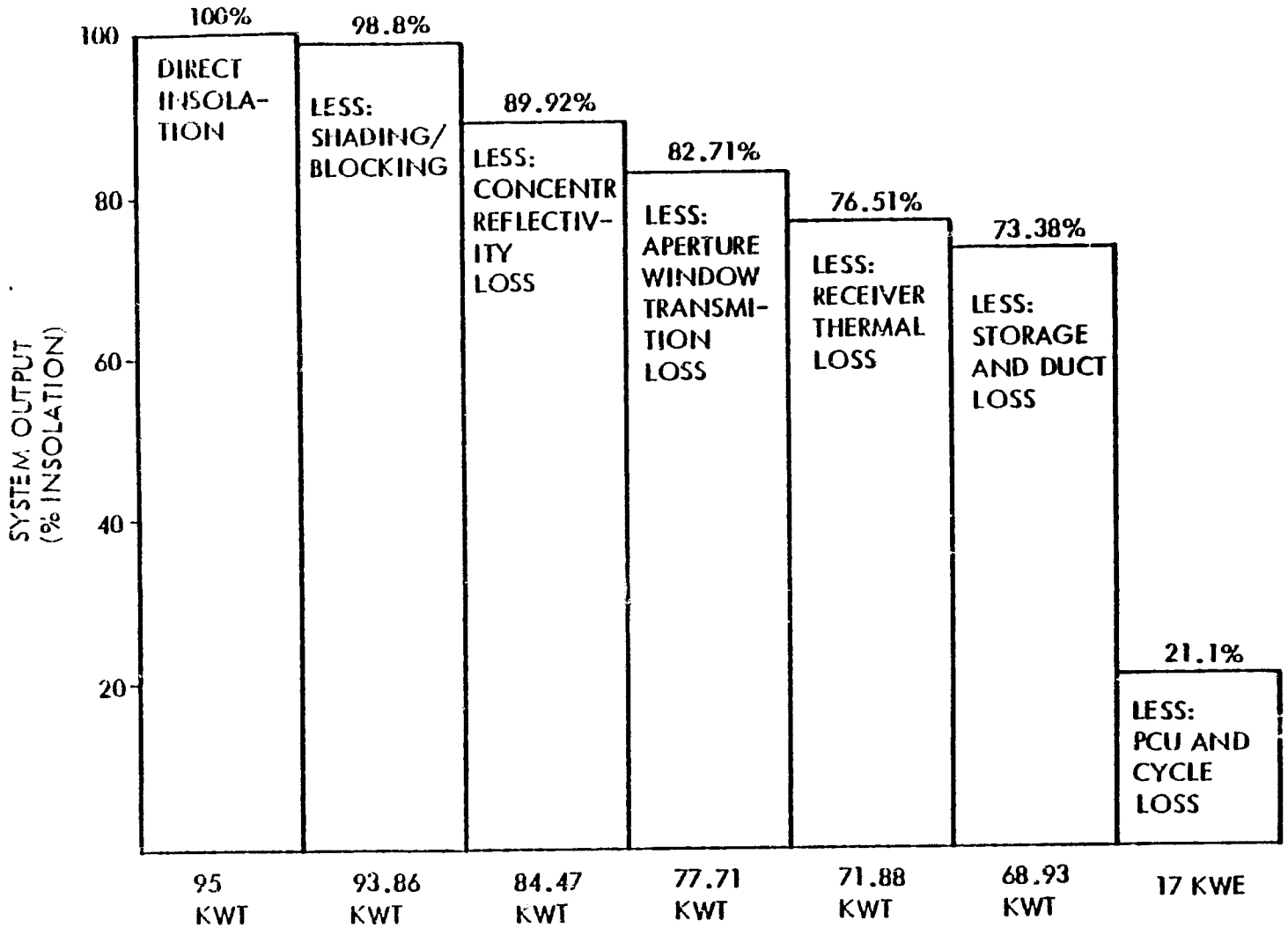

Figure 5-25. System performance considers each component the system resulting in an overall cycle efficiency of 0.21.

The pressurized matrix receiver is designed with a quartz window at the aperture to maintain cavity pressure. A transmission of 92% is due to reflection of the incident rays from the window. Therefore, the power available in the receiver is further reduced to 77.71 KWt. Accounting for reradiation and conduction losses from the receiver cavity, a 7.5% loss reduces the thermal power available to 71.88 KWt. Combining the transmission loss with reradiation and conduction, the overall receiver efficiency is calculated to be 0 85.

The storage module and ducting contribute 4% in conduction losses. The thermal energy available at the turbine is 61.93 kW. Finally, 17 KWe power output is obtained by deducting the thermal and electrical losses associated with the power conversion module. This results in an overall cycle efficiency of 0.21.

SECTION 6

INTERFACE REQUIREMENTS

The solar receiver is only one component of the Brayton cycle solar powered electric generating system. The Air Brayton Solar Receiver (ABSR) will be installed with its aperture at the focal point of a sun-tracking parabolic concentrator. The power conversion module, consisting of engine, generator, and recuperator is interfaced with and mounted in direct proximity to the receiver. The ABSR/power conversion module assembly is supported on a set of four struts with its center of gravity on the optical axis of the (parabolic) concentrator.

6.1 RECEIVER TO CONCENTRATOR

During daily operation, the concentrator tracks the sun and reflects its image into the receiver aperture. Table 6-1 relates energy capture to spot diameter for a range of combined mirror tracking and surface accuracies; the sun is assumed here to have a Gaussian shape with a radial standard deviation of 4.4 mrad.

The data of Table 6-1 support the selection of a 7.34 inch aperture diameter. The 7.34 inch diameter aperture receives nearly 99% of the incident light and at the same time minimizes reradiation. The maximum intensity of light which lands outside the limits of the aperture is 18 watts/cm^2. Stainless steel radiation shields which are cooled by natural convection protect the front surface of the receiver

TABLE 6-1. ENERGY CAPTURE AND SPOT SIZE

DEVIATION				CAPTURE							INTENSITY - w/cm²						
Sun	Tracking & Surface	Combined	r, inches	1.0	1.5	2.0	2.5	3.0	3.5	4.0	1.0	1.5	2.0	2.5	3.0	3.5	4.0
4.4	0.0	4.4	1.14	31.9	57.9	74.5	91.9	96.9	99.1	99.6	1100.	680.	347.	146.	50.6	14.5	3.33
	0.5	4.43	1.15	31.5	57.3	78.6	90.6	96.7	99.0	99.8	1090.	678.	350.	149.	52.1	15.5	3.75
	1.0	4.51	1.17	30.6	56.0	76.5	89.8	96.3	98.9	99.7	1065.	674.	356.	156.	57.3	17.5	4.44
	1.5	4.65	1.21	28.6	53.6	74.5	88.2	95.4	98.5	99.6	1020.	665.	366.	170.	68.4	21.9	6.06
	2.0	4.93	1.25	27.4	51.3	72.2	86.5	94.4	98.0	99.4	976.	654.	374.	192.	75.4	26.7	8.03
	2.5	5.06	1.31	25.3	48.1	69.3	83.8	92.7	97.2	99.1	914.	635.	382.	198.	88.9	34.5	11.6
	3.0	5.33	1.38	23.1	44.6	65.0	80.8	90.6	96.0	98.5	848.	611.	366.	214.	104.	44.2	16.5
	3.5	5.62	1.46	20.9	41.0	60.9	76.9	87.9	94.3	97.7	779.	481.	396.	227.	119.	55.7	23.1
	4.0	5.95	1.54	19.0	37.8	57.0	73.2	85.0	92.4	96.6	717.	551.	381.	237.	133.	669.	30.4
	4.5	6.29	1.63	17.2	34.5	52.9	69.2	81.6	90.0	95.1	655.	518.	372.	244.	145.	78.8	38.9
	5.0	6.66	1.73	15.4	31.3	49.7	64.8	77.8	87.1	93.1	594.	482.	360.	247.	156.	90.6	48.4

1. Intensity as a function of distance from the center of aperture, $I_r = 2100 \cdot \exp\left(-\frac{r^2}{2\sigma^2}\right)$

2. Reradiation from the cavity at 1700°F as a function of aperture radius, $R = 10.9 \cdot \sigma^{-2}$

3. Optimum aperture size to maximize net capture (capture - reradiation) as a function of tracking accuracy: $D_{\sigma=0} = 7.21"$; $D_{\sigma=1} = 7.36"$; $D_{\sigma=2} = 7.76"$.

from the spilled sunlight. The optical axis of the receiver must be closely aligned with the axis of the parabolic reflector to assure symmetrical flux distribution within the receiver.

The receiver support struts will be adjustable to provide the necessary minor alignment of axes at assembly. The four struts will be 4.0 inches outside diameter x 0.025 inch thick to hold the 1100 pound receiver/generator system within 0.25 inch of axis, regardless of reflector orientation. These struts have a safety factor of 1.70 based on Euler's buckling criteria. The strut stiffness/receiver mass combination has a natural frequency of 6-7 Hz. Turbo machinery induced vibration (at a much higher frequency) will not induce any support resonance.

6.2 RECEIVER TO POWER CONVERSION MODULE

The Power Conversion Module (PCM) interfaces with the receiver module, via a mechanical mounting plate and hot gas ducting. The mounting plate will have the necessary hole patterns to mount the receiver on one side and the PCM on the opposite side. Clearance and lightening holes will be included in the prototype system(s). Production systems would use a pressed sheet metal interface to sharply reduce piece cost and to simplify installation.

Duct interfacing will consist of flanged ducts, sealed with pressed steel gaskets, which are ring (marmon) clamped together. The suitability of ball-socket, gasketless interconnects typical of mass

produced motor vehicular applications will be investigated. The higher temperature/pressure requirements may preclude their use in this application, but potential product cost benefits cannot be ignored.

SECTION 7

PRODUCTION FABRICATION PLAN

7.1 GENERAL

The production plan required for volume fabrication of the Air Brayton Solar Receiver (ABSR) is an outgrowth of cost considerations which involve the physical design of this product. Figure 7-1 displays a production configuration of the receiver developed during the Phase I contract. This concept fabrication technique provides a base design with minimum parts count and minimum assembly effort on which to base production planning. In addition, Figure 7-2 displays a typical breakdown of target cost dollars, making a production budget available for design, tool and fabrication analyses. An allocation of direct material and direct labor dollars from this budget is made for each element of the device. These allocations are shown on the analysis sheets of Figure 7-3.

Volume production planning is keyed on a 100,000 unit per year quantity. This amount can clearly justify the capital investment needed to attain target piece costs. Smaller yearly rates will be burdened with a greater portion of startup cost. Larger volumes (1,000,000 per year) may well prove to be more efficient as geographic dispersions of multiples of 100,000. Shipping costs for a bulky, low dollar item will determine this approach when definite figures result from the upcoming contract task (see Figure 7-4 for quantity cost relation).

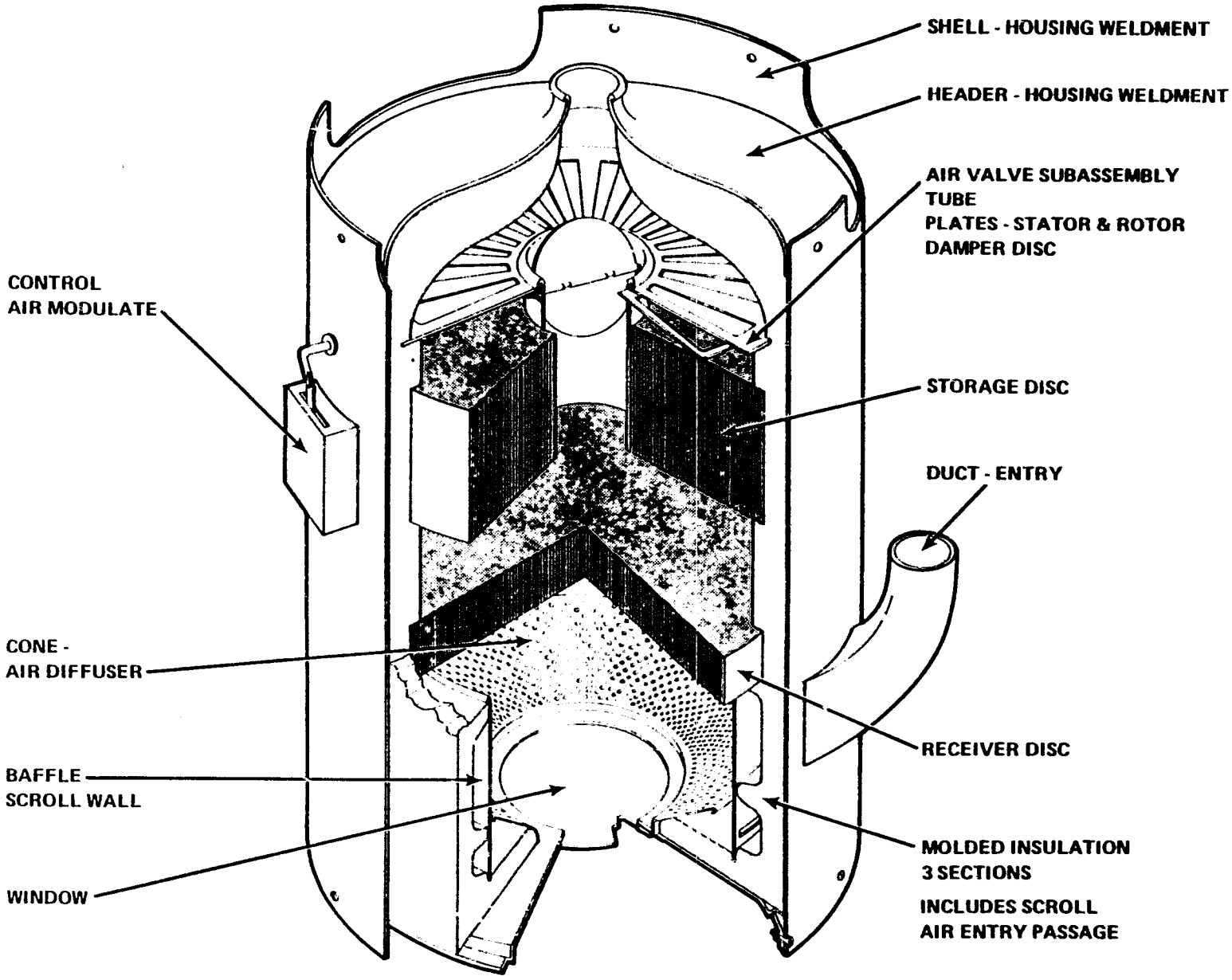

Figure 7-1. This is the production configuration of the receiver which was developed during the Phase I contract.

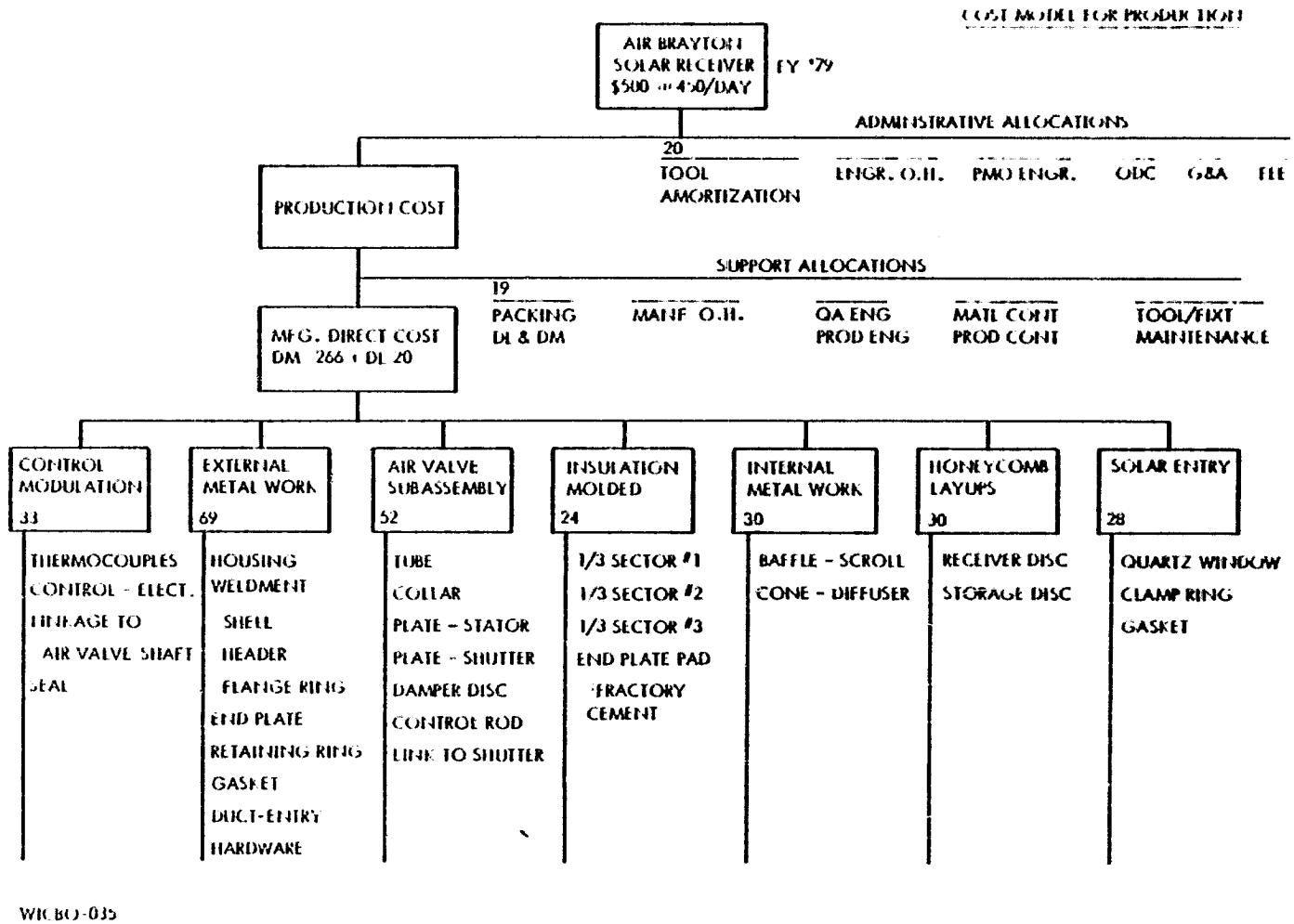

WICBO-035

Figure 7-2. A typical breakdown of target cost makes a production budget available for design, tool and fabrication analysis.

UNIT QTY	PART DESCRIPTION	DIRECT MAT'L	ASSEMBLY HOURS	TEST HOURS	TEST EQUIP	CAPITAL EQUIP
	AIR BRAYTON SOLAR RECEIVER ASSEMBLY	-	1.00			
1	TRAY SUB ASSEMBLY - INTERNAL ELEMENTS	-	1.00			
	INSULATION - MOLDED SEGMENT #1	5	.25			
1	AIR VALVE SUB ASSEMBLY		.25			
1	TUBE	6				
1	COLLAR	8				
1	PLATE-STATOR	12				
1	PLATE-SHUTTER	12				
1	DAMPER DISC	6				
1	CONTROL ROD-DAMPER	4				
1	LINK TO SHUTTER	4				
1	STORAGE DISC HONEYCOMB LAYUP	20	.2			
1	RECEIVER DISC HONEYCOMB LAYUP	10	.14			
1	BAFFLE - SCROLL WALL	10	-			
AR	REFRACTORY CEMENT	5	-			
2	THERMO COUPLES	4	.05			
2	INSULATION MOLDED SECTIONS 2 & 3	10	.1			
24	BANDING STOCK					
1	HOUSING WELDMENT	25	-			
1	SHELL	-				
1	HEADER	-				
1	FLANGE RING	-				
1	DIFFUSER CONE	30	-			
1	END PLATE SUB ASSEMBLY		.15			
1	END PLATE	8				
1	INSULATION PRD MOLDED	3				
AR	REFRACTORY CEMENT	1				
1	WINDOW	2				
1	GASKET	2				
1	CLAMP RING	6				
1	RETAINING RING (TO OUTER SHELL)	10				
1	GASKET	4				
1	DUCT - ENTRY	20				
1	CONTROL - AIR VALVE MODULATION	25				
1	LINKAGE TO DAMPER SHAFT	2				
1	SEAL	2				
-	HARDWARE 25 PC	2				
1	PACKAGE FOR SHIPMENT		.25			
1	CRATE	10				
-	DUNNAGE	7				
-	STRAPPING	2				
-	LABELING	.25				

NICBO-036

Figure 7-3. Direct material and labor are allocated from the production budget.

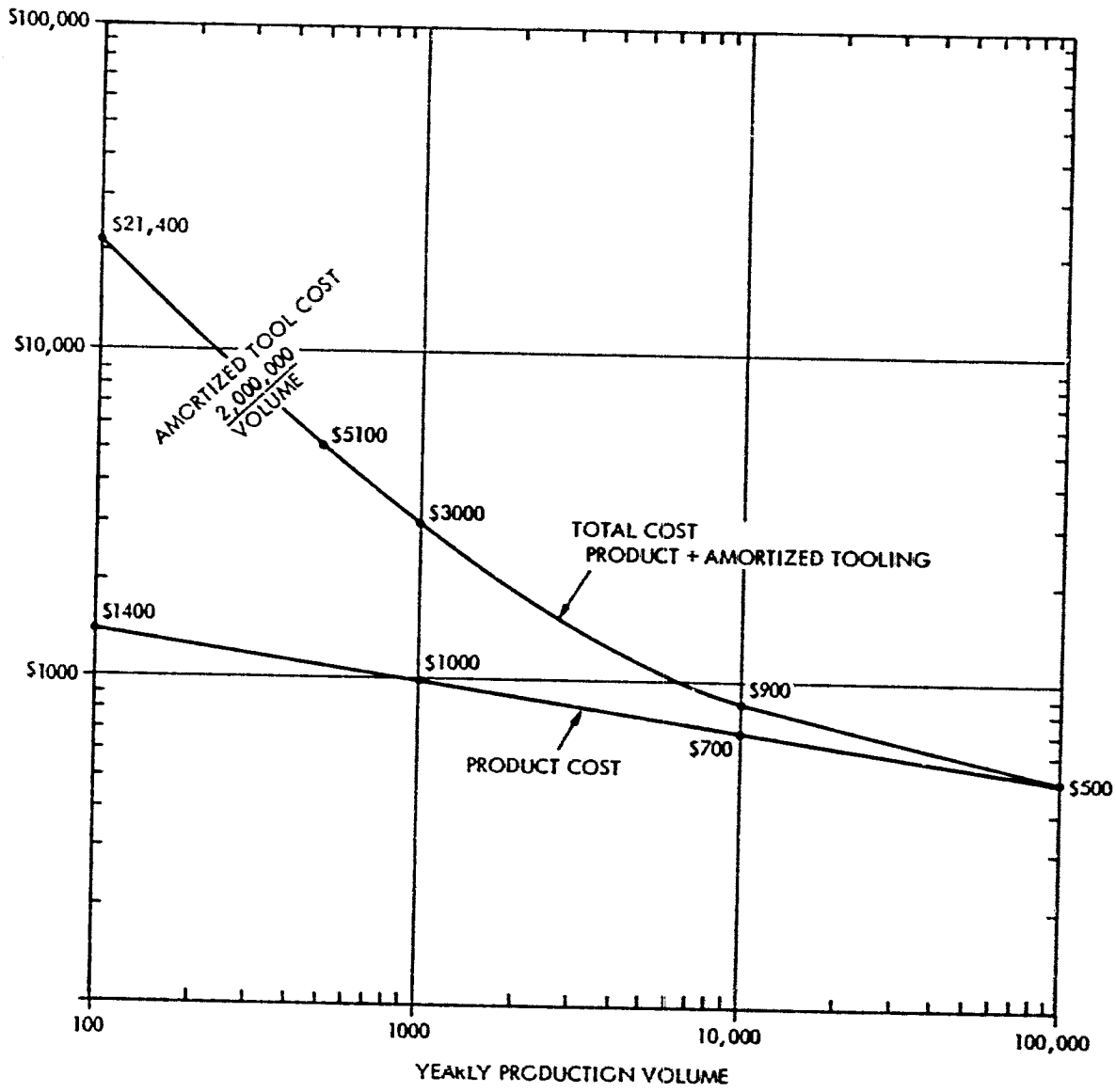

WICBO-0

Figure 7-4. Unit receiver cost decreases with increased volume production.

A target cost of $500 per unit (FY'79) has been assigned to the 100,000 yearly quantity. Considering effictive yearly work weeks, this equates to a daily factor flow rate of 450 sets per day. Process flow plan and manpower loading required are shown by Figure 7-5, and Figure 7-3, respectively.

It is planned to fabricate the molded insulation, honeycomb receiver and honeycomb storage elements in house for achievement of cost goals. This choice will also remove breakage and stress factors from the cost of shipping these parts from outside vendors.

Metal work of the exterior housing and end plate, and the elements of the air flow valve assembly is fabricated by very common methods used in producing hot water tanks and heavy sheet metal parts. These can be procured in volume by competitive bid. The existing Quartz window is a part currently satisfactory for prototype exposure and cost. Cost reduction is anticipated with volume production of these windows.

A total of several million dollars is anticipated for tooling and factory setup costs. Precise tool and fixture costing is a function of the next contract reporting task.

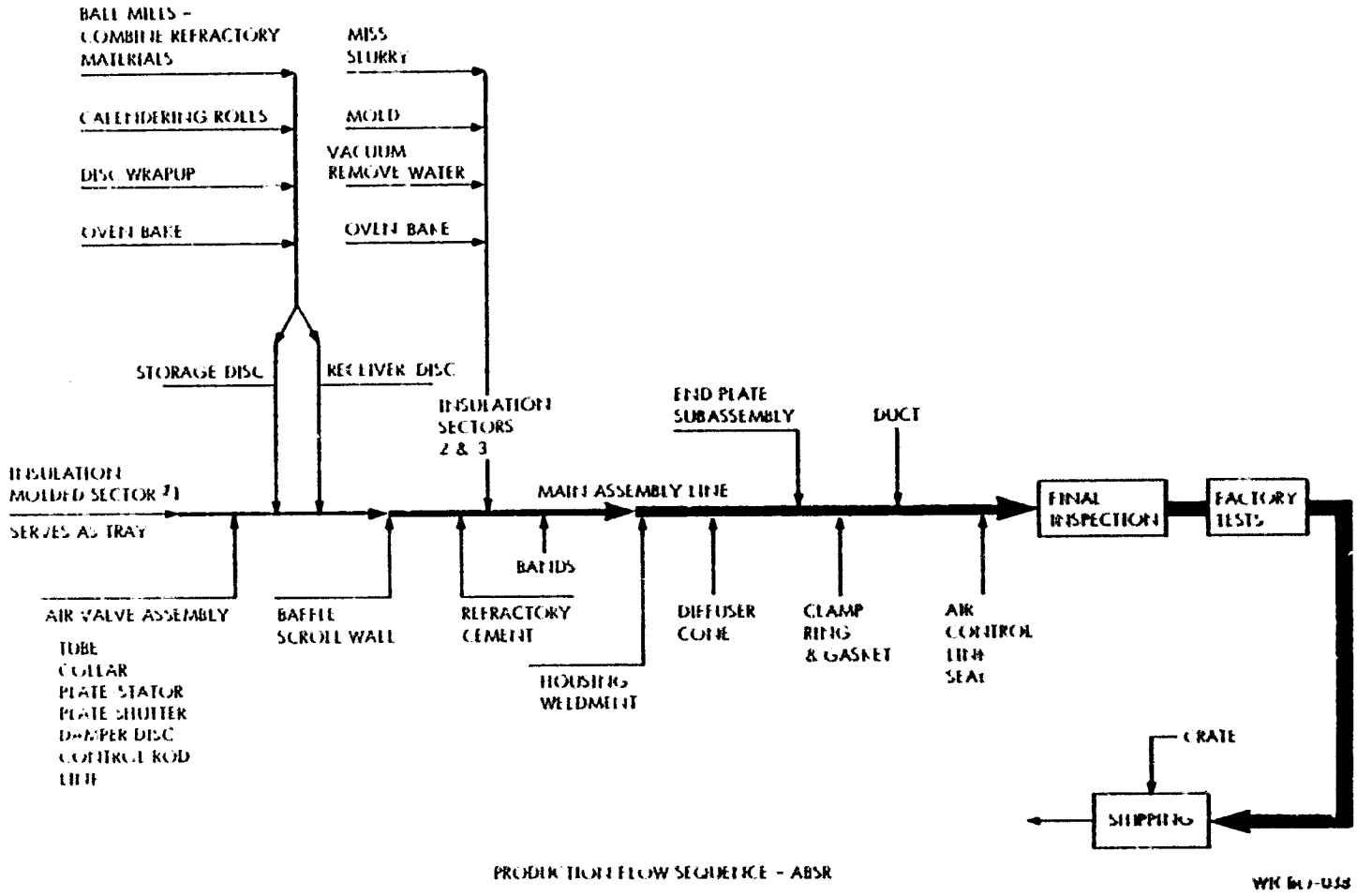

WICBO-038

Figure 7-5. The production flow sequence has been organized to assure the smoothest possible flow.

7.2 MANUFACTURING PROCESSES

7.2.1 General

Fabrication of three prototype units of the ABSR will not require the use of capital expenditure for production equipment or facilities. Sanders' present production facilities have been used to manufacture infrared countermeasures (IRCM) systems (AN/ALQ-147) for aircraft self-defense. The IRCM systems utilize the same kinds of materials and have similar hot gas flow requirements. The required low volume setups for refractory discs (receiver and storage) already exist and they are obtainable from the vendors used in prior development.

Metal forming is common to the water and boiler tank industry for housing work. Air valve parts may be readily blanked and rolled either at Sanders or at the vendor's facility.

A quartz window of the style used during the 10 KWt Receiver contract will be used in this receiver. Assembly fixtures and tools will be concerned with single unit work (a rate of one ABSR per week). No exotic methods will be needed for Phase II prototype development.

7.2.2 Implementation of Fabrication Plan

The schedule of Figure 7-6 gives the timing of design release, parts procurement (purchase and/or in-house fabricate), and assembly/test of the prototypes. The prototype systems (001-003) are designed

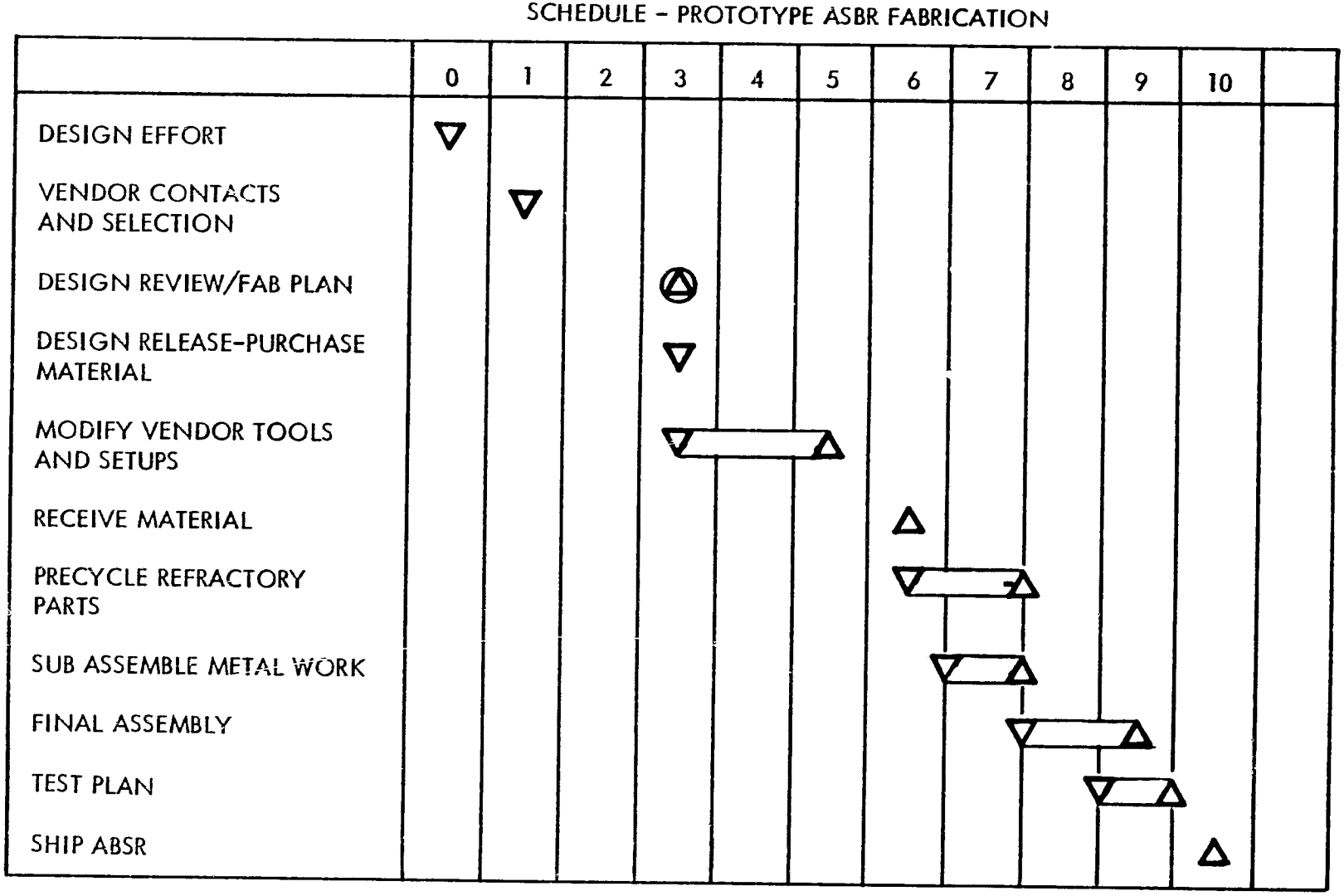

WICB0-032

Figure 7-6. The Prototype ABSR fabrication schedule will extend for 10 months, culminating in the delivery of three ABSR units.

to be functionally equivalent to the high volume production unit. Physical differences between the prototype and production units represent a realistic trade-off to cost-effectively provide a working system demonstration unit with extra instrumentation to collect engineering test data, and extra design flexibility to facilitate any required modifications, which may be necessary as a result of preliminary test findings.

The first unit (prototype 001) components will be closely inspected for design compliance. During the assembly and instrumentation of 001, manufacturing processes and component compatibility will be validated. Any necessary processes and/or component dimension changes will be incorporated in the fabrication process sheets, and dimension changes will be recorded by the appropriate drawing revisions.

After completion of unit 001, units 002 and 003, if purchased, will be assembled in accordance with the updated documentation.

Fabrication of the prototype units will be in accordance with the system drawing level breakdown. The process corresponds in principle with the Production Flow Sequence ABSR shown in Figure 7-5. Major differences are in the receiver and storage matrices; Sanders will purchase completed ceramic matrices for the prototype because in-house fabrication is not warranted for small lots.

Insulation in the prototype unit will be supplied in cylindrical sections approximately 14 inches long to minimize tooling cost.

A moving assembly line will not be used for the prototype lot. Tooling adjustments and secondary setup effort, by ceramics and insulation vendors has been planned. Sanders will prepare fixtures and dollies while awaiting parts. The necessary materials handling equipment will be identified and supplied from production support. Manpower allocation is shown in Figure 7-7. The production sequence will follow the flow shown in Figure 7-5.

7.3 SPECIAL PROCESSES AND EQUIPMENT

Extensive tooling will not be required for fabrication or assembly of the prototype receiver. There are, however, special forming techniques which have already been developed and are routinely used by our ceramic vendors.

The mullite storage mass will be extrusion formed and fired.

The Cordierite receiver matrix is formed from a roll press embossed tape of green stock which is then coiled to the required diameter.

Insulation sections will be joined by Sanders at assembly with an (aluminum) phosphate refractory cement.

MANPOWER ALLOCATION - PROTOTYPE FABRICATION

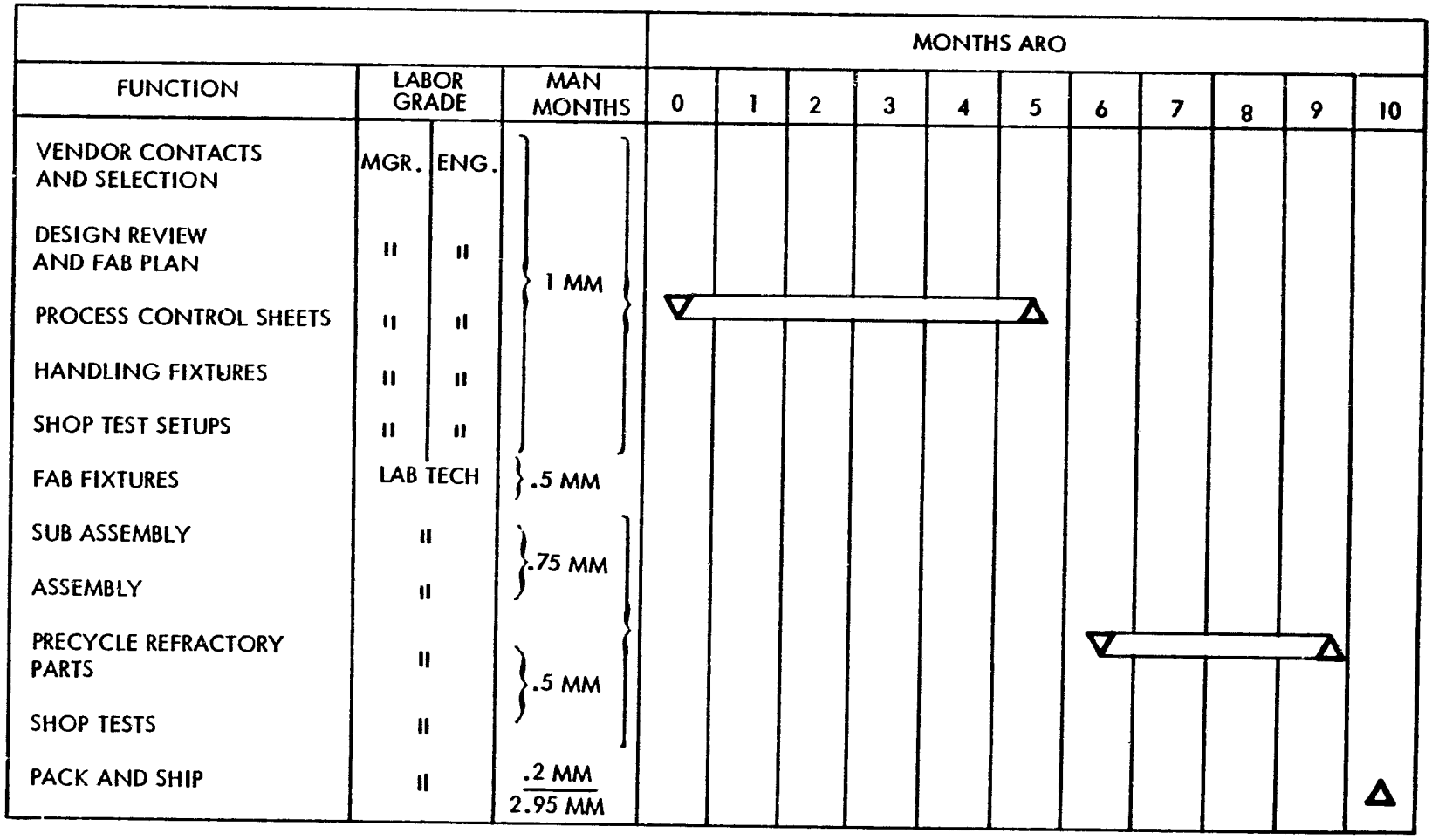

WICBO-033

Figure 7-7. Manpower will be allocated to provide the smoothest work flow during the program

SECTION 8

CONCLUSIONS

The parametric study on Air Brayton Solar Receivers indicated that the Pressurized Matrix receiver is the best candidate for meeting the performance and cost goals of Point Focusing Solar Thermal Power Conversion Systems. The compelling reasons for this decision are:

- Analytically and experimentally validated high heat transfer efficiency
- Low receiver pressure drops, that result in overall improvement in cycle efficiency
- Low thermal stresses that minimizes mechanical failure of receiver performance
- Compatibility with automated, manufacturing processes that minimize requirement for labor intensive operations of drawing, fusing, brazing and welding. Utilization of these manufacturing cost efficiencies offers the potential for complete receiver modules of low cost and high reliability
- Proven fabrication, design and test experience with similar matrix receiver and storage modules that insures satisfactory operating performance well within the time frame of the Jet Propulsion Laboratory's schedule.

APPENDIX A

HEAT EXCHANGER MATERIAL PROPERTIES

HEAT EXCHANGER MATERIAL PROPERTIES

	CONDUCTIVITY (BTU/HR-FT-°F)	EMISSIVITY SOLAR	EMISSIVITY AT 2000°F	RELATIVE COST
SiC	39	.9	.9	HIGH
CORDIERITE	.867	.2	.4	LOW
S.S.	9.4	.5	.5	MEDIUM

PROPERTIES OF CORDIERITE

SAFE OPERATING TEMP. °C (°F)	1200 (2192)
SPECIFIC GRAVITY	1.7
SPECIFIC HEAT	0.19
COEF. OF THERMAL EXPANSION IN/IN/°F (70 - 1400°F)	2.1×10^{-6}
THERMAL SHOCK RESISTANCE	EXCELLENT
COMPRESSIVE STRENGTH (Psi)	
PARALLEL TO PASSAGES	2750
PERPENDICULAR TO PASSAGES	70
MODULUS OF RUPTURE (Psi)	1800
THERMAL CONDUCTIVITY BTU/HR-FT-°F @ 570°F	0.867
DENSITY (lb/ft^3)	55

PROPERTIES OF SiC

SPECIFIC GRAVITY	3.1	
WORKING TEMPERATURE		
- INERT ATMOSPHERE	4200°F Max	
- OXIDIZING ATMOSPHERE	3000°F Max	
MODULUS OF RUPTURE (psi)	22,800	(2200°F)
MODULUS OF ELASTICITY (psi)	56×10^6	(70°F)
	51×10^6	(2200°F)
COMPRESSIVE STRENGTH (psi)	150,000	(70°F)
TENSILE STRENGTH (psi)	20,650	(70°F)
THERMAL CONDUCTIVITY	60	(1140°F)
BTU/HR-FT-F°	39	(1574°F)
	21	(2086°F)
	15	(2292°F)
	7.8	(2782°F)
THERMAL COEFF. OF EXPANSION	1.88×10^{-6}	(70 - 800°F)
IN/IN/F°	2.60×10^{-6}	(70 - 1800°F)
	2.80×10^{-6}	(70 - 2500°F)
MEAN SPECIFIC HEAT	0.34	(70 - 2800°F)
SPECTRAL EMISSIVITY	0.9	
THERMAL SHOCK RESISTANCE	EXCELLENT	

PROPERTIES OF S.S.

DENSITY	500 LB/FT^3
COEFFICIENT OF THERMAL EXPANSION IN/IN-$^\circ$F	9.9×10^{-6}
THERMAL CONDUCTIVITY (BTU/LB-FT-$^\circ$F)	9.4
SPECIFIC HEAT (BTU/LB-$^\circ$F)	.12
MODULUS OF ELASTICITY (PSI)	28×10^6
POISSON'S RATIO	0.29
YIELD STRESS PSI	39000